Public Interest Energy Research (PIER) Program

White Paper

DEVELOPMENT AND APPLICATION OF DOWNSCALED HYDROCLIMATIC PREDICTOR VARIABLES FOR USE IN CLIMATE VULNERABILITY AND ASSESSMENT STUDIES

A White Paper from the California Energy Commission's California Climate Change Center

Prepared for: California Energy Commission

Prepared by: University of California, Davis

JULY 2012

CEC-500-2012-010

James H. Thorne
Ryan Boynton
Lorraine Flint
Alan Flint
Thuy N'goc Le

University of California Davis
1 Shields Ave.
Davis, CA 95616

ACKNOWLEDGEMENTS

The authors thank the Information Center for the Environment co-directors, Dr. Jim Quinn and Dr. Karen Beardsley, for logistical and work space support. Alan and Lorraine Flint of the United States Geological Survey provided methods and code for the downscaling of climate data for climate change impacts.

PREFACE

The California Energy Commission's Public Interest Energy Research (PIER) Program supports public interest energy research and development that will help improve the quality of life in California by bringing environmentally safe, affordable, and reliable energy services and products to the marketplace.

The PIER Program conducts public interest research, development, and demonstration (RD&D) projects to benefit California. The PIER Program strives to conduct the most promising public interest energy research by partnering with RD&D entities, including individuals, businesses, utilities, and public or private research institutions.

PIER funding efforts are focused on the following RD&D program areas:

- Buildings End-Use Energy Efficiency
- Energy Innovations Small Grants
- Energy-Related Environmental Research
- Energy Systems Integration
- Environmentally Preferred Advanced Generation
- Industrial/Agricultural/Water End-Use Energy Efficiency
- Renewable Energy Technologies
- Transportation

In 2003, the California Energy Commission's PIER Program established the California Climate Change Center to document climate change research relevant to the states. This center is a virtual organization with core research activities at Scripps Institution of Oceanography and the University of California, Berkeley, complemented by efforts at other research institutions.

For more information on the PIER Program, please visit the Energy Commission's website http://www.energy.ca.gov/research/index.html or contract the Energy Commission at (916) 327-1551.

ABSTRACT

This paper outlines the production of 270 meter grid-scale maps for 14 climate and derivative hydrologic variables for a region that encompasses the State of California and all the streams that flow into it. The paper describes the Basin Characterization Model (BCM), a map-based, mechanistic model used to process the hydrological variables. Three historic and three future time periods of 30 years (1911–1940, 1941–1970, 1971–2000, 2010–2039, 2040–2069, and 2070–2099) were developed that summarize 180 years of monthly historic and future climate values. These comprise a standardized set of fine-scale climate data that were shared with 14 research groups, including the U.S. National Park Service and several University of California groups as part of this project. The paper presents three analyses done with the outputs from the Basin Characterization Model: trends in hydrologic variables over baseline, the most recent 30-year period; a calibration and validation effort that uses measured discharge values from 139 streamgages and compares those to Basin Characterization Model-derived projections of discharge for the same basins; and an assessment of the trends of specific hydrological variables that links historical trend to projected future change under four future climate projections. Overall, increases in potential evapotranspiration dominate other influences in future hydrologic cycles. Increased potential evapotranspiration drives decreasing runoff even under forecasts with increased precipitation, and drives increased climatic water deficit, which may lead to conversion of dominant vegetation types across large parts of the study region, as well as have implications for rain-fed agriculture. The potential evapotranspiration is driven by air temperatures, and the Basin Characterization Model permits it to be integrated with a water balance model that can be derived for landscapes and summarized by watershed. These results show the utility of using a process-based model with modules representing different hydrological pathways that can be interlinked.

Keywords: Downscaled climate, Basin Characterization Model, BCM, climatic water deficit, water balance, climate change

Please use the following citation for this paper:

Thorne, James, Ryan Boynton, Lorraine Flint, Alan Flint, and Thuy-N'goc Le (University of California, Davis and U.S. Geological Survey). 2012. *Development and Application of Downscaled Hydroclimatic Predictor Variables for Use in Climate Vulnerability and Assessment Studies.* California Energy Commission. Publication number: CEC-500-2012-010.

TABLE OF CONTENTS

LIST OF TABLES

LIST OF FIGURES

Unless otherwise noted, all tables and figures are provided by the authors.

Section 1: Introduction

1.1 PIER Vulnerability and Adaptation Study

The California Energy Commission (Energy Commission) Public Interest Energy Research (PIER) 2010 Climate Change Vulnerability and Adaptation (V&A) study includes the development of downscaled climate and hydrologic variables for the State of California and the watersheds that flow into it. These fine-scaled climate data can be used in a variety of applications and analyses that may permit better research, modeling, and interpretation for resource management in the state. These variables were also developed to provide a standard set of downscaled climate of historic and baseline conditions, and future emissions scenarios for use by researchers in multiple sectors involved in the overall PIER V&A study. The idea was that even when future projections are uncertain, if the same projections are used by groups working in multiple sectors, then the results from each sector study may be more cross-comparable. We arrived at the grid-scale and scenarios presented here through a series of steps that started with the identification of appropriate scenarios for California, based on Cayan et al. (2008), and the use of fine-scale downscaling for application to a regional hydrological model that can be evaluated on the basis of measured streamgage data.

This paper documents the methodology used to develop 14 climatic and hydrologic variables at 270 meters (m) for a 90-year retrospective and a 90-year forward projection, under two emissions scenarios and using two global climate models (GCMs), as well as potential applications, accuracies, and uncertainties. It also describes the data preparation and distribution, and acknowledges the studies being conducted in parallel that have used the data for the V&A study and other ongoing studies. We provide detail on trends in the hydrologic variables, but not temperature, as this paper is primarily focused on hydrology.

1.2 Hydroclimatic Variables for Future Climate Studies

Much of climate change impact assessment and adaptation planning centers on water availability, for both human populations and ecological systems (e.g., Trnka et al. 2011; Parmesan 2006). Projections of future climates from GCMs include the amount and timing of precipitation, as well as increases in air temperature, and are widely used in climate impact assessments (Girvetz et al. 2009). One of the needs in these assessments is a better understanding of what happens to precipitation in terrestrial ecosystems. The three main pathways—returning to the air via evaporation and plant transpiration; infiltration into soils and recharge to aquifers; and runoff—represent the water balance. Quantifying the relationship between these pathways can permit much more detailed predictions of the impacts of changing water availability to ecosystems and their inhabitants. Although climate change studies are fraught with uncertainty on the basis of emissions scenarios and GCMs used, the application of climate projections to mechanistic, process-based, hydrologic modeling should not be cause to amplify the uncertainty in the GCM projections. In fact, the incorporation of deterministic processes and landscape characteristics can potentially be employed to reduce uncertainty in the projected hydrologic outcome. Validation of spatially explicit hydrologic models that

quantify the water balance by comparing measured streamflow with model output is a promising approach to providing defensible mechanistic hydrologic relationships between climate and landscape in baseline time, that can then be applied to future climate projections for potentially more detailed forecasts. These will have increased utility over existing models for studies investigating climate impacts to species and ecosystems. Such a spatially vetted mechanistic model could then provide more robust projections of runoff, and thereby the other components of the water balance under future climates. Such capacity for these more detailed hydrologic predictions is critical for ecological studies and planning in the face of climate change.

1.3 Development of Variables at Fine Spatial Scales

The search for operational scales of analysis to inform natural resources management drives a need for finer-scale climate models. Global climate model outputs, typically range from 1.5–4.5 degrees (e.g. 2.5 degrees is approximately 250km x 250km), is too coarse for watershed-specific assessments on all but the largest watersheds (Fowler et al. 2007; Girvetz et al. 2009), requiring the need to convert this output to scales that appropriately reflect the environmental processes under consideration. Downscaling can bring climate projections to a spatial dimension for grid cells that can be validated using watershed-based methods, applied to local landscapes, or analyzed across large regions. Depending on the process of concern, this downscaling may range from spatial extents of kilometers to meters. Downscaling was, therefore, the first step we took to develop projections of water-balance components for California watersheds that are robust for use under climate change scenarios. As projections maintain their own set of uncertainties on the basis of the assumption chosen for global climate modeling and greenhouse gas emissions scenarios, it is advisable to incur the least additional uncertainty attributable to the downscaling scheme itself.

1.4 Hydrologic Modeling Background

Many approaches to hydrologic modeling have been developed. The U.S. Geological Survey (USGS) Precipitation-Runoff Modeling System (PRMS) is being used to simulate flows under future climate conditions at the watershed scale (Leavesley et al. 1992; Hay et al. 2011). This approach requires daily temperature and precipitation values that are applied to individual watersheds and used in a deterministic, distributed-parameter setting (Risley et al. 2011). The Variable Infiltration Capacity model (VIC) is a spatially explicit physical hydrology model, generally run regionally at coarse spatial scales, that balances energy and water budgets (Liang et al. 1994) and also runs using daily data (Wood et al. 2002). This model has also been applied to monthly climate in a model comparison study by Maurer et al. (2010), who found that model selection was less important for capturing high flow timing but that for the low flows, the models they tested varied, implying a need to vet model performance, particularly for aridifying regions. These rainfall-runoff models are specifically calibrated to streamgage data.

Other hydrologic modeling approaches have used streamgage data to validate the model projections as well. Alkama et al. (2011) developed the Interactions between Soil, Biosphere, and Atmosphere-Total Runoff Integrating Pathways (ISBA-TRIP) and looked at multi-decadal

variability in continental runoff from 1960–1994 using 154 large rivers with varying lengths of streamgage data for validation. Chiew et al. (2010) found that five different downscaling techniques all reproduced observed rainfall, and the runoff models used were capable of reproducing observed streamflows for eight basins in Australia. The range of applications and modeling platforms using streamflow for calibration indicates the utility of using the integrated measurement of streamflow in calibration exercises.

All of these rainfall-runoff models rely on soil storage in some capacity and do not incorporate bedrock properties; thus, they neglect the influence of bedrock permeability in estimates of recharge. There have been many experimental evaluations of hillslope processes and a few that have investigated the influence of bedrock permeability on hydrologic response to climate (Hutchinson and Moore 2000; Tromp-van Meerveld et al. 2007). Fewer still that have numerically modeled watersheds with the incorporation of bedrock properties (Flint and Flint 2006; Jones et al. 2008; Hopp and McDonnell 2009). Generally, these models are two- or three-dimensional, finite-element models that explicitly incorporate bedrock, but are computationally expensive and cover small areas. Historically, recharge estimates have relied on monthly water-balance models that incorporate simulations of evapotranspiration (Alley 1984), inverse modeling (Sanford 2001), or lysimetry and tracer tests (Gee and Hillel 1988). Water-balance modeling to assess both recharge and runoff has been done at the site scale (Flint et al. 2002; Ragab 1996) and integrated with various measurements addressing different spatial scales (Flint et al. 2002). Watershed-scale or regional-scale modeling to estimate recharge and runoff has been done using water-balance modeling by Hevesi et al. (2003), Flint et al. (2004, 2011, 2012, in review), and Flint and Flint (2007).

Water-balance models have been used to assess the impacts of climate change on hydrology, and in California the following water-balance models have been previously used: VIC and CALSIM (Vicuña et al. 2007; Maurer et al. 2010), the Precipitation-Runoff Modeling System (PRMS) (Dettinger et al. 2004; Koczot et al. 2011), Water Evaluation And Planning (WEAP) (Purkey et al. 2008, Sacramento Valley), and the Watershed Environmental Hydrology (WEHY) model (Chen et al. 2004), either at the watershed scale, or regionally. While many studies have evaluated impacts of climate change on ecological processes and the response of species to these changes (e.g., Lenihan et al. 2003; Lawler et al. 2009; Heller and Zavaleta 2009), these evaluations are predominantly based on climate variables, without the integrating effects of hydrologic response. Indeed, most species-distribution models rely solely on climatic variables and topography (Franklin 2010, ch. 5). Analyses of climate change impacts on ecosystems using climatic water deficit, with estimates of actual evapotranspiration, are beginning to emerge in the literature (e.g., Lutz et al. 2010; Breshears et al. 2009; van Mantgem and Stephenson 2007; Crimmins et al. 2011). However, the hydrologic results presented in this paper are provided at a fine spatial scale not yet seen applied in the literature that has the potential to further enhance the science and interpretation of climate change impacts on ecological systems.

1.5 Regional Water-Balance Modeling to Evaluate Hydrologic Response to Climate in California

The Basin Characterization Model (BCM) is a regional water balance model (Micheli et al., in review; Flint and Flint 2007) that has been applied to numerous watersheds in California at a fine scale of 270 m grid cells to assess impacts of climate change on both water availability and ecosystems. Using downscaled precipitation and air temperatures surfaces from 1971–2000, projections of runoff and recharge were produced for model calibration and assessment of model performance.

This paper reports historic and future trends from the climatic input variables and from variables generated by the BCM: snowpack, potential evapotranspiration, actual evapotranspiration, and climatic water deficit (Appendices A and B). The future condition analyses are for four climate scenarios representing a range of projected outcomes and model sensitivity to greenhouse gas forcing, and an analysis of the resulting hydrologic impacts.

To develop confidence in the application of historic and future climate projections to hydrologic modeling, this paper evaluates the reliability of hydrologic model performance by comparing basin discharge, a product of the runoff and recharge values modeled by the BCM with basin discharge values measured at streamgages. We assembled historical streamgage data from 138 mostly unimpaired basins (Figure 1; Appendix C) and used the monthly and yearly summaries from streamgages to test how well the BCM model outputs perform on watersheds with varying bedrock permeability, soil properties, impermeable surfaces, and degrees of aridity. The results of this model testing permit better interpretation of where hydrologic simulations perform better or worse due to influences of landscape variables. Tests were conducted by calculating discharge from BCM model outputs and comparing that to streamgage data.

1.6 Other Studies Using the Data

A number of other efforts under the PIER 2010 Climate Change Vulnerability and Adaptation effort are using the outputs from this data modeling effort. These include research groups working on:

- modeling the expected optimum movement corridors for biodiversity as it shifts suitable range (Hannah et al. 2012);
- modeling of fire return interval under future climatic and hydrological conditions (Krauchuk and Moritz 2012);
- a study that integrates historic vertebrate surveys, vegetation data, and historical climate data (Santos et al. 2012);
- an assessment of agricultural vulnerability, that includes among many factors the projections developed here (Jackson et al. 2012); and
- in the projections of future energy consumption by integrating the temperature values with projected future urban footprints (Thorne et al. 2012).

The idea behind using the same base climate and ecohydrological data for these studies is that, even if the projections turn out not to be correct, the results of the studies are cross-comparable.

In addition, there are a number of recent and ongoing studies in California that have relied on these datasets. Among these are a number of projects in the USGS California Water Science Center, including the following:

- A collaboration with the California Department of Water Resources that focuses on snowmelt in the southern Sierra Nevada and the contribution of soils to uncertainties in future streamflows
- A U.S. Forest Service study on mortality in high-elevation white bark pine (*Pinus* albicaulis) (Millar et al., in press)
- A Sonoma County Water Agency study on climate change impacts to the Russian River, future streamflows, and groundwater availability
- A USGS study on climate change impacts on streamflow and temperature in the Klamath River basin
- A study on climate change impacts on water resources in Santa Cruz County (Santa Cruz Health Department)
- USGS studies requiring upper recharge boundary conditions for groundwater models in Antelope Valley, Fort Irwin, San Gorgonio Pass, Santa Rosa Plain, Borrego Valley, Central Valley
- Ecological applications for the U.S. Fish and Wildlife's California Landscape Conservation Cooperative projects on wolverines in the Sierra Nevada, Central Valley waterbirds, and Central Valley rangelands

Other groups using the data include researchers at the University of California (UC) Berkeley, UC Santa Barbara, UC Riverside, Arizona State University, Sonoma Ecology Center, Pepperwood Foundation, and Creekside Center for Earth Observation.

Section 2: Data and Methods

2.1 Study Area

Hydrologic analyses rely on the topographic boundary of watersheds and drainages, and therefore we applied the BCM to hydrologic California, defined as all basins that drain within or into the State of California. All future references to California in this report infer this larger boundary. We report results for 5,128 watersheds (USGS 12-digit hydrologic units; sub-basins defined on the basis of the USGS National Hydrography Dataset; http://nhd.usgs.gov/index.html), and by ecoregion (Figure 1; modified from Hickman (1993) to include all basins draining into California).

Fluctuations in runoff or recharge across multiple watersheds can be monotypic or varied in response, indicating the need to calibrate hydrologic models to the watershed scale. In addition, relatively few watersheds are gaged, requiring modeling of hydrologic dynamics for most landscapes. For example, for our study area, approximately 1,700 streamgages have been in

operation within the 1971–2000 period, their periods of record ranging from 1 to 109 years; but only 1,400 record five or more years. These streamgages represent less than a third of the 5,128 subwatersheds in California; many of these gages are on the same streams (replicates), and California is presumably one of the better-instrumented regions of the world.

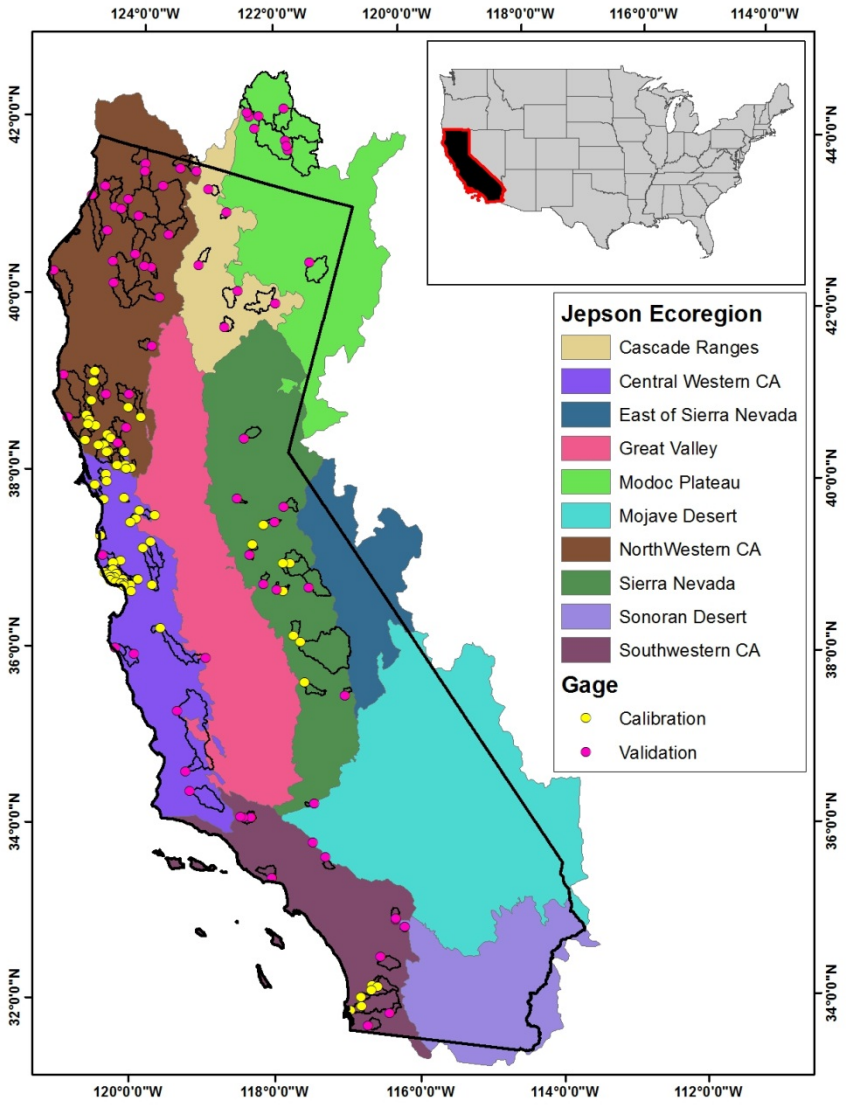

Figure 1: Study Area of the "Hydrologic" California with Study Basins, Modified Jepson Ecoregions, and Watersheds with Streamgages Used for Calibration or Validation

Streamgages record a variety of discharge dynamics, from flashy with high runoff peaks as a result of low permeability bedrock (such as granites in the Sierra Nevada or impervious urban surfaces), to high baseflows with very permeable bedrock composition (e.g., volcanic rock; Flint and Flint 2007; Flint et al. 2011; Tromp-van Meerveld et al. 2007). The degree of climate aridity and soil type also affects hydrologic response to climate, with the deep unsaturated zones (in arid regions or the deep soils of California's Central Valley) storing water when available from wet climate cycles for use as groundwater during dry periods (Flint and Flint 2007). These

factors are implicitly addressed when projections of hydrologic change due to changes in climate are considered; however, they are potentially confounding with projections of basin discharge.

2.2 Future Climate Scenarios

Global climate models are generally available for the continental United States at a 2.5 x 2.5 degree spatial resolution (IPCC 2001, 2007). A set of these projections have been downscaled to 1/8 x 1/8 degree (approximately 12 x 12 kilometers [km]) spatial resolution for the State of California and its environs by researchers at USGS and Scripps Institute of Oceanography using the constructed analogs method of Hidalgo and others (2008). These provide a basis for our further downscaling for model application. On the basis of analyses done by Cayan et al. (2008; 2009), several criteria were followed in the selection of models to downscale for the PIER V&A study. Models selected were required to produce a realistic simulation of aspects of California's recent historical climate, particularly the distribution of monthly temperatures and the strong seasonal cycle of precipitation. They were required to contain realistic representation of some regional features, such as the spatial structure of precipitation, and similar degree of variability. In addition, models selected were to have differing levels of sensitivity to greenhouse gas forcing.

As a result, for our analysis, two GCMs were selected: the Parallel Climate Model (PCM) developed by National Center for Atmospheric Research (NCAR) and the U.S. Department of Energy (U.S. DOE) (see Washington and others 2000; Meehl and others 2003) and National Oceanic and Atmospheric Administration (NOAA) Geophysical Fluid Dynamics Laboratory CM2.1 model (GFDL) (Stouffer and others 2006; Delworth and others 2006). The choice of greenhouse gas emissions scenarios included A2 (medium-high emissions) and B1 (low or "mitigated" emissions), and was guided by considerations presented by the Intergovernmental Panel on Climate Change (IPCC) (Nakic'enovic' and others 2000). Thus we developed a range of hydrology estimates based on four specific scenarios; two models each representing two emissions scenarios. We refer to these scenarios as "GFDL A2," "GFDL B1," "PCM A2," and "PCM B1." These four projections span the range of future climates in California and represent "warmer (B1) and wetter (PCM)," and "much warmer (A2) and drier (GFDL)."

The above approach could be described as a precision-based approach, which is one that, instead of examining all possible (or modeled) futures, focuses on projections thought to be most relevant for a particular area. An alternative that is frequently used in climate studies is the ensemble approach, wherein a stack of GCM projections or emission scenarios are considered in concert to determine consensus in the direction or magnitude of change (e.g., Pierce et al. 2009). Consensus studies were conducted as part of the PIER V &A effort by other groups, including Krauchuk and Moritz (2012). This study uses the precision approach and illustrates a range of possible outcomes for projections previously described by Cayan et al. (2008), and listed above.

To put these scenarios in a larger context, the Krawchuk and Moritz paper (2012) compares these four scenarios to an ensemble of 16 models of global climate model output from the World

Climate Research Programme's (WCRP) Coupled Model Intercomparison Project phase 3 (CMIP3) multi-model dataset (Meehl et al. 2007). In the 2010–2039 period, the GFDL falls in the mid-range for temperature increases and low range for precipitation; the PCM falls in the low range for temperature and precipitation. By 2070–2099, the GFDL is still in the mid-range among GCMs for temperature but among the lowest of the 16 GCMs for precipitation, thus supporting its use in representing a warmer, drier future. The PCM falls in the low range for temperature and low-mid range for precipitation; annual precipitation shows little change, but higher amounts than the GFDL. Though by no means high-ranking in precipitation amounts within the 16 GCM ensemble, the comparison to the GFDL supports its use in representing a warmer, wetter future.

Climate projections are model simulations that describe potential future changes in climate. Unless bias corrected, GCM projections of current time climate (here also called baseline) often do not match measured current climate conditions. In order for future projections to match baseline climate, the entire record requires adjustment to establish the correct mean and variability of the baseline model simulations. The four scenarios of our study were therefore downscaled from the 12 km grid scale to the historical data scale (4 km^2) of the Parameter-Elevation Regressions on Independent Slopes Model (PRISM; Daly et al. 1994), by using the Gradient-Inverse-Distance-Squared (GIDS) spatial interpolation approach (see Section 2.3.1). The purpose of this adjustment was to then apply a bias correction. The bias correction brings the projected future conditions into alignment with baseline conditions, thereby making the calibration so that future conditions are tied to current climate levels.

To make the correction possible, the GCM is run for an historical time period to establish a baseline for modeling to match baseline climate. The baseline period for this study is defined as the PCM and GFDL model runs for 1950–2000, when climate change forcings are assumed absent from the model, representing baseline (pre-2000) atmospheric greenhouse gas conditions. This baseline period was then adjusted using the PRISM data from 1950–2000, for each month and for each grid cell. Our approach to bias correction is a simple scaling of the mean and standard deviation of the projections to match those of the PRISM data following Bouwer and others (2004) and described in detail in Flint and Flint (2012). Once the bias correction is complete, the 4 km projections are further downscaled to 270 m spatial resolution using the GIDS spatial interpolation approach for model application.

2.3 Data Development

Development of data to run BCM for hydrologic climate change assessments required downscaling the climate inputs from 12 km grids to 270 m for historic and future projections. This included downscaling the PRISM data from 4 km^2 to 270 m^2 grids, and doing the same for the four future scenarios. We then had month-by-month and year-by-year data for minimum temperature (Tmin), Maximum temperature (Tmax), and precipitation (PPT). These were used as inputs for running the BCM (see below, and Appendix A) to create the additional 11 hydrologic variables (see Appendix B). Finally, we summarized each variable for six 30-year time slices: 1911–1940, 1941–1970, 1971–2000, 2011–2040, 2041–2070, and 2071–2100, calculating

the mean, standard deviation, rate of change within the 30-year period, and several other values (see Appendix B).

2.3.1 Downscaling Historic and Future Datasets

Historical climate maps (Tmin, Tmax, PPT) were derived from the empirically based PRISM monthly precipitation and air temperature database and maps that are available at 4 km spatial resolution (Daly et al. 2004). We downscaled the PRISM data, described below, to the 270 m operational grid scale for model application.

All historical and future climate grids and maps of properties need to be at the same grid scale—in this case, 270 m—for model operation. Spatial downscaling was used to interpolate precipitation and air temperature grids from coarse-scale grids (4 km) to fine-scale (270 m). The approach applies a spatial GIDS weighting to monthly point data by developing multiple regressions for every fine-resolution grid cell for every month. Using the PRISM climate variables and the 4 km-resolution digital elevation model, parameter weighting is based on the location and elevation of the coarse-resolution cells surrounding each fine-resolution cell to predict the climate variable of the fine-resolution cell (Flint and Flint, 2012; modified from Nalder and Wiens 1998). To remove the "bullseye" effect often associated with certain interpolation schemes (e.g., kriging, inverse distance squared), the program was modified to have a search radius that is specified as the size of gridcell of the coarse-resolution grid. The modified GIDS spatial downscaling technique does not introduce additional uncertainty in the downscaling process, and may indeed improve the estimate of the climate variable by incorporating the deterministic influence (such as lapse rates or rain shadows) of location and elevation on climate. The details of the methodology and the evaluation of uncertainty are discussed in Flint and Flint (2012).

2.3.2 Description of the Basin Characterization Model (BCM)

The hydrology of a region is a function of the water balance, including the climatic input precipitation, and how it is partitioned into evapotranspiration; snow accumulation, sublimation, and melt; changes in soil moisture storage; and subsequently, runoff and recharge. Basin discharge can subsequently be calculated from runoff and recharge. The BCM mechanistically models the pathways of a basin's precipitation into evapotranspiration, infiltration into soils, runoff, or percolation below the root zone to recharge groundwater. The evapotranspiration component of the BCM is derived through the use of potential evapotranspiration equations (PET; Priestley and Taylor 1972), solar radiation, slope and aspect, and topographic shading. For the purposes of comparison across watersheds (or other landscape units), PET in the BCM is not interactive with the other segments. In other words, water demand from plants is independent from other hydrodynamic components in the model. The soil storage component of the model uses soil parameters to calculate how much water is available in the soil, a parameter of particular use to plant ecologists, and is also independent from the other major hydrologic dynamics, except that groundwater recharge, calculated as infiltration below the zone of evapotranspiration, is calculated only from surplus, after soil moisture capacity has been filled. Groundwater recharge (recharge) is also tied to runoff, and the relationship between the two is driven by the level of permeability of bedrock.

The unique response of any given watershed to climate is primarily related to its energy balance (based on latitude, longitude, elevation, slope, and aspect), soil moisture storage capacity, and the characteristics of the materials that are deeper than the rooting zone of vegetation, including deep alluvial valleys or channels or bedrock that lead to deep percolation into the groundwater system. The monthly water balance can be calculated using the BCM that was originally developed for arid and semi-arid lands with minimal streamflow data upon which rainfall-runoff models rely for calibration (Flint and Flint 2007). The BCM calculates hydrologic variables on a grid cell basis and can be run at any spatial resolution, generally limited by computing power or file storage capabilities. For this application we developed a spatial resolution of 270 m, not so fine-scale to be computationally prohibitive, but fine enough to capture differences on hillslopes due to variable radiation and soil properties. Grid cell values can be summarized for any spatial pattern, here using the USGS hydrologic unit code (HUC) 12 watersheds.

The BCM has a number of subroutines or modules. Figure 2 is a schematic of the processes and calculations addressed in the BCM. The modeling approach begins with the climate as precipitation and air temperature. This is followed by the calculation of PET. This calculation relies on an hourly energy-balance calculation that is based on solar radiation, air temperature, and the Priestley-Taylor equation (Flint and Childs, 1991). Clear sky PET is calculated using a solar radiation model that incorporates seasonal atmospheric transmissivity parameters and site parameters of slope, aspect, and topographic shading (to define the percentage of sky seen for every grid cell) (Flint and Childs 1987). Hourly PET is aggregated into monthly time series, and cloudiness corrections are made using cloudiness data from National Renewable Energy Laboratory (NREL). Modeled PET for the southwest United States has been calibrated to measured PET from California Irrigation Management Information System (CIMIS) and Arizona Meteorological Network (AZMET) stations.

Using PET and gridded precipitation, maximum and minimum air temperature, and the approach of the National Weather Service Snow-17 model (Anderson 1976), snow is accumulated, sublimated, and melted to produce available water (Figure 2). These driving forces for the water balance have been calibrated regionally to solar radiation and PET data, and snow cover estimates have been compared to Moderate Resolution Imaging Spectroradiometer (MODIS) snow cover maps (Flint and Flint 2007). However, the final calibrations of snowmelt and runoff have illustrated goodness-of-fit, as will be shown in the results.

The calculation of excess water provides the water that is available for watershed hydrology. Available water occupies the soil profile, where water will become actual evapotranspiration, and may result in runoff or recharge, depending on the permeability of the underlying bedrock. Total soil-water storage is calculated as porosity multiplied by soil depth. Field capacity (soil water volume at -0.3 megapascals [MPa]) is the soil water volume below which drainage is negligible, and wilting point (soil water volume at -1.5 MPa) is the soil water volume below which actual evapotranspiration does not occur (Hillel 1980).

Once available water is calculated, it may exceed total soil storage and become runoff, or it may be less than total soil storage but greater than field capacity and become recharge. Anything less

than field capacity will be calculated as actual evapotranspiration at the rate of PET for that month until it reaches wilting point. When soil water is less than total soil storage and greater than field capacity, soil water greater than field capacity equals recharge. If recharge is greater than bedrock permeability (K), then recharge = K and excess becomes runoff, else it will recharge at K until field capacity.

Runoff and recharge combine to calculate basin discharge, and actual evapotranspiration is subtracted from PET to calculate climate water deficit.

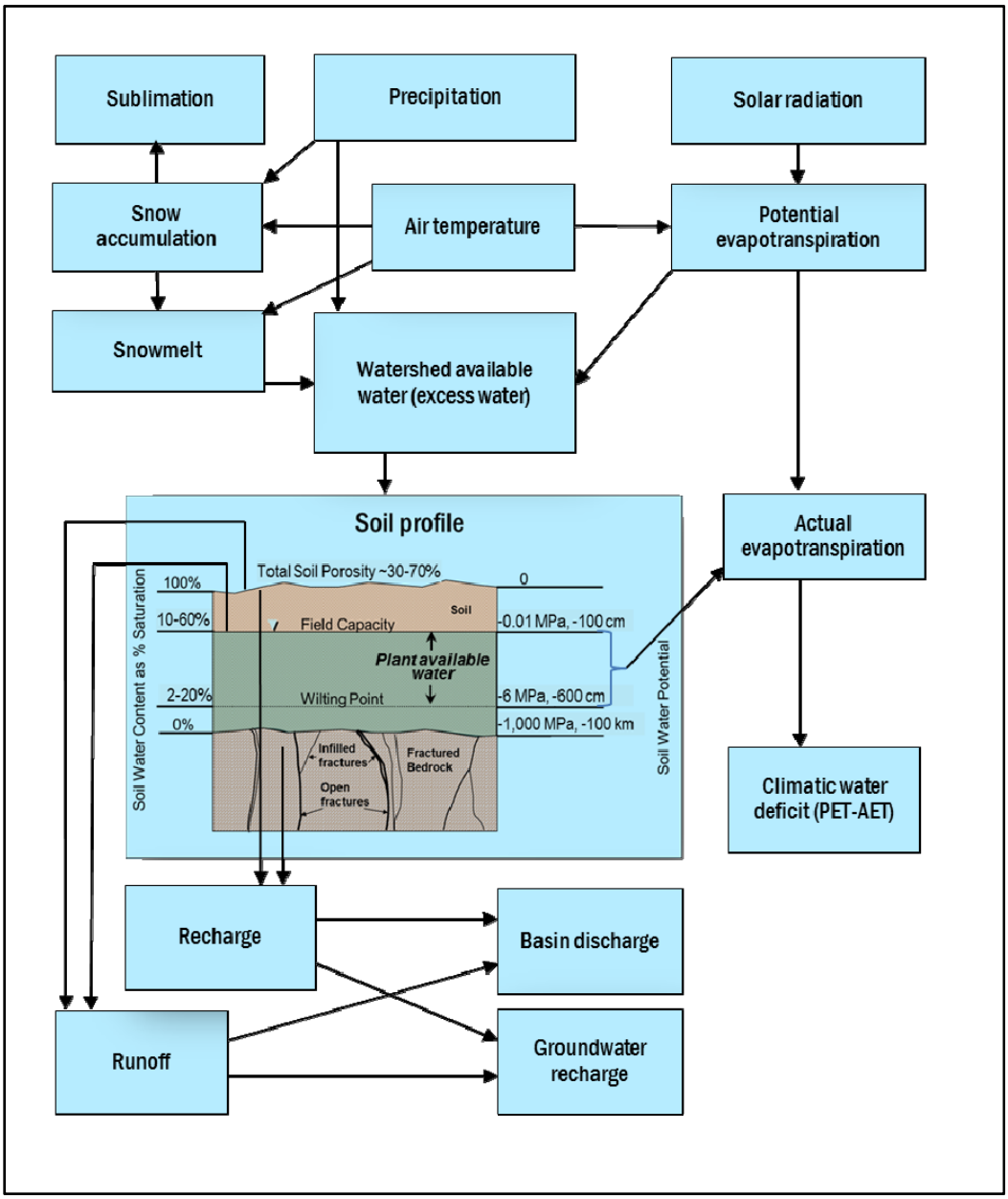

Figure 2: Schematic Describing Relation of Components of the Basin Characterization Model. Arrows indicate the sequence of calculations.

The BCM can be used to identify locations and climatic conditions that generate excess water by quantifying the amount of water available either as runoff generated throughout a basin, or as in-place recharge (Flint and Flint 2007). Because of the grid-based, simplified nature of the model, with no routing of runoff to downstream cells, long time series for very large areas can be simulated easily. However, if local unimpaired streamflow is available, estimated recharge and runoff for each grid cell can be used to calculate basin discharge that can be extrapolated through time for varying climates. In addition, the application of the model across landscapes allows for grid-based comparisons between different areas. Because of the modular and mechanistic approach used by the BCM, it is flexible with respect to incorporating new input data or updating of algorithms should better calculations be derived. A flow chart indicating all input files necessary to operate the BCM, and the output files resulting from the simulations, is shown in Appendix A.

After running the BCM, the 14 climate and hydrologic variables were produced in raster format for every month of every year modeled (summarized in Appendix B). To evaluate hydrologic response to climate for all basins in hydrologic California, we used the BCM to calculate hydrologic conditions across the landscape for 1971–2000 and to project them for the two GCMs and two emission scenarios for 2001–2100. Trends in climate, hydrologic derivatives of runoff and recharge, and climatic water deficit are separately analyzed for both historical-to-baseline, and baseline-to-future time periods (1911–1940 to 1971–2000, and 1971–2000 to 2071–2100).

2.3.3 Model Performance: Calibration and Validation

Although recharge and runoff were calculated for every grid-cell and summarized as totals for basins, the estimate of basin discharge as a time series requires a further calculation of streamflow. Calculation of streamflow uses a series of equations that can be calibrated with coefficients from existing streamgage data, that then permit estimation of basin discharge for time periods when there are no streamflow measurements. We calculated basin discharge for each of 138 basins for which we also obtained streamgage data, and used the 138 streamgage datasets for calibration and validation.

The regional BCM developed for the southwest United States (California, Nevada, Utah, Arizona, and parts of New Mexico and Idaho; Flint and Flint 2007, 2009, 2011) was applied to California following regional calibrations for solar radiation, PET, snow cover, (described above), and groundwater (described in Flint and Flint 2009, 2011). The California calibration is based on study areas with ongoing studies (Figure 1, calibration basins) that were designed to provide runoff and recharge for historic, baseline, and future climatic conditions. Generally the watersheds used for calibration basins were identified on the basis of lack of impairments, such as urbanization, agriculture, reservoirs, or diversions, although this was not always possible. We used 68 basins for which bedrock permeability was iteratively changed to optimize the match between calculated basin discharge and measured streamflow. Calibration basins represent 9 of the 14 dominant geologic types in California, and have been calibrated to bedrock permeability on the basis of mapped geology for California (Jennings 1977; Figure 3; Appendix C).

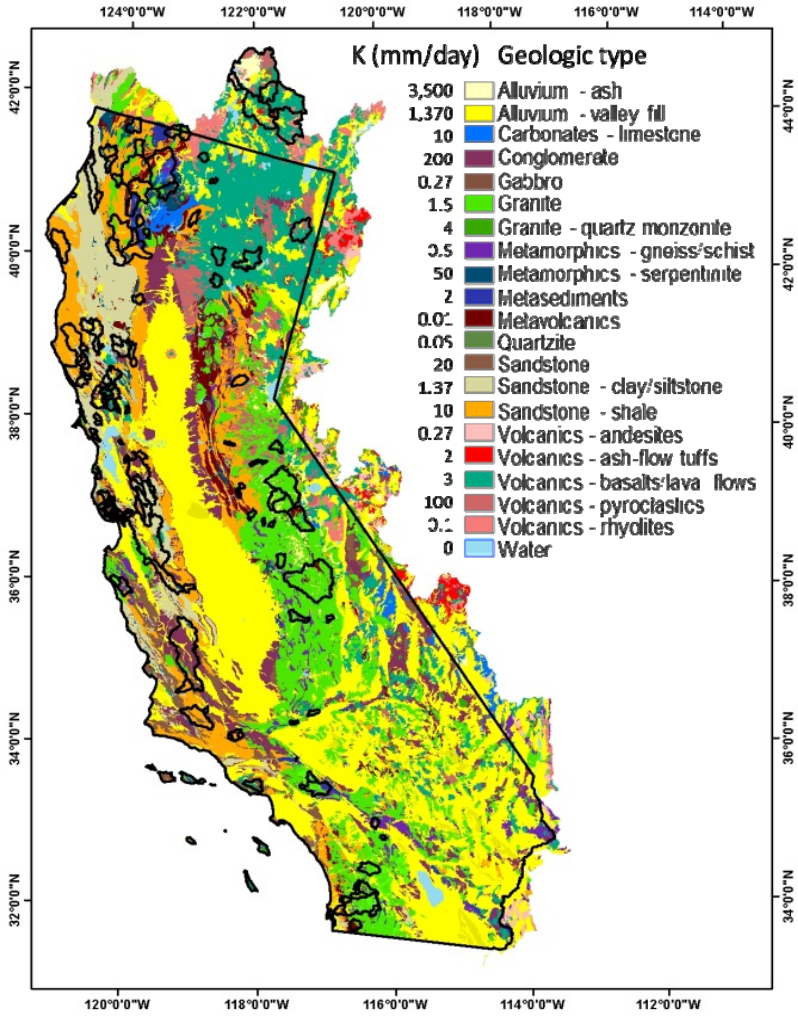

Figure 3: Map of Geology for Study Area with Study Basins

The BCM performs no routing of streamflow, which is done as post-processing to produce total basin discharge for any basin outlet or pour point of interest, such as streamgages or reservoirs. The 68 calibration basins were calibrated to optimize the match between BCM-derived discharge and streamflow by iteratively adjusting the bedrock permeability corresponding to the geologic types located within the basins to alter the proportion of excess water that becomes recharge or runoff. (This is iterative among all calibration basins because the geologic units are mapped consistently across the entire state, and if the permeability is changed to optimize the fit in one basin it changes the permeability wherever the geology is mapped.) This part of the calibration process is followed by accounting for stream channel gains and losses to calculate basin discharge, optimize the fit between total measured volume and simulated volume for the

period of record for each gage, and maintain a mass balance among streamflow and BCM recharge and runoff.

As described, BCM simulates recharge (BCM_{rch}) and runoff (BCM_{run}) for each 270 m grid cell for each month *(i)*. To compare them to gaged mean monthly streamflow, all gridcells upstream of the streamgage are summed for each month to create time series for BCM_{run} and BCM_{rch}. To transform these results into a form that can be compared to the pattern and amount of gaged streamflow, the water balance is conceptualized as consisting of two units that are hydraulically connected through a shallow storage zone ($GW_{shallow(i)}$). The two units are the basin discharge ($Stream_{(i)}$) and regional aquifer ($GW_{deep(i)}$). A set of empirical flow-routing equations defines storage in successive time-steps (*i*) and performs partitioning. $GW_{shallow(i)}$ is the computational method used to extend streamflow for time-steps when $BCM_{run(i)}$ and $BCM_{rch(i)}$ are zero (e.g., during seasonal and annual dry periods). For time-steps when $BCM_{run(i)}$ and $BCM_{rch(i)}$ are non-zero, the amounts are accumulated for the grid cells upstream of a streamgage. Initially the water in $GW_{shallow(i)}$ is evaluated as

$$GW_{shallow(i)} = (1\text{-}Runscaler)* BCM_{run(i)} + BCM_{rch(i)} + GW_{stor(i-1)} \quad \text{(Eq. 1)}$$

Runscaler is a coefficient (< 1) that is used to match peak flows, and (*1-Runscaler*) is the direct loss of peak flows to $GW_{shallow}$. Carryover of groundwater storage from the previous time-step $(GW_{stor(i-1)})$ is set by the parameter *exp* (< 1).

$$GW_{stor(i)} = (GW_{shallow(i-1)})^{exp} \quad \text{(Eq. 2)}$$

The overland flow component is comprised of the direct runoff and baseflow. The direct runoff is calculated (Eq. 3) from $BCM_{run(i)}$ and the *Runscaler* (from Eq. 1), and the baseflow/recession component is partitioned from $GW_{shallow(i)}$ minus carryover to the next month ($GW_{stor(i)}$, see Eq. 2) using the parameter *Rchscaler* (< 1).

$$Runoff_{(i)} = BCM_{run(i)}* Runscaler + Baseflow_{(i)} \quad \text{(Eq. 3)}$$

$$Baseflow_{(i)} = (GW_{shallow(i)} - GW_{stor(i)}) * Rchscaler \quad \text{(Eq. 4)}$$

To maintain mass-balance, the carryover ($GW_{stor(i)}$) is subtracted from the $Baseflow_{(i)}$. The sum of $Runoff_{(i)}$ and $Baseflow_{(i)}$ is the storage water partitioned to $Stream_{(i)}$.

$$Stream_{(i)} = Runoff_{(i)} + Baseflow_{(i)} \quad \text{(Eq. 5)}$$

$Stream_{(i)}$ is the post-processed portion of the BCM water-balance that is compared to the pattern and amount of gaged streamflow. The amount partitioned to the regional aquifer is the residual water in the shallow storage zone, minus carryover ($GW_{stor(i)}$) to the next month,

$$GW_{deep(i)} = GW_{shallow(i)} - GW_{stor(i)} - Baseflow_{(i),} \quad \text{(Eq. 6)}$$

which is equivalent to (*1-Rchscaler*) + $Baseflow_{(i)}$. Together these equations represent a conceptual routing scheme. It is not based on extensive system properties, nor is it a formal mass balance; however, it is an aggregate mass-balance check for all time-steps in the water-balance period (Eq. 7).

$$\sum BCM_{run} + \sum BCM_{rch} - \sum Discharge - \sum GW_{deep} = 0 \quad \text{(Eq. 7)}$$

The mass-balance, aggregated for all time steps, is checked (see Eq. 7). In practice, *Runscaler* is estimated to visually match measured streamflow peaks, and *exp* is adjusted to preserve the mass balance described in Eq. 7. The parameter *Rchscaler* is then used to match measured streamflow. Bedrock permeability, which is initially assigned on the basis of geology, is also iteratively adjusted to improve the match between gaged streamflow and the basin discharge, $Stream_{(i)}$, and the mass balance.

BCM_{rch} and BCM_{run} reflect natural hydrologic conditions and do not account for diversions, reservoir storage or releases, urban runoff, groundwater pumping, or other impairments, and therefore will not exactly match measured streamflow in impaired basins.

Generally, regions with low summer flows in more arid environments have low baseflow exponents, *exp*; whereas, regions with a large groundwater component, such as the volcanics in the upper Klamath basin, will have a large *exp*. The multiplier used to reduce the recharge component that makes it to the streamgage, *Rchscaler* (Eq. 4), is generally very low in desert areas with deep unsaturated zones and high in large basins with high baseflows. This allows for deep groundwater flow, GW_{deep}, to be calculated as in Equation 6, for application to groundwater flow models.

For comparison to the calibration basins, and to evaluate model performance representing the state, 71 additional validation basins were identified for the calculation of discharge on the basis of general lack of impairments, as well as statewide coverage of landscapes and geology. Hydrologic results for these basins were developed on the basis of the calibration to bedrock permeability performed using the calibration basins. The calibrations and validation basins are distributed across the range of elevation, aridity (calculated as average annual precipitation divided by PET), and bedrock permeability, in comparison to all basins in California (Figure 4, left panels), and we also show the relationship between them for the same three environmental conditions (Figure 4, right panels). Study basins generally cover the range of elevations for the state (Figure 4). Bedrock permeability as a representation of geology is dominated by lower permeability basins because very high permeability basins, such as those with alluvial valley fill, do not generate streamflow (Figure 4).

The range of climates in the state, represented by the UNESCO Arid Zone Research program aridity categories (precipitation divided by PET; UNEP 1997), is covered less well by the study basins and neglects the hyper-arid and arid locations due to lack of streamflow data (Figure 4). The representation of study basins within the ecoregions in the state also reflects the lack of streamgage data in the desert areas, as well as in the eastern side of the Sierra Nevada, and in the deep soils of the Central Valley (Great Valley), where any gaged streams are very impaired.

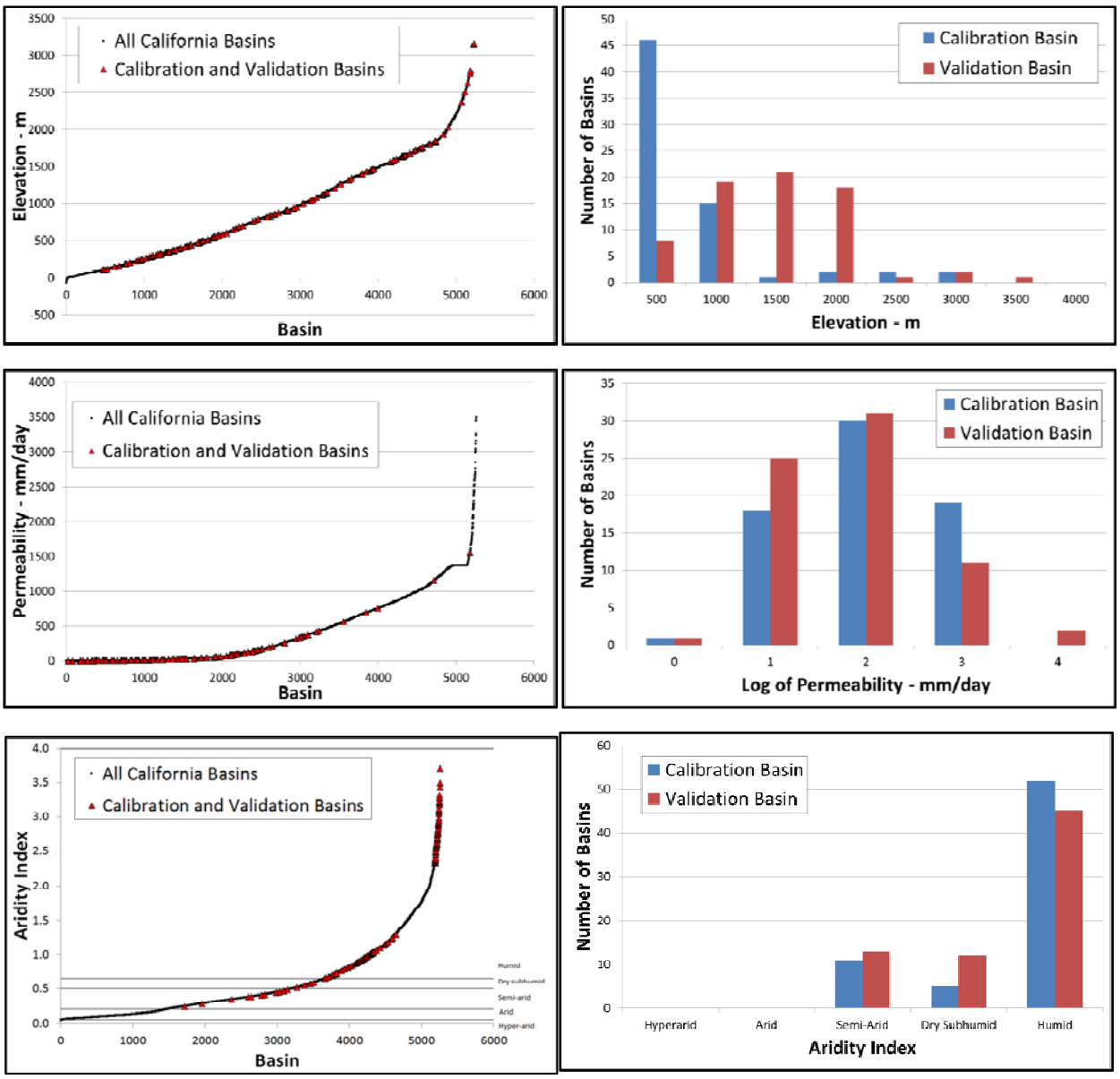

Figure 4: Plots on the Left Show All 5128 Watersheds in California (black) and Study Basins (red) Illustrating the Range of Representation by Study Basins for Elevation, Bedrock Permeability, and Aridity. Plots on the right show the distribution of Calibration and Validation gages for the same.

Example calibrations are shown for Dry Creek near Cloverdale in the Russian River basin, the Napa River near Calistoga in the North Bay Counties, and Big Creek above Pine Flat Reservoir near Trimmer, in the Kings River basin in the southern Sierra Nevada (Figure 5). All three have moderate baseflows, but Dry Creek loses 40 percent of both the calculated runoff and recharge to the groundwater system, the Napa River loses none of the runoff and 30 percent of the recharge to the groundwater system, and Big Creek, located in granitic geology toward the lower elevations of the Kings River basin, loses nothing to the groundwater system (Appendix C). Also shown are calibrations for two locations considered impaired: Aptos Creek at Aptos, California, and Sprague River, near Beatty, Oregon.

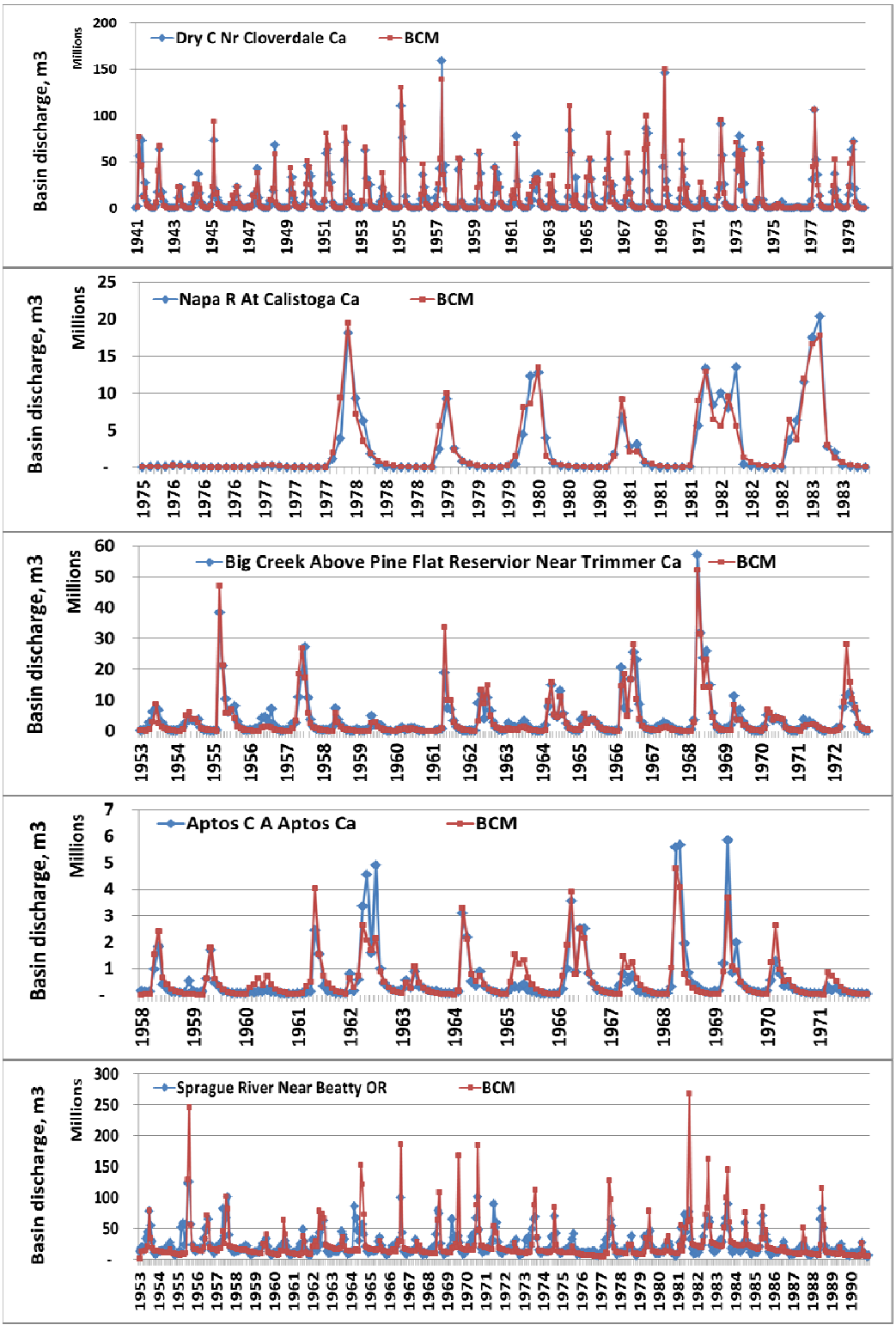

Figure 5: Calibration Time Series Comparing Measured and Estimated Basin Discharge in Millions of Cubic Meters, for Five Calibration Basins: (a) Dry Creek near Cloverdale, California, (b) Napa River at Calistoga, California, (c) Big Creek above Pine Flat Reservoir near Trimmer, California, (d) Aptos Creek at Aptos, California, and (e) Sprague River near Beatty, Oregon.

Calibration statistics are shown in Appendix C and spatially in Figure 6, with the linear regression r^2 for monthly and yearly comparison of measured and simulated basin discharge, and the Nash-Sutcliffe efficiency statistic (NSS; Nash and Sutcliffe 1970) calculated as 1 minus the ratio of the mean square error to the variance. The NSS is widely used to evaluate the performance of hydrologic models, generally being sensitive to differences in the observed and modeled simulated means and variances, but is overly sensitive to extreme values, similarly to r^2 (Legates and McCabe 1999). The NSS ranges from negative infinity to 1, with higher values indicating better agreement. Average calibration statistics for all basins are NSS = 0.65, monthly $r^2 = 0.70$, and yearly $r^2 = 0.86$.

In our study, calibration basins have a mean NSS of 0.71 (standard deviation 0.18), with the higher values for the Russian River basin, just north of the San Francisco Bay Area, and lower values for the Santa Cruz basins, just south of the Bay Area, where there are many urban impacts (Figure 6 top; Appendix C). There are several cases where urbanization and agriculture were identified as factors resulting in the inability to calculate a mass balance. The measured streamflow at Aptos Creek at Aptos (Figure 5d) had very high peaks that were not reproduced by the BCM. This basin is dominated by urbanization, suggesting that the high peak flows were a result of urban landscapes enhancing runoff, both during precipitation events where there is reduced infiltration and during the summer when urban runoff is enhanced—neither of which is taken into account in the BCM. In order to match measured volumes and streamflow patterns, the runoff is reduced by 80 percent, and the recharge is reduced by 50 percent. An example of diversions and groundwater pumping for public use can be seen in the difference between the Merced River at Happy Isles, upstream of Yosemite Village, and the Merced River at Pohono, downstream of Yosemite Village, where the percentage of runoff is reduced to 45 percent to match measured flows (Appendix C).

The basin discharge for the validation basins, not used for calibration, was developed using the adjusted bedrock permeability values developed during calibration. The mean NSS for these basins is 0.61 (standard deviation 0.20), with the upper Klamath and small basins in the Modoc Plateau volcanics performing the poorest (Figure 6a). This is likely due to the large groundwater reservoir in the volcanics that has very long travel times from precipitation input to outflow in streams. An example of a calibration in the volcanics for the Sprague River basin illustrates the large baseflow component with high baseflow exponent (Figure 5e). The Sprague River basin also has a large agricultural component and return flows, so the attempt to maintain a match in volumes results in an overestimate of the peak flows. The presence of a groundwater reservoir also shows in the differences between the r^2 values for the monthly and yearly values (Figures 6 left and 6 right), which identifies lags in the monthly calibration between measured and simulated discharge that are negated when calculated yearly. There is a large difference for the Kings River above the North Fork near Trimmer, for example, indicating the potential for a lag in groundwater flows becoming baseflows that appear at the base of the basin and not being accounted for in a monthly model; whereas, the yearly r^2 is very high. The basins in the volcanics consistently show a larger range in the two r^2 values, which is also illustrated in the Sprague River near the Beatty, Oregon, calibration (Figure 5e) by the mismatch in the timing of the peaks.

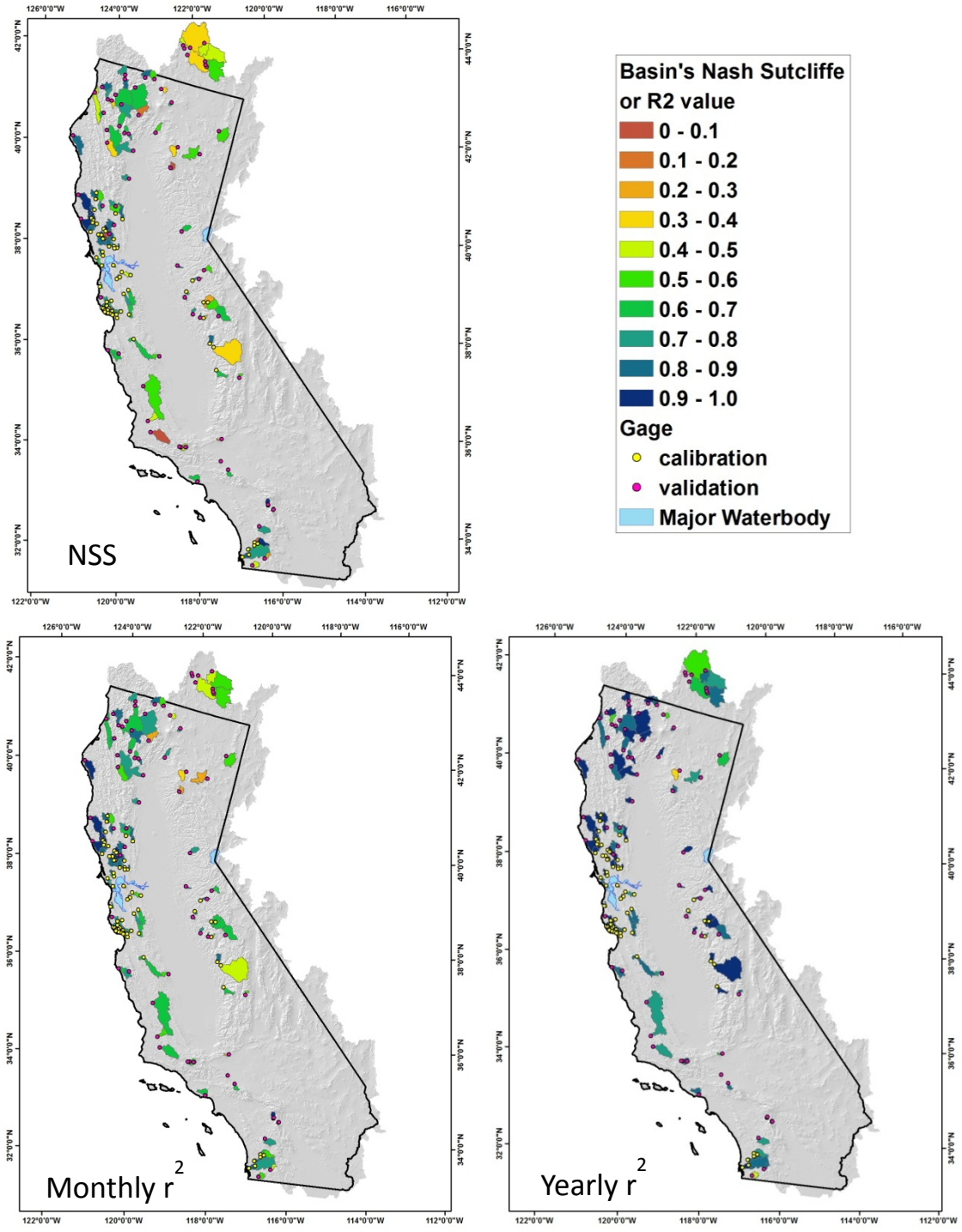

Figure 6: Map of Study Basins Illustrating the Spatial Distribution of the Calibration Statistics for the (top) Nash-Sutcliffe Efficiency Statistic, (left) Monthly r^2, and (right) Yearly r^2

2.3.4 Post Processing: 30-year and 10-year Summaries and Statistics

For California, we produced 270 m grids to represent historic and future climates from 1900 to 2100, resulting in 6,594,862 grid cells statewide, and a map for each of the 14 variables for each month. For the historic data and four future scenarios, this produced over 11 terabytes of data. We then created water year summaries of the 14 variables. The water year starts in October and ends in September. For the two temperature variables we averaged the temperature over the water year, and for the other 12 variables we summed all data for 12 months

Since retaining yearly values for this region results in unwieldy large files, we reduced the data size for distribution and analysis to 30-year summaries, providing monthly average values for variables historically for 1911–1940, 1941–1970, and 1971–2000. Future climate values are based on 100-year simulations, with 2010–2039, 2040–2069, and 2070–2099 time slices produced. We also developed summaries for 10-year periods based on time slices starting with 1911–1920 and running through 2090-2099. Appendix D has a list of all available variables, file size, format, and acronym.

We wrote a program to summarize the 30-year datasets by various statistical measures, to create a manageable dataset for analysis of long-term trends. We calculated these statistics for both annual (water year) and monthly average values. Statistics were developed for each 30-year time period by applying a linear regression model to the input rasters, which produced the seven statistics (average, standard deviation, coefficient of variation, variance, coefficient of determination, slope, and intercept) for each variable for each 30-year time period. The linear regression model used equations from Zar (1999). Change over the historical baseline period 1971–2000 was described as the slope of the regression model multiplied by 30 years.

To test the statistical significance of change between two time slices, t-values were calculated on a per grid cell basis. This was computed as:

$$t = \frac{\bar{X}_2 - \bar{X}_1}{\sqrt{\frac{var_2}{n_2} + \frac{var_1}{n_1}}} \quad \text{(Eq. 8)}$$

Where $\bar{X}$ the 30-year mean and var is the 30-year variance (both outputs from the linear regression model explained above). The n variable was set to 30 since both time periods were 30 years in length. The subscripts represent the different time periods, "1" is used for the base and "2" is used for the future. Therefore, for historical change analyses 1 was 1911–1940 and 2 was 1971-2000; for future change analyses 1 was 1971–2000 and 2 was 2070–2099. Once the t-value was determined, 2.045 was used as the threshold for determining if the change was statistically significant or not. This threshold reflects a 95 percent confidence interval using 29 degrees of freedom.

The development of the PRISM climate data itself is not corrected for new or terminated stations or changes in measurement methods over time, which can lead to artifacts in spatial maps of long-term changes, as well as in temporal changes in areal averages. This analysis is intended to indicate large-scale, general patterns of change over the study area, which is

appropriate for using PRISM, not to calculate statistical significance. Therefore, general direction and magnitude of change within ecoregions, for example, is the appropriate use of the data.

Sector 3: Results

3.1 BCM Climate and Hydrology Results

We characterized the variables calculated by the BCM for watersheds and for ecoregions, and compared historical summaries and patterns to future projections. We report three analyses: (1) trends in the time slice characterizing the baseline time period (1971–2000); (2) the calibration and validation of basin discharge by comparing post-processed runoff and recharge measures to derive discharge, and comparing that value to streamgage measurements; and (3) a comparison of the historical and future conditions for BCM variables—precipitation, potential evapotranspiration, runoff, recharge, and climatic water deficit. We present the map-based assessments, using the difference in magnitude (absolute value) for each variable; the number of standard deviations by which projected future conditions will differ from the standard deviation of baseline conditions; and the geographic variations across California of both historical and future projections. Temperature values are available, but for brevity, and because temperature has previously been more widely reported, this paper focuses on hydrological components.

3.1.1 Patterns in Baseline 30-year Climate and Hydrology

The process used to estimate hydrologic impacts of climate change at fine scales involved downscaling climate data for model input. Pre-processing included development of PET estimates from the downscaled air temperature. The BCM then generated outputs as a series of hydrologic and associated variables. This section discusses: precipitation, air temperature, PET, snowpack, runoff, recharge, and climatic water deficit.

During the 30-year baseline period of 1971–2000, precipitation generally increased, with the exception of the deserts and eastern Sierra Nevada (Table 1). Largest percentage increases are in the Great Valley, Central Western California, and Sierra Nevada. Both minimum and maximum air temperatures increased for all ecoregions, ranging from 0.5°C to 1.6°C (0.9°F to 2.9°F) for minimum air temperature and much less of an increase for maximum air temperature (Table 1). Potential evapotranspiration increased throughout the state by about 3 percent. Recharge decreased by up to 24 percent in southwestern California, and by 11 percent in northwestern California, while all other ecoregions increased in recharge. Recharge in the Mojave Desert increased by 51 percent (an increase of 1.4 millimeters per year [mm/yr]), and in the Modoc Plateau by 42 percent (an increase of 18.2 mm/yr) (Table 1).

The change in climate over the 30-year period is exemplified by the changes in snowpack in California, which integrates effects of precipitation and air temperature on the dominant water resource in California for water supply. The snowpack in this region is the warmest in the western United States (Lundquist et al. 2004) and is the most sensitive to small changes in air temperature. This is illustrated by the change in April 1 snowpack (Figure 7), where snowpack

has diminished the most in extent in the northern portions of the state; whereas, the highest elevation snowpack in the southern Sierra Nevada mountains and Mount Shasta have actually increased in some locations. However, the dominant loss of April 1 snowpack results in less runoff to extend surface water resources throughout the summer season. This situation has implications for recharge and climatic water deficit as well.

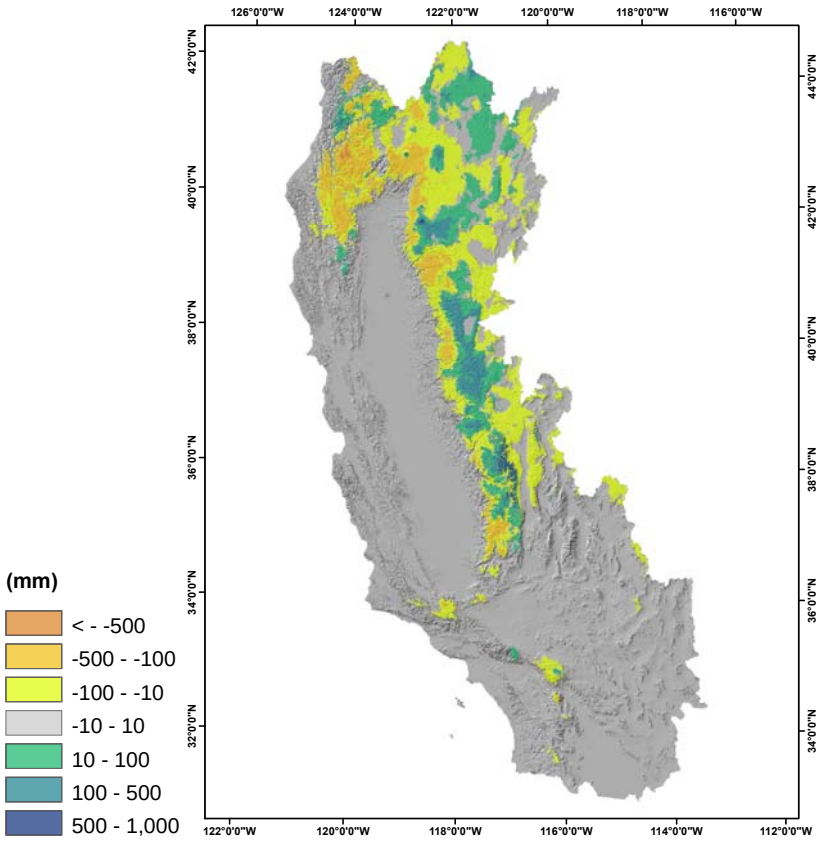

Figure 7: Map of Change in April 1 Snowpack, Calculated as Snow Water Equivalent, for 1971–2000

Corresponding to increases in precipitation, runoff increased over the baseline period in most locations in the state, notably the northern Sierra Nevada Mountains and parts of the Trinity Mountains in the northwestern ecoregion (Table 1; Figure 8). Some declines are noted in the northwest, where the smallest change in precipitation occurred. Decreases in recharge are notable in the northwest portions of the state, with moderate decreases in the Sierra Nevada foothills and southern California mountains (Figure 8). Generally locations with little to no recharge, such as areas with deep soils or arid climate, also had little to no change in recharge indicated. Some increases in recharge are indicated in the northeast and in parts of the high Sierra. Detailed views of basins in the Russian River watershed (north of San Francisco Bay) and Santa Cruz mountains (south of San Francisco Bay) are shown in Flint and Flint (in review), illustrating the dominance of runoff in the Russian River watershed, where water supply relies heavily on reservoirs, in contrast to the reliance on groundwater resources and recharge in the Santa Cruz mountains.

Table 1: Climate and Hydrologic Variables for Modified Jepson Ecoregions in California. Mean value and change for 1971–2000.

	Ecoregion	Northwestern CA	Cascade Ranges	Modoc Plateau	Central Western CA	Great Valley	Sierra Nevada	East of Sierra Nevada	Southwestern CA	Mojave Desert	Sonoran Desert
Precipitation (mm)	mean	1,450	1,132	442	559	346	947	320	481	162	116
	change	38	142	54	121	83	143	-1	32	-2	-5
	% change	3%	13%	12%	22%	24%	15%	0%	7%	-1%	-5%
Minimum Air Temperature (C)	mean	5.4	2.5	0.5	7.3	9.2	2.9	0.1	8.7	10.4	14.2
	change	0.5	1.2	0.8	1.0	1.2	1.4	1.4	1.3	1.6	1.1
Maximum Air Temperature (C)	mean	18.9	17.1	15.5	21.9	24.2	16.9	16.2	22.8	25.2	29.9
	change	0.8	0.7	0.2	0.7	0.6	0.8	1.4	1.0	1.2	1.2
Potential Evapotranspir-ation (mm)	mean	1,032	1,043	1,025	1,267	1,353	1,151	1,164	1,373	1,464	1,511
	change	20	39	20	37	35	49	69	54	63	46
	% change	2%	4%	2%	3%	3%	4%	6%	4%	4%	3%
Recharge (mm)	mean	457.7	351.4	43.4	65.3	11.1	215.9	47.0	39.5	2.8	1.0
	change	-51.3	28.7	18.2	2.5	2.3	12.5	3.1	-9.6	1.4	0.1
	% change	-11%	8%	42%	4%	21%	6%	7%	-24%	51%	8%
Runoff (mm)	mean	476.6	277.0	40.5	97.8	6.0	300.2	46.6	69.8	1.3	1.8
	change	52.8	84.5	18.3	73.2	7.4	97.6	3.5	25.9	0.9	0.9
	% change	11%	30%	45%	75%	124%	32%	8%	37%	73%	53%
Climatic Water Deficit (mm)	mean	489	425	544	868	1,016	557	743	985	1,290	1,344
	change	-4	25	16	-8	-42	30	93	45	75	48
	% change	-1%	6%	3%	-1%	-4%	5%	12%	5%	6%	4%

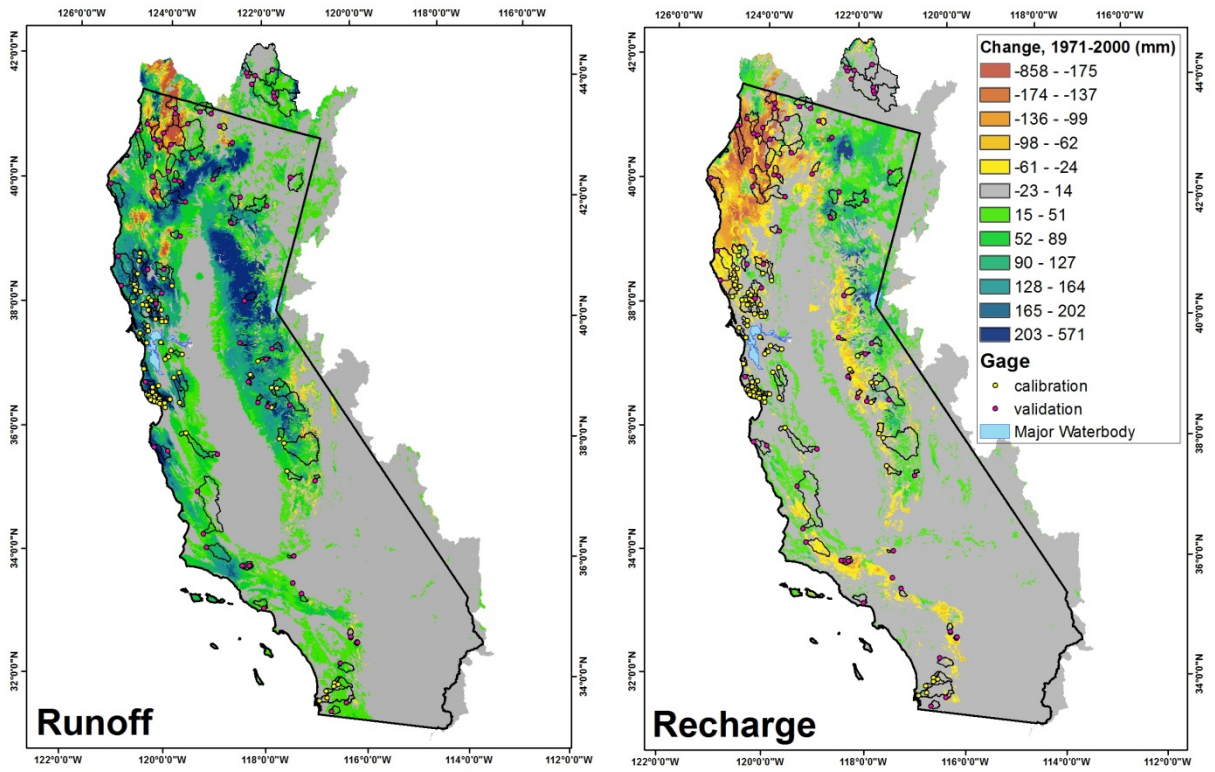

Figure 8: Maps of Change in Runoff and Recharge over the 1971–2000 Baseline Period, Binned as ½ Standard Deviation from the Mean, and Including Study Basins. The locations where increases have occurred in runoff or recharge are indicated by cool colors, greens and blues, and decreases by warm colors, yellows, and oranges.

Increases in runoff in snow-dominated regions, due to warming air temperatures, diminishes recharge, which is more likely to occur during the slow snowmelt season. This is confirmed for the northwestern ecoregion, where the Trinity Alps decreased in snowpack, and shows small increases for the Sierra Nevada, in contrast to other regions (Figure 7).

Figure 9a shows the average annual climatic water deficit for 1971–2000. There is high climatic water deficit in the southern Central Valley and Mojave and Sonoran Deserts, and low climatic water deficit in the north coast and Sierra Nevada. Climatic water deficit declined (that is, it became wetter) over the baseline period in the central and northwestern California ecoregions and the Great Valley, while in all other regions, despite the increases in precipitation, climatic water deficit increased (Figure 9b). This variable integrates energy loading and moisture availability from precipitation with soil water holding capacity. The distribution of moisture conditions that generally define the amount of water in the soil that can be maintained for plant use throughout the growing season and summer dry season corresponds very well to the established distribution of vegetation types. However, in many locations, shallow soils limit the contribution of precipitation. The lowest climatic water deficits in California are in regions with snowpack that, as it melts in the springtime, provides a longer duration of available water, thus maintaining a lower annual climatic water deficit, even despite shallow soils. Locations in the south with higher PET have higher climatic water deficits.

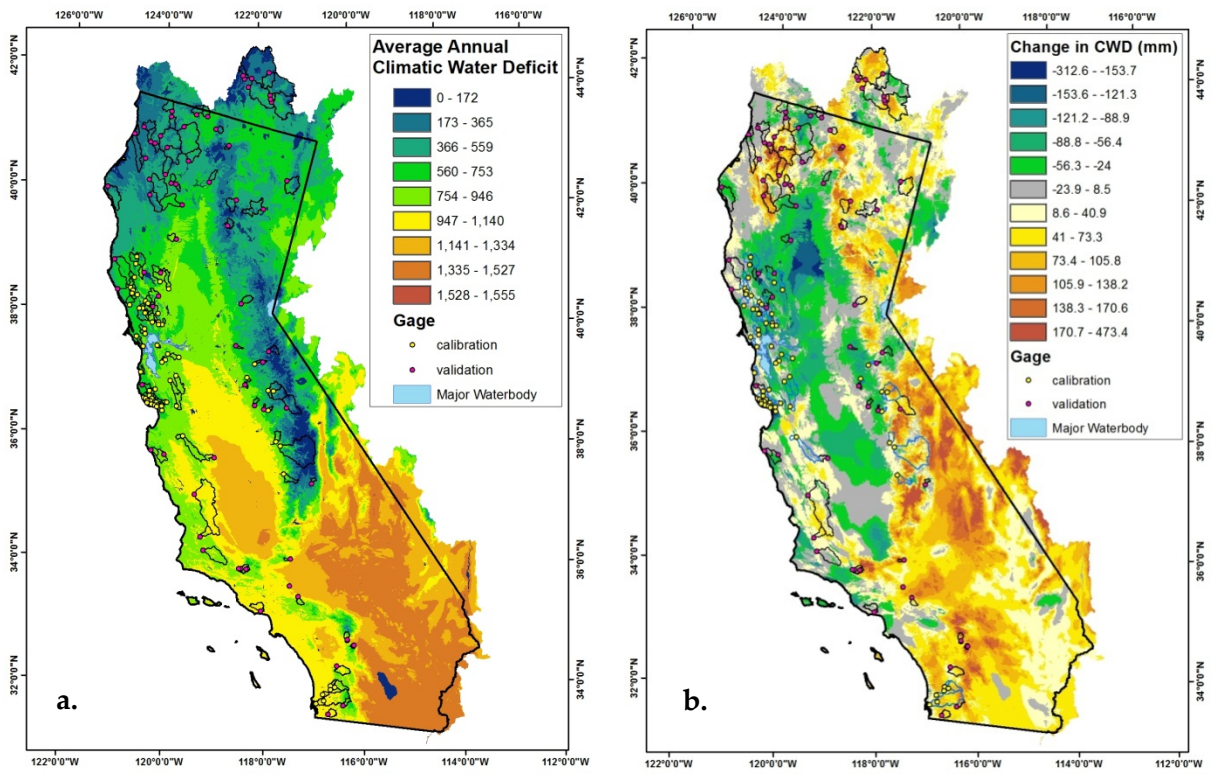

Figure 9: Maps of (a) Average Annual Climatic Water Deficit and (B) Change in Climatic Water Deficit over the 1971–2000 Period, Binned as ½ Standard Deviation from the Mean

Precipitation has increased in most locations, but has declined in the desert and eastern Sierra Nevada. Air temperature and PET have increased in all ecoregions (Table 1). This translates into increases in climatic water deficit in nearly all locations, and particularly those dominated by snowpack, such as the Sierra Nevada ecoregion and Trinity Mountains in the northwestern California ecoregion. The recorded increases in air temperature, particularly minimum air temperature, result in earlier snowmelt and reduce the ability of the snowpack to sustain the water available throughout the summer season. The deserts all increased in deficit with declining precipitation and increasing air temperature. However there are some small areas in the Great Valley ecoregion that experienced small decreases in deficit because of the ability of the deep soils to store the additional precipitation rather than result in recharge or runoff. Some moderating effects of coastal climatic conditions are seen in small valleys along the coast with decreases in deficit.

3.1.2 Historic to Future Climate and Hydrology

In the analysis of the impacts from historic (1911–1940) to future (2070–2099) climate on hydrology, we characterized the changes in precipitation, PET, runoff, recharge, and climatic water deficit from the BCM for watersheds and for ecoregions, and compared changes in variables from historical to baseline periods and from the baseline period to the end of the twenty-first century. Three types of map analyses were applied to this comparison:
(1) assessment of the difference in magnitude (absolute value) for each variable; (2) the number

of standard deviations of baseline conditions (defined as the 30-year time slice representing baseline time, 1971–2000) by which historic and projected future conditions differ; and (3) a geographic review of the variations in hydrologic conditions across California for both historical and future time periods.

A summary of variables by modified Jepson ecoregion (Table 2) and for the HUC 12 watersheds averaged for the extent of California (Appendix E) was calculated. Overall, mean precipitation increased by 80 millimeters (mm) between 1911–1940 and 1971–2000 (baseline, Appendix E). Under the PCM scenarios, precipitation continued to increase to 2070–2099 (36 to 66 mm), but it decreased under the GFDL scenario (-74 to -113 mm). Potential evapotranspiration increased 10 mm from historic to baseline time frames, and increased under all future time frames between 51 and 104 mm. Runoff increased historically 36 mm. It increased under future PCM projections by 51 to 77 mm, but decreased under GFDL projections by 38 to 42 mm. Finally, climate water deficit (CWD) decreased by 16 mm from historic to baseline time; however, it increased under all projections between 40 and 174 mm, indicating increases in PET and decreases in available soil moisture resulting in lower actual evapotranspiration.

3.1.2.1 Precipitation

While most of northern California got wetter from the historic to baseline time, only the northeast, an eastern area representing the high Sierra Nevada and Inyo/White mountains, and a few scattered watersheds saw an increase that was even one-half a standard deviation (SD) from the baseline SD for the 30-year mean, a pattern that is mostly repeated when looking at the statistically significant trends (Figure 10). This suggests that the trend in increased moisture is well within the baseline variability of precipitation from year to year. The same is true for the southern half of the region, which mostly shows a drying trend. As expected, given the GCMs selected, the PCM future scenarios forecast increased precipitation, and GFDL forecasts a drier future (Figure 11, Table 2). However, compared to baseline precipitation variability and statistically significant change, only the desert ecoregions receive more than 0.5 SD more precipitation under PCM, while under GFDL A2, the northern half of California loses precipitation mostly between 0.5 and 0.9 SD (Figures 12 and 13).

Table 2: Climate and Hydrologic Variables for Modified Jepson Ecoregions in California. Mean and standard deviation for 30-year time periods from 1911–2000 and 2070–2099.

		Historic (1911–1940)	Historic (1941–1970)	Current (1971–2000)	PCM B1 (2070–2099)	PCM A2 (2070–2099)	GFDL B1 (2070–2099)	GFDL A2 (2070–2099)
	Modified Jepson Ecoregions	mean / std	mean / std	mean / std	mean / std	mean / std	mean / std	mean / std
Precipitation	Cascade Ranges	967 / 426	1111 / 490	1132 / 494	1219 / 522	1158 / 493	978 / 397	925 / 406
	Central Western CA	496 / 170	519 / 196	559 / 196	607 / 213	604 / 204	463 / 155	448 / 151
	Mojave Desert	133 / 63	133 / 59	162 / 64	206 / 76	189 / 69	155 / 60	136 / 55
	Sonoran Desert	104 / 52	92 / 45	116 / 52	163 / 62	153 / 64	126 / 58	103 / 47
	Great Valley	302 / 122	315 / 137	346 / 139	383 / 148	382 / 148	293 / 113	276 / 103
	Modoc Plateau	366 / 153	428 / 176	442 / 178	478 / 197	450 / 178	413 / 172	373 / 163
	North Western CA	1258 / 539	1446 / 625	1450 / 598	1571 / 625	1475 / 573	1281 / 560	1197 / 528
	Sierra Nevada	832 / 356	919 / 417	947 / 424	1032 / 448	1016 / 431	816 / 364	763 / 336
	East of Sierra Nevada	281 / 236	297 / 221	320 / 231	359 / 249	345 / 246	282 / 202	256 / 189
	Southwestern CA	461 / 160	439 / 154	481 / 157	572 / 185	545 / 169	435 / 135	404 / 134
	California	511 / 467	561 / 541	586 / 534	649 / 566	622 / 535	518 / 467	481 / 442
Potential Evapotrans-piration	Cascade Ranges	1047 / 81	1035 / 83	1043 / 77	1093 / 75	1116 / 73	1099 / 73	1139 / 71
	Central Western CA	1246 / 69	1245 / 67	1267 / 67	1315 / 71	1343 / 73	1325 / 72	1370 / 76
	Mojave Desert	1448 / 78	1444 / 76	1464 / 77	1519 / 75	1547 / 74	1528 / 73	1578 / 71
	Sonoran Desert	1495 / 46	1491 / 51	1511 / 46	1555 / 43	1578 / 43	1563 / 43	1605 / 42
	Great Valley	1342 / 81	1337 / 82	1353 / 79	1397 / 81	1420 / 82	1403 / 81	1442 / 83
	Modoc Plateau	1019 / 57	1013 / 57	1025 / 55	1077 / 55	1102 / 55	1085 / 56	1128 / 58
	North Western CA	1025 / 107	1023 / 110	1032 / 108	1073 / 110	1095 / 111	1081 / 109	1119 / 110
	Sierra Nevada	1149 / 132	1138 / 134	1151 / 135	1210 / 131	1238 / 129	1215 / 130	1263 / 127
	East of Sierra Nevada	1162 / 118	1156 / 121	1164 / 128	1225 / 124	1256 / 123	1238 / 124	1296 / 122
	Southwestern CA	1352 / 63	1338 / 64	1373 / 66	1429 / 62	1458 / 62	1437 / 63	1486 / 62
	California	1241 / 194	1235 / 194	1251 / 198	1302 / 199	1328 / 199	1310 / 199	1355 / 200

Table 2: (continued)

		Historic (1911–1940)	Historic (1941–1970)	Current (1971–2000)	PCM B1 (2070–2099)	PCM A2 (2070–2099)	GFDL B1 (2070–2099)	GFDL A2 (2070–2099)
	Modified Jepson Ecoregions	mean / std	mean / std	mean / std	mean / std	mean / std	mean / std	mean / std
Runoff	Cascade Ranges	200 / 249	255 / 304	277 / 311	327 / 341	298 / 323	192 / 230	198 / 239
	Central Western CA	73 / 104	79 / 121	98 / 133	131 / 153	128 / 150	60 / 90	66 / 94
	Mojave Desert	1 / 7	1 / 6	1 / 7	4 / 13	2 / 8	1 / 5	1 / 5
	Sonoran Desert	2 / 9	1 / 5	2 / 9	4 / 16	4 / 18	2 / 11	2 / 10
	Great Valley	4 / 19	4 / 20	6 / 25	10 / 34	10 / 36	4 / 16	3 / 16
	Modoc Plateau	24 / 65	33 / 85	41 / 91	46 / 100	34 / 83	27 / 75	22 / 68
	North Western CA	354 / 392	459 / 474	477 / 456	581 / 477	516 / 441	383 / 404	368 / 379
	Sierra Nevada	240 / 244	281 / 292	300 / 297	346 / 315	342 / 309	212 / 226	200 / 214
	East of Sierra Nevada	42 / 117	42 / 108	47 / 122	51 / 128	48 / 123	31 / 91	25 / 76
	Southwestern CA	59 / 93	56 / 88	70 / 97	113 / 130	94 / 113	50 / 68	55 / 75
	California	102 / 222	125 / 271	134 / 274	164 / 305	150 / 284	100 / 223	96 / 212
Recharge	Cascade Ranges	294 / 243	367 / 291	351 / 274	352 / 269	330 / 254	269 / 218	246 / 207
	Central Western CA	56 / 60	59 / 71	65 / 70	66 / 66	69 / 66	42 / 50	46 / 51
	Mojave Desert	2 / 7	2 / 8	3 / 9	5 / 11	3 / 10	1 / 6	2 / 6
	Sonoran Desert	1 / 4	1 / 4	1 / 4	2 / 5	2 / 6	1 / 4	1 / 4
	Great Valley	8 / 27	9 / 31	11 / 34	13 / 37	14 / 38	6 / 21	7 / 22
	Modoc Plateau	29 / 60	38 / 77	43 / 82	46 / 88	37 / 74	31 / 68	25 / 59
	North Western CA	416 / 336	483 / 378	458 / 356	438 / 334	426 / 324	382 / 313	350 / 284
	Sierra Nevada	188 / 213	219 / 256	216 / 250	218 / 246	213 / 238	165 / 195	152 / 176
	East of Sierra Nevada	42 / 87	44 / 85	47 / 90	62 / 109	58 / 108	38 / 76	34 / 72
	Southwestern CA	39 / 48	37 / 46	40 / 46	40 / 42	43 / 44	28 / 31	27 / 29
	California	106 / 212	123 / 246	121 / 234	120 / 226	116 / 218	95 / 195	88 / 178

Table 2: (continued)

		Historic (1911–1940)	Historic (1941–1970)	Current (1971–2000)	PCM B1 (2070–2099)	PCM A2 (2070–2099)	GFDL B1 (2070–2099)	GFDL A2 (2070–2099)
	Modified Jepson Ecoregions	mean / std	mean / std	mean / std	mean / std	mean / std	mean / std	mean / std
Climatic	Cascade Ranges	459 / 200	427 / 202	425 / 196	490 / 185	541 / 181	523 / 184	626 / 182
Water	Central Western CA	878 / 133	861 / 140	868 / 136	904 / 142	935 / 143	960 / 140	1032 / 141
Deficit	Mojave Desert	1299 / 150	1296 / 150	1290 / 153	1314 / 148	1356 / 145	1364 / 145	1437 / 140
	Sonoran Desert	1341 / 268	1348 / 270	1344 / 268	1346 / 268	1378 / 273	1386 / 275	1450 / 284
	Great Valley	1050 / 191	1030 / 205	1016 / 201	1034 / 210	1058 / 210	1112 / 188	1172 / 182
	Modoc Plateau	576 / 197	530 / 198	544 / 194	619 / 202	665 / 195	657 / 198	756 / 201
	North Western CA	509 / 192	486 / 193	489 / 192	512 / 201	559 / 196	553 / 196	633 / 197
	Sierra Nevada	574 / 296	551 / 290	557 / 294	631 / 270	683 / 256	670 / 271	775 / 255
	East of Sierra Nevada	762 / 319	751 / 309	743 / 319	830 / 313	888 / 302	886 / 307	994 / 292
	Southwestern CA	972 / 142	973 / 142	986 / 136	1003 / 132	1042 / 126	1071 / 135	1156 / 132
	California	869 / 381	852 / 391	853 / 387	892 / 372	934 / 365	942 / 375	1025 / 363

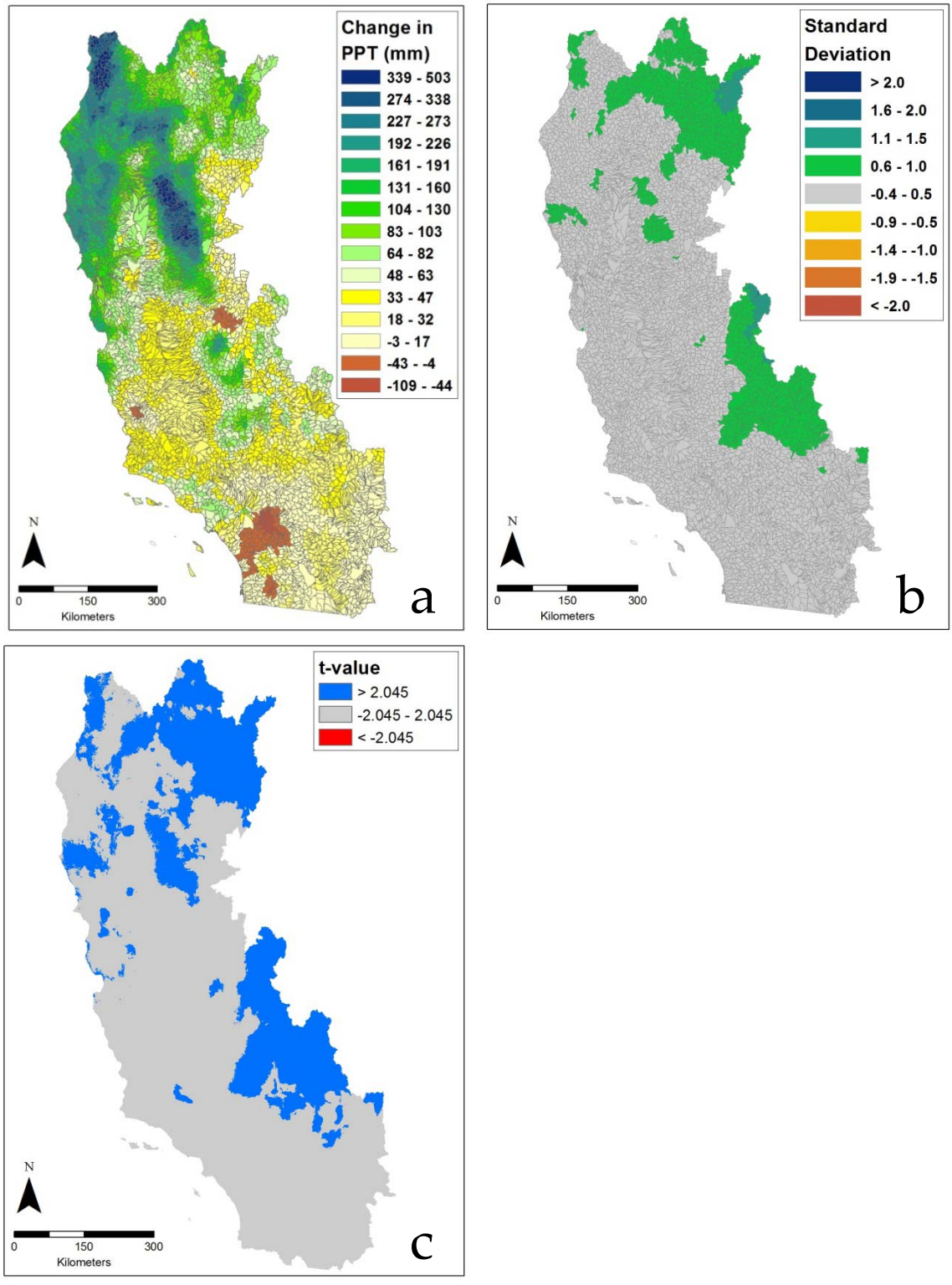

Figure 10: The Difference in Annual Precipitation for HUC 12 Watersheds between 1911–1940 and 1971–2000 (a), Normalized to the Standard Deviation over the 1971–2000 Period (b), and Statistically Significant Areas of Change, as Measured Using a T Test at α = .05 Significance Level (c)

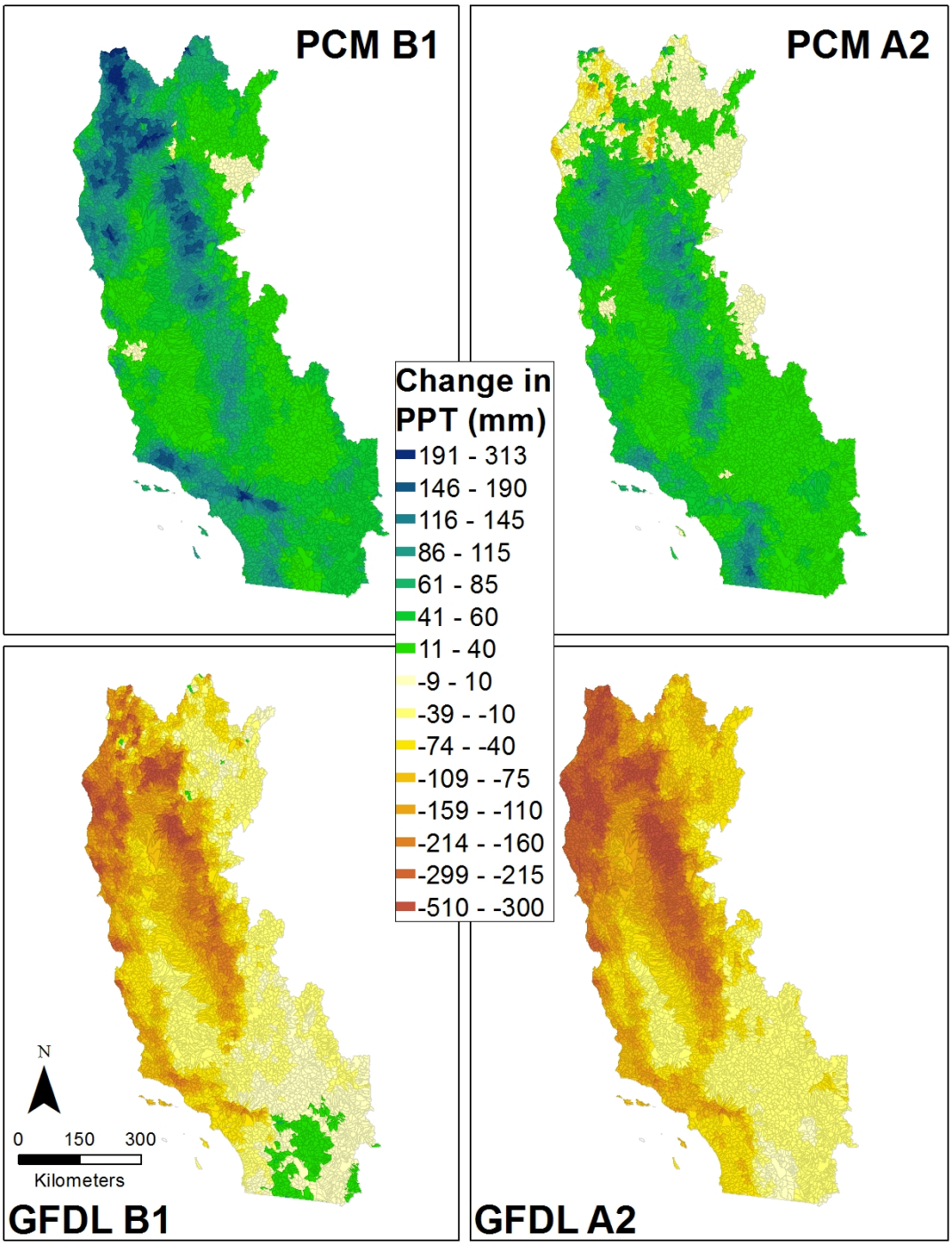

Figure 11: Difference in Annual Precipitation (PPT) for HUC 12 Watersheds between Future (2071–2100) and Baseline (1971–2000) for the GFDL and PCM A2 and B1 Scenarios

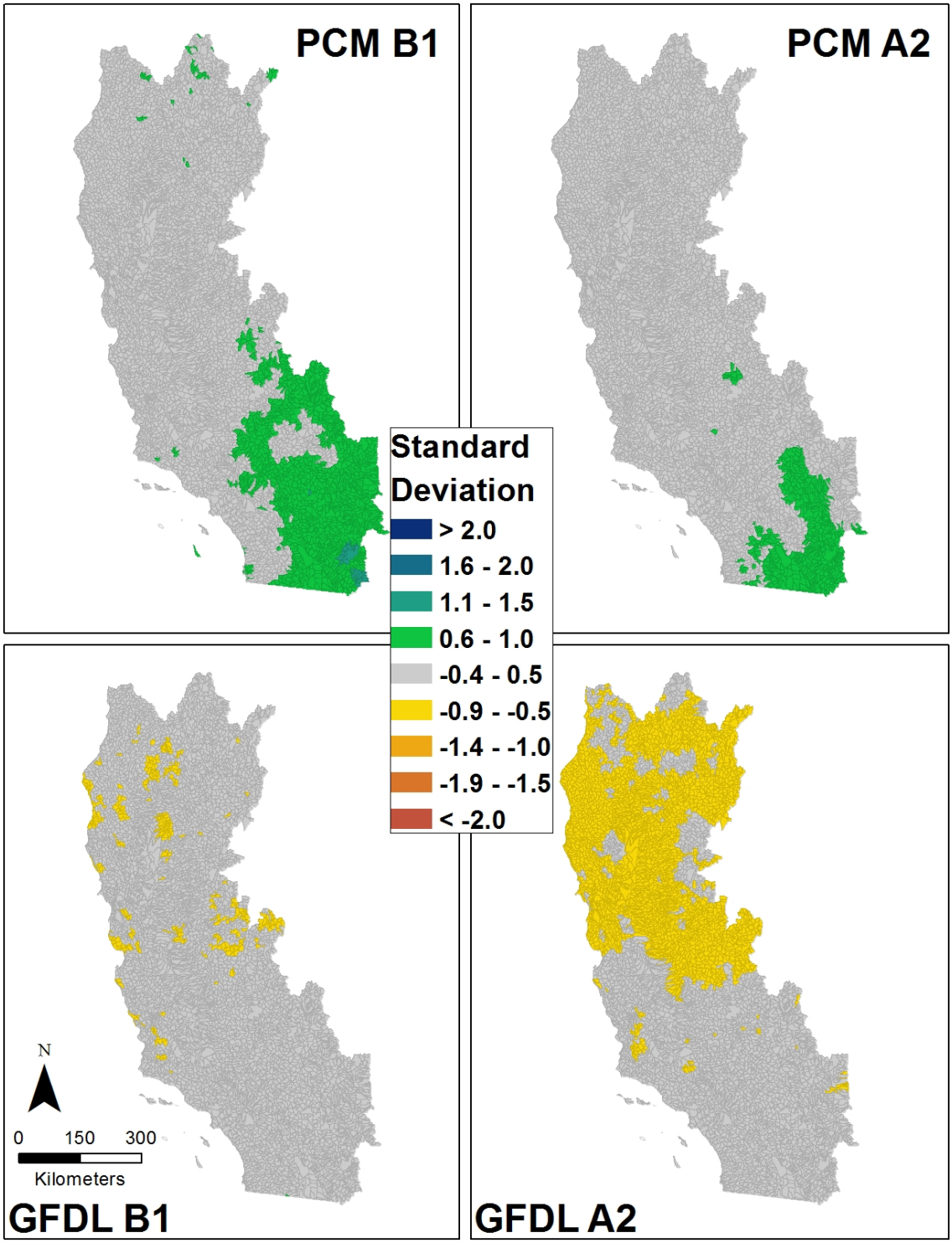

Figure 12: The Difference in Precipitation for HUC 12 Watersheds between Future (2071–2100) and Baseline (1971–2000), Normalized to the Standard Deviation over the Period 1971–2000

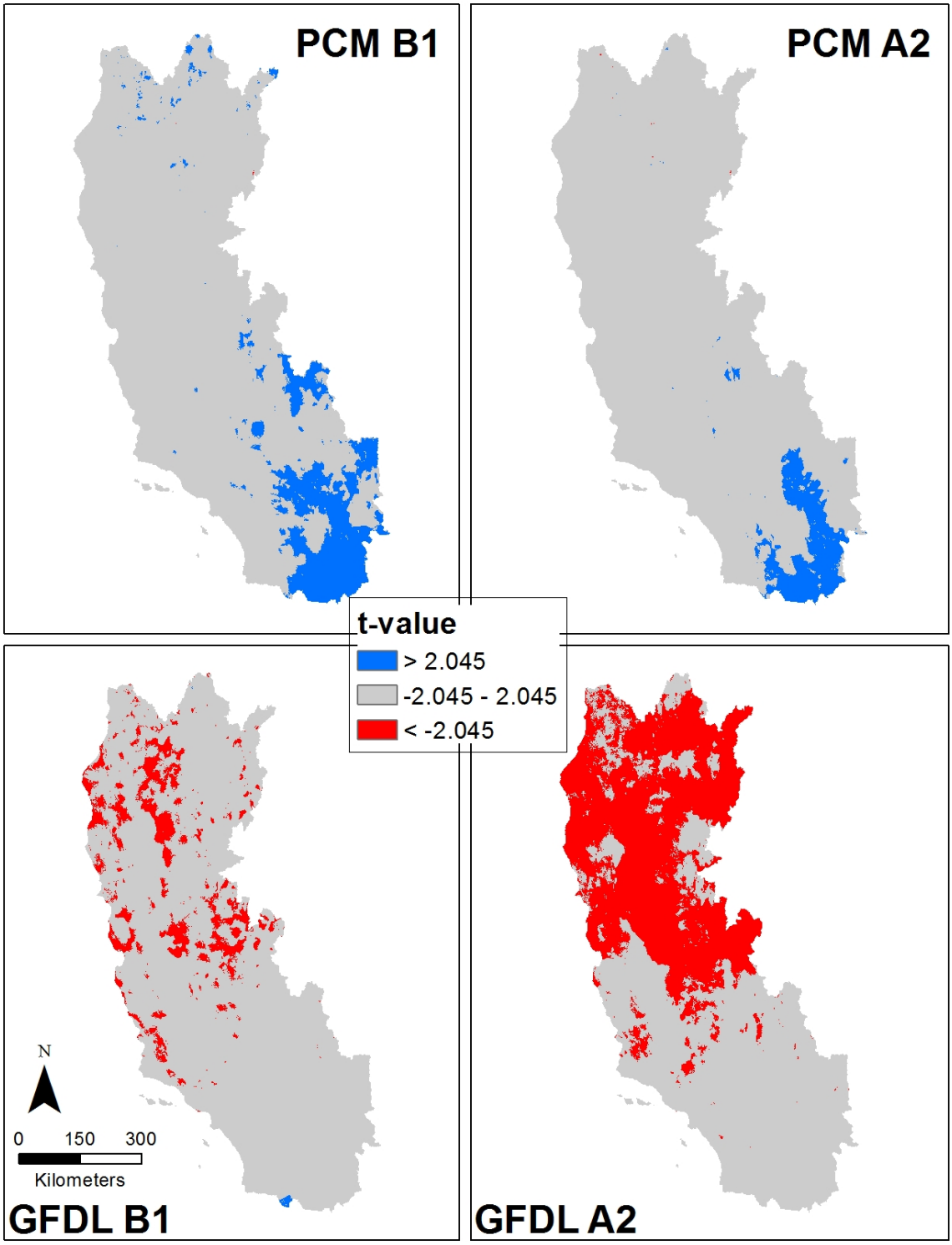

Figure 13: Statistically Significant Areas of Precipitation change between Future (2071–2100) and Baseline (1971–2000), as Measured Using a T Test at α = .05 Significance Level

3.1.2.2 Potential Evapotranspiration

The calculation of PET using the Priestley-Taylor equation assumes that PET is a function of, and is non-linearly related to, air temperature. The application of PET in the BCM assumes that plants are in equilibrium with their environment and will transpire at maximum rates until the soil reaches the wilting point. Potential evapotranspiration increased from historical to baseline time periods in most of California, with the exception of a few places in the Sierra Nevada, where it decreased between 0.5 and > 2 SD of baseline PET values, with similar patterns in the significance values (Figure 14). The extreme change in these locations is due to cooling air temperature, but because PET is already low in these locations, due to the non-linear relation between PET and air temperature, the change is greater than if the PET were initially high. Potential evapotranspiration is projected to increase under all scenarios and for all ecoregions (Figure 15, Table 2) and shows one of the strongest spatial patterns of all the variables, with nearly the entire region increasing by at least 1 SD, and statistically significant under the PCM projections, and by > 2 SD under the GFDL projections (Figures 16 and 17).

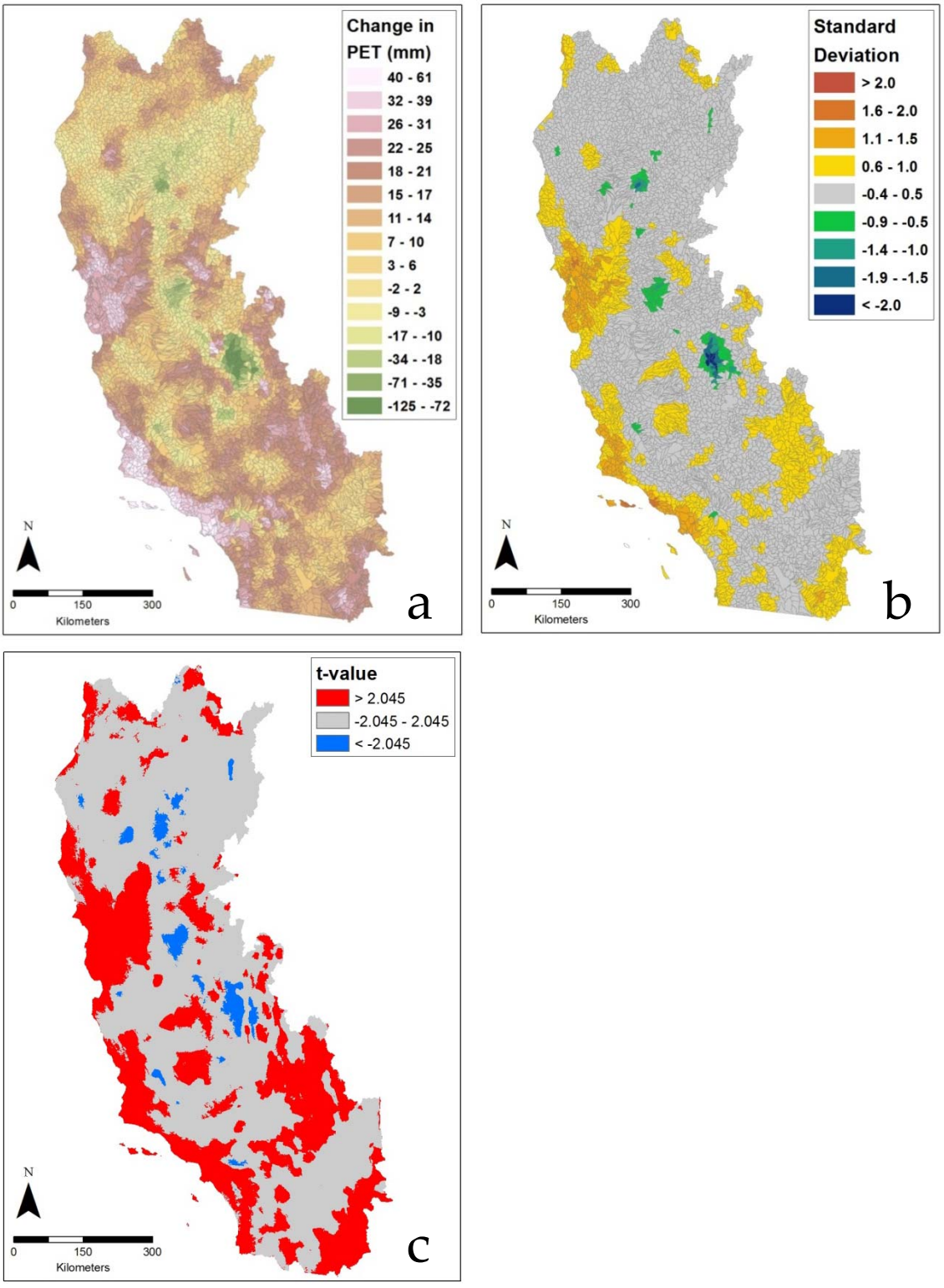

Figure 14: The Difference in Annual Potential Evapotranspiration (PET) for HUC 12 Watersheds between 1911–1940 and 1971–2000 (a), Normalized to the Standard Deviation over the 1971–2000 Period (b), and Statistically Significant Areas of Change, as Measured Using a T Test at α = .05 Significance Level (c)

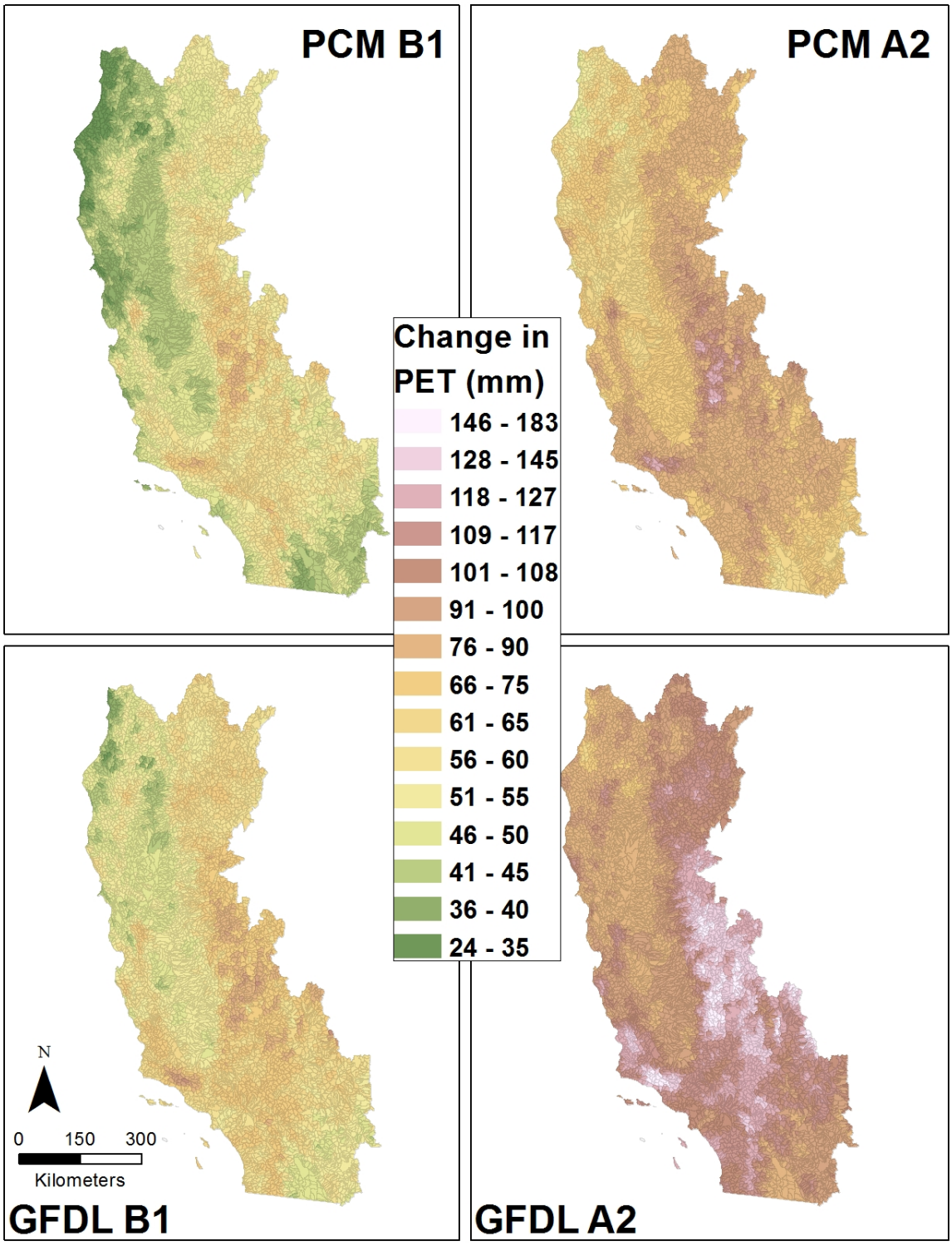

Figure 15: The Difference in Annual Potential Evapotranspiration (PET) for HUC 12 Watersheds between Future (2071–2100) and Baseline (1971–2000) for GFDL and PCM A2 and B1 Scenarios

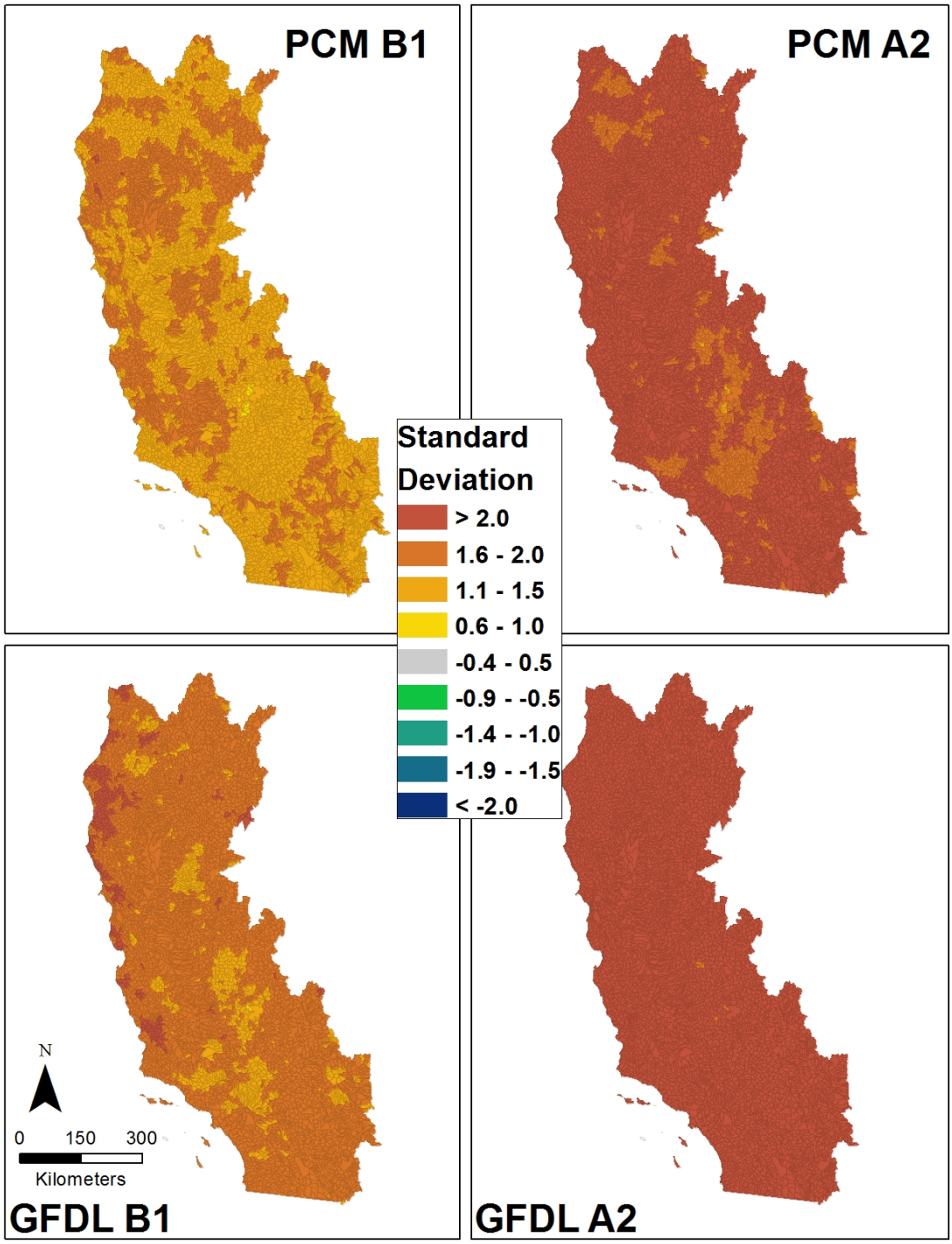

Figure 16: The Difference in Potential Evapotranspiration for HUC 12 Watersheds between Future (2071–2100) and Baseline (1971–2000) Normalized to the Standard Deviation over the 1971–2000 Period for GFDL and PCM A2 and B1 Scenarios

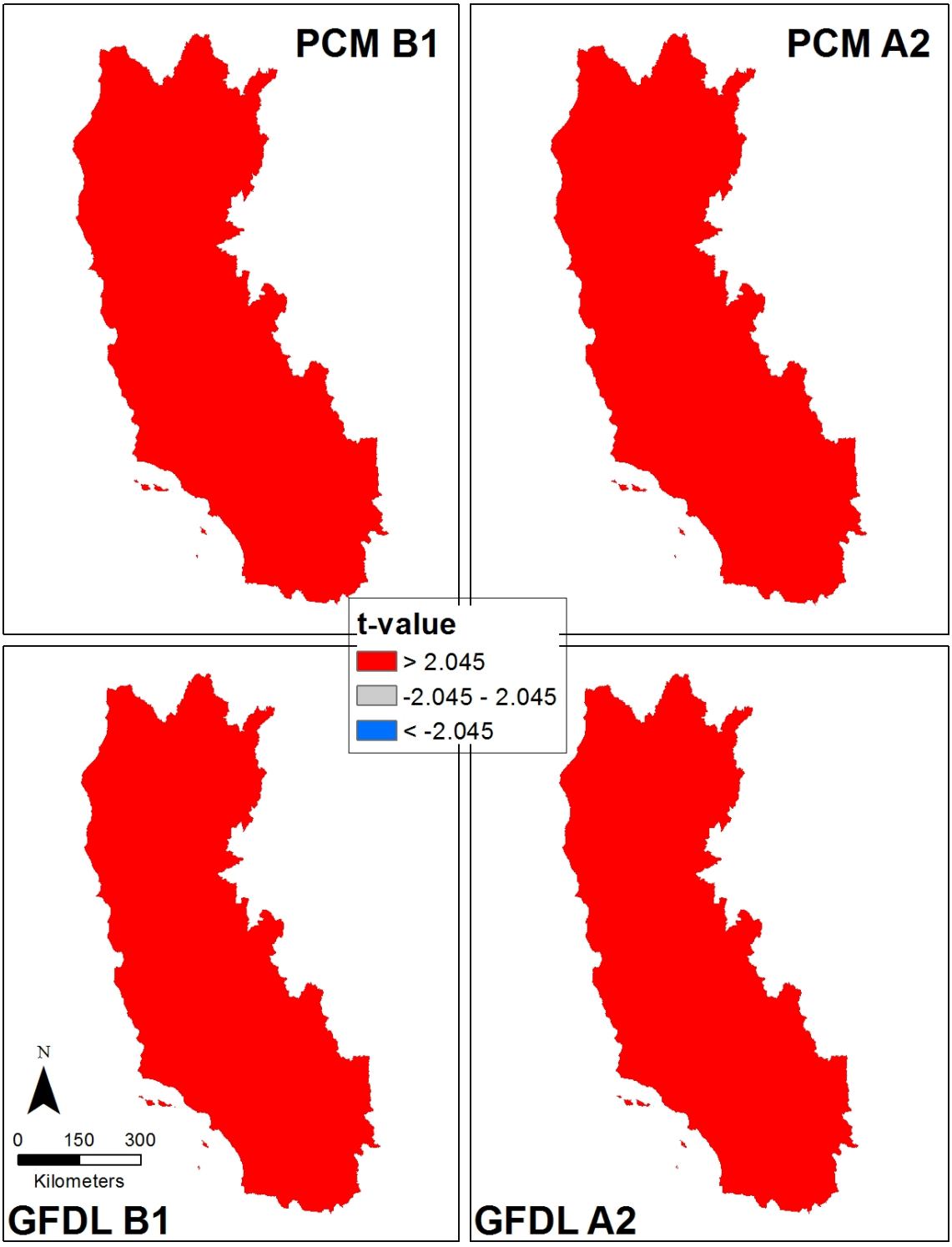

Figure 17: Statistically Significant Areas of Potential Evapotranspiration change between Future (2071–2100) and Baseline (1971–2000), as Measured Using a T Test at α = .05 Significance Level

3.1.2.3 Runoff

Annual runoff values increased slightly in California between 1911–1940 and 1971–2000 (Figure 18), a change driven by increases throughout the northwest ecoregion, and in the northern Sierra Nevada. Looking at this difference relative to the standard deviation during the baseline time period, none of the watersheds had runoff increase by more than one standard deviation, but a few (40) in the desert ecoregions decreased by more than one. This is because the annual runoff in these watersheds was less than 3 mm in 1911–1940 and less than 1 mm in 1971–2000. Comparing the baseline conditions to future scenarios (2070–2099), the PCM model shows an increase in runoff for all ecoregions except the Modoc Plateau (Table 2), and especially in the Sierra Nevada and the coast ranges, while the GFDL model shows an almost inverse pattern of drying (Figure 19). Because of the very low runoff values in the baseline time period, the incremental increases in the desert regions of the study show future runoff to be above 1 SD (and in many places above 2 SD) under the PCM model. For the GFDL model, parts of the Sierra Nevada and the northeast region of the state show decreases in runoff above 0.5 SD of baseline (Figures 20). Note that statistically significant change differs from the SD view under the future scenarios, particularly in the desert systems, where much of the change while high in terms of standard deviations is not significant at the 0.05 level (Figure 21).

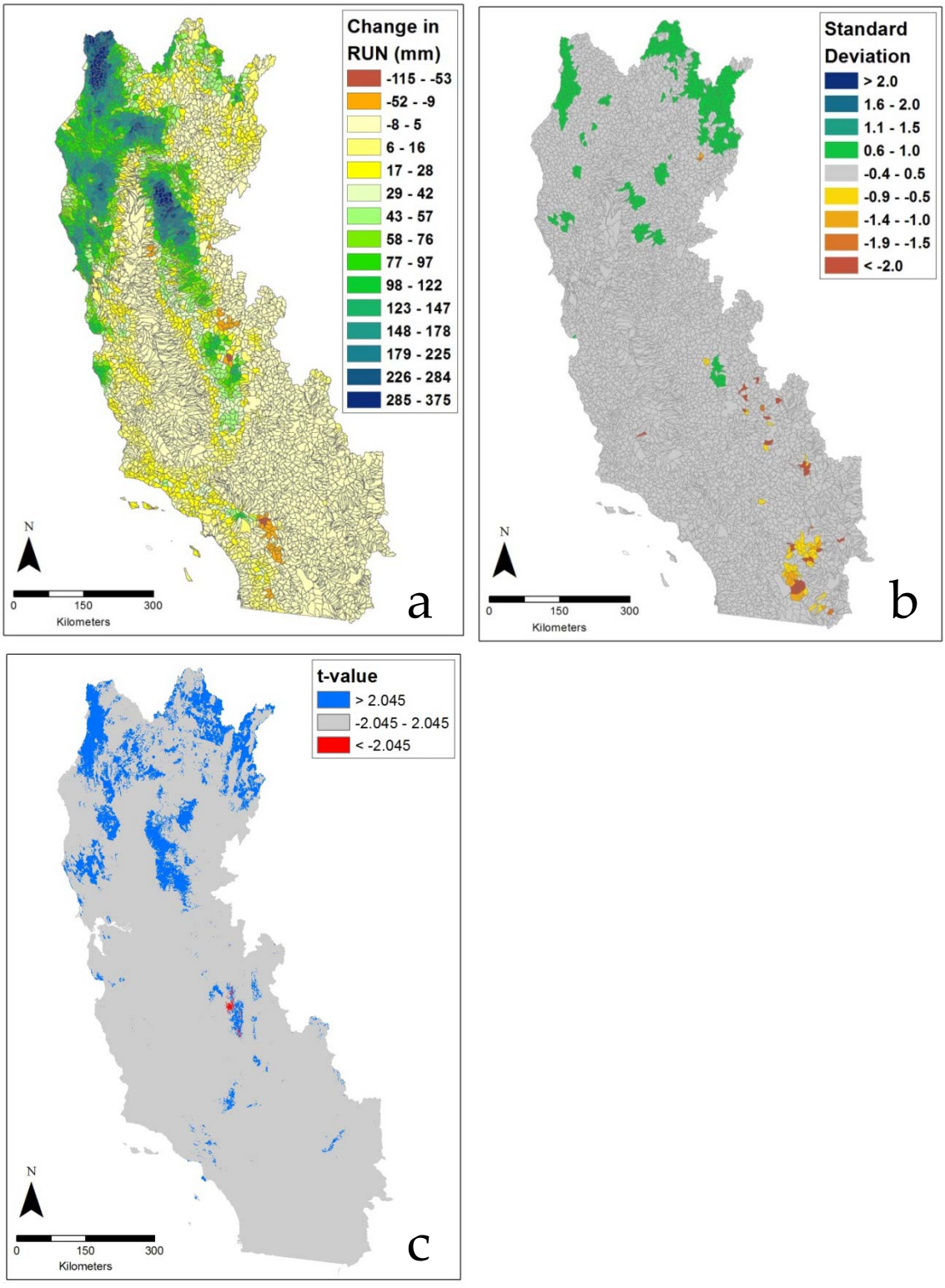

Figure 18: The Difference in Annual Runoff (RUN) for HUC 12 Watersheds between 1911–1940 and 1971–2000 (a), Normalized to the Standard Deviation over the 1971–2000 Period (b), and Statistically Significant Areas of Change, as Measured Using a T Test at α = .05 Significance Level (c)

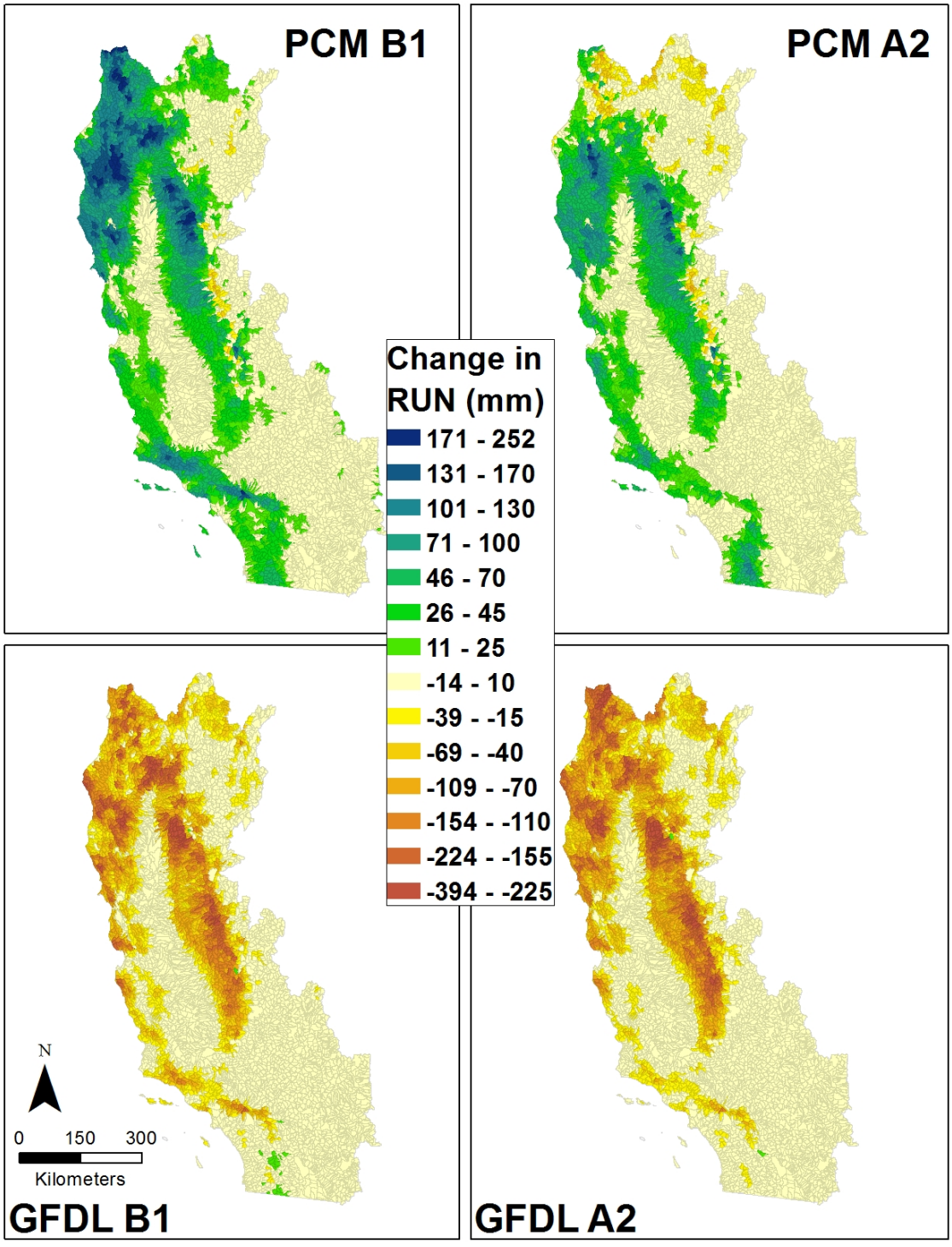

Figure 19: Difference in Annual Runoff (RUN) for HUC 12 Watersheds between Future (2071–2100) and Baseline (1971–2000) for GFDL and PCM A2 and B1 Scenarios

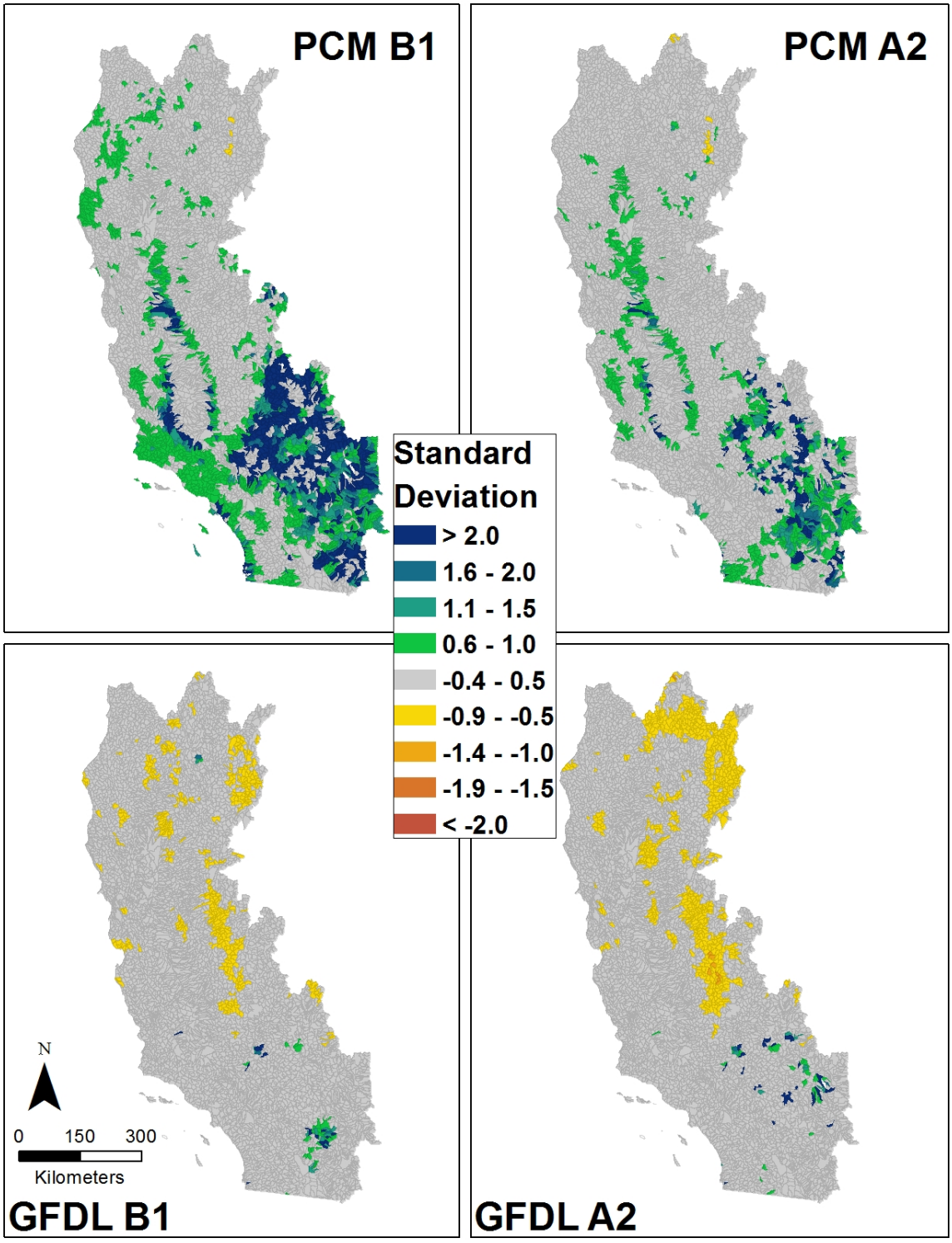

Figure 20: The Difference in Runoff for HUC 12 Watersheds between Future (2071–2100) and Baseline (1971–2000), Normalized to the Standard Deviation over the 1971–2000 Period for the GFDL and PCM A2 and B1 Scenarios

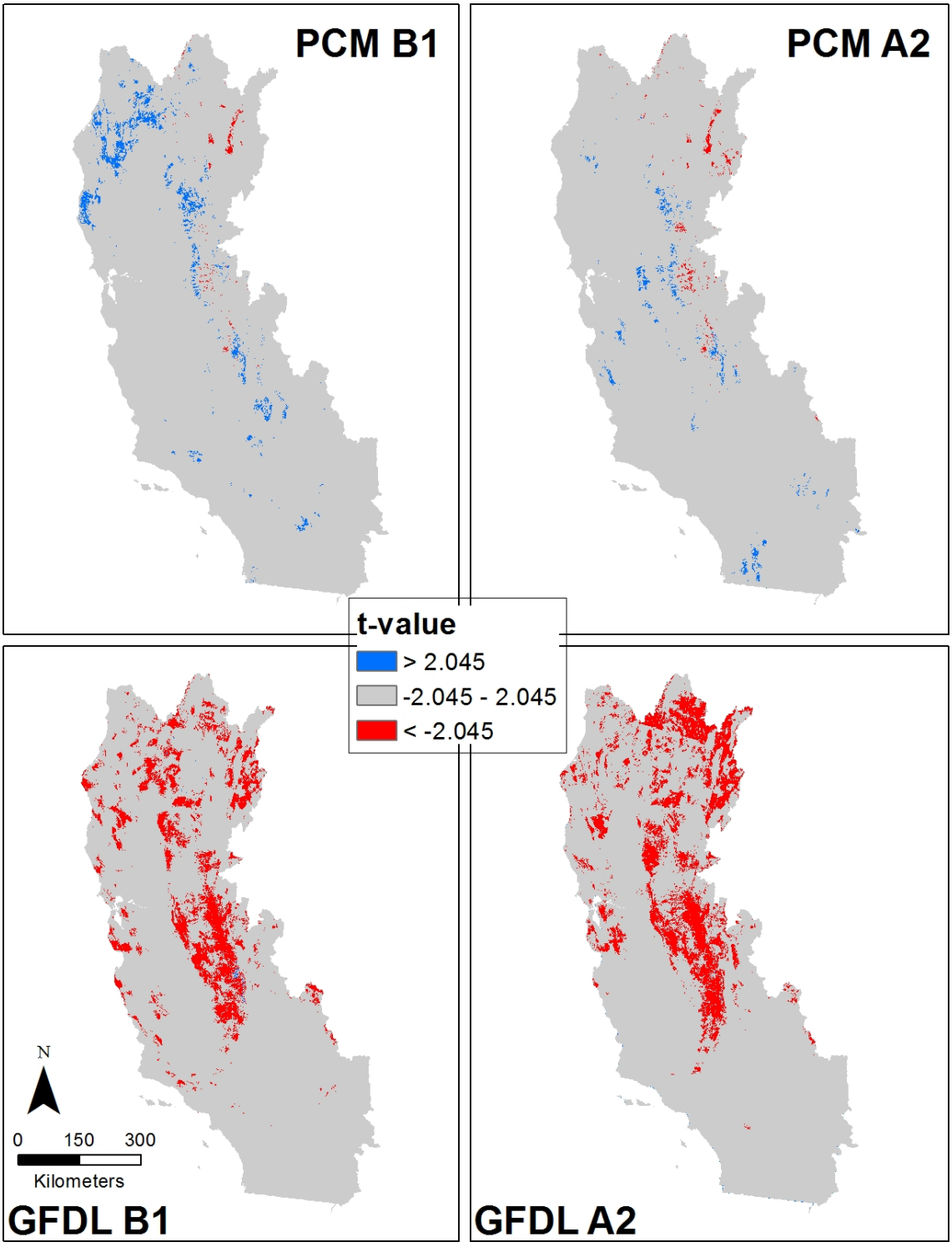

Figure 21: Statistically Significant Areas of Runoff change between Future (2071–2100) and Baseline (1971–2000), as Measured Using a T Test at α = .05 Significance Level

3.1.2.4 Recharge

Annual recharge values increased throughout the mountains and coast of northern California between 1911–1940 and 1971–2000 (Figure 22), similarly to runoff in distribution, but at a lower magnitude. Declines in recharge in the southern parts of the state and the Central Valley are at a similar magnitude. The difference between the time periods relative to the standard deviation during the baseline time period indicated very small changes outside the normal variability. The differences between recharge and runoff are more pronounced in the changes between baseline and the future scenarios (2070–2099) (Figure 23). This difference is exemplified by a very important characteristic that results from warming, regardless of the direction of change in precipitation in future projections, and that is the alteration of seasonality, with a shorter wet season and longer dry season.

For the wet scenarios (PCM model), there are slight increases in recharge in the Central Western and Great Valley ecoregions (B1 and A2), and the Cascade and Sierra Nevada (B1 only) (Table 2), but in contrast to runoff there are declines in recharge in the Sierra foothills and the northwestern part of the state. Because of the compression of the wet season with warming, (i.e., precipitation starts later in the fall and declines earlier in the spring), in addition to the earlier onset of springtime snowmelt, there is less time with conditions conducive to recharge. Even if there is increased precipitation and more excess water for any given month, this favors the partitioning of excess water into runoff because of the limitation of soil storage. Therefore, shorter wet seasons translate into reductions in recharge, and amount of runoff is related to if there is more or less precipitation.

The dry model, GFDL, has declines for both scenarios. The calculation of increases in SD beyond the baseline SD and T test indicate fairly small changes not present in the baseline variability, with the exception of the deserts and low-precipitation locations in the wet scenarios, as with runoff, and the mountains in the dry scenarios (Figure 24 and 25).

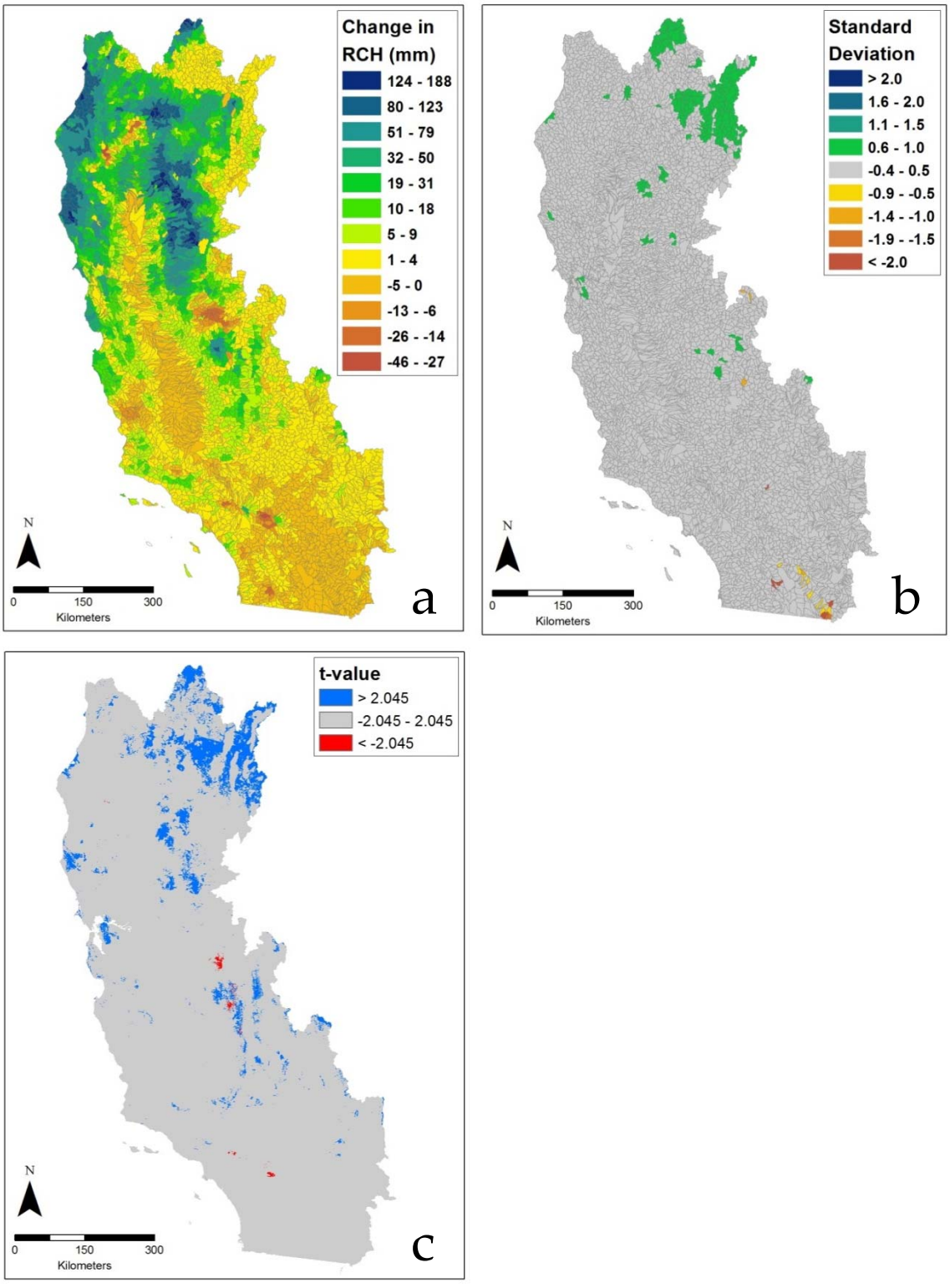

Figure 22: The Difference in Annual Recharge (RCH) for HUC 12 Watersheds between 1911–1940 and 1971–2000 (a), Normalized to the Standard Deviation over the 1971–2000 Period (b), and Statistically Significant Areas of Change, as Measured Using a T Test at α = .05 Significance Level (c)

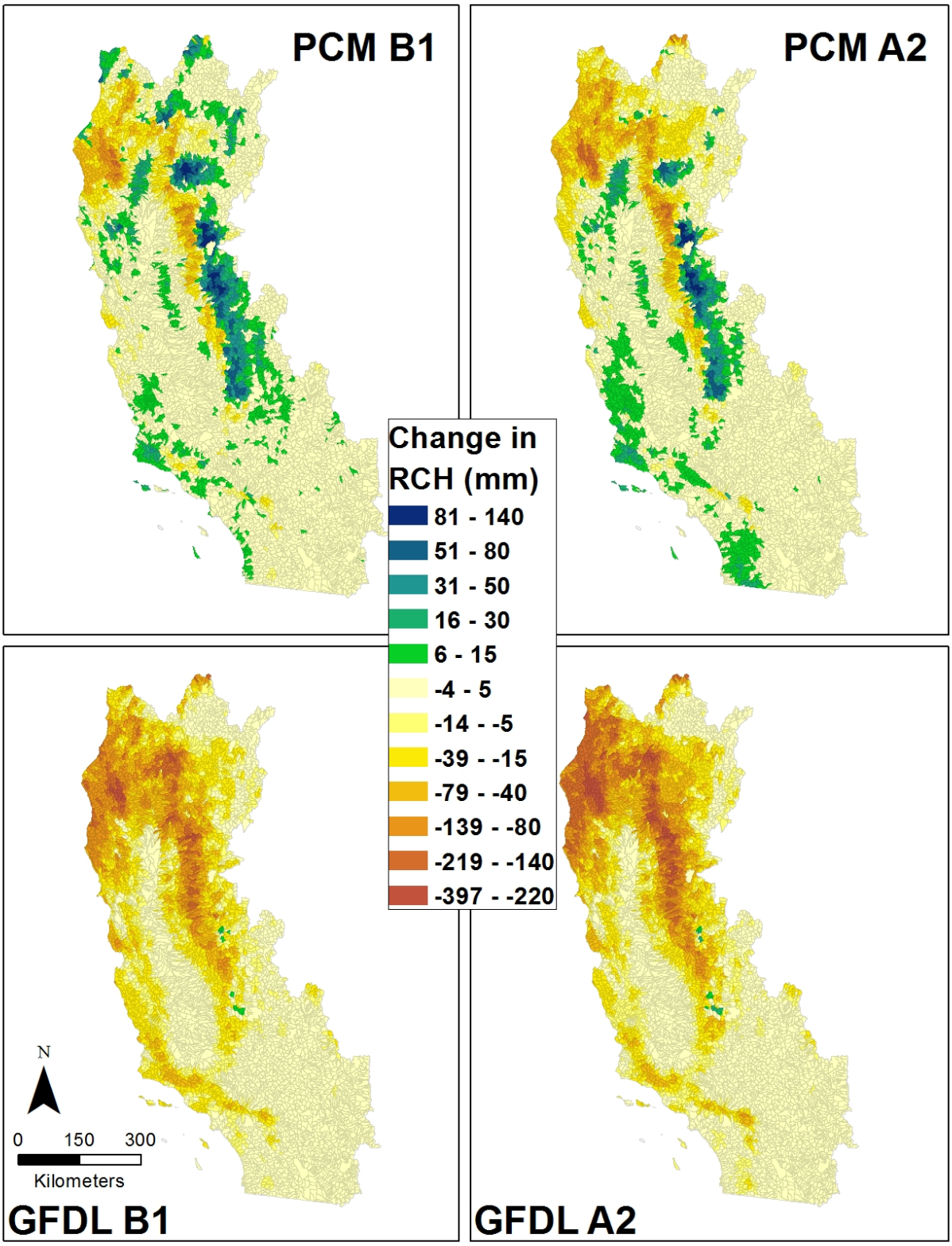

Figure 23: Difference in Annual Recharge (RCH) for HUC 12 Watersheds between the Future (2071–2100) and Baseline (1971–2000) for the GFDL and PCM A2 and B1 Scenarios

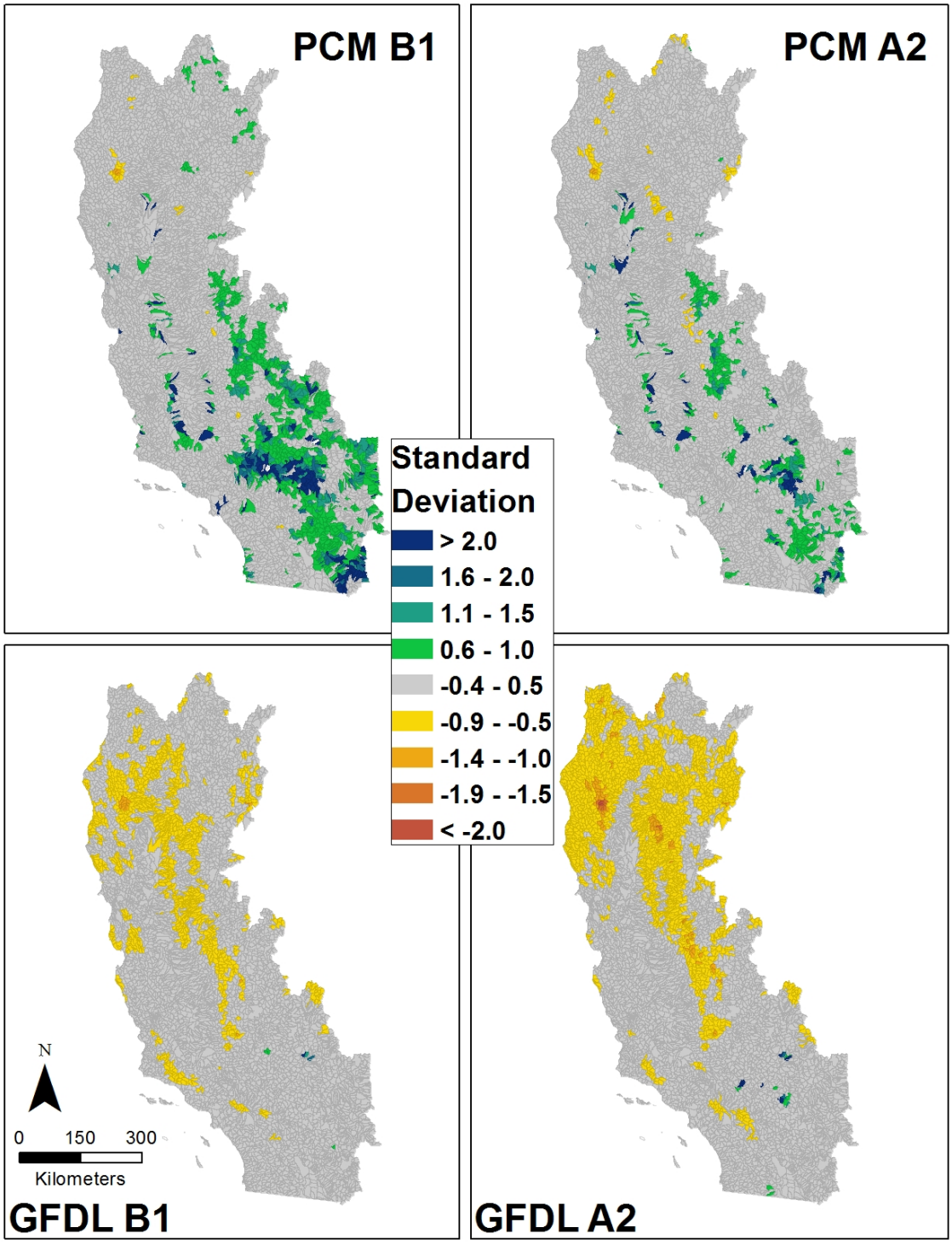

Figure 24: The Difference in Annual Runoff for HUC 12 Watersheds between Future (2071–2100) and Baseline (1971–2000), Normalized to the Standard Deviation for the 1971–2000 Period for GFDL and PCM A2 and B1 Scenarios

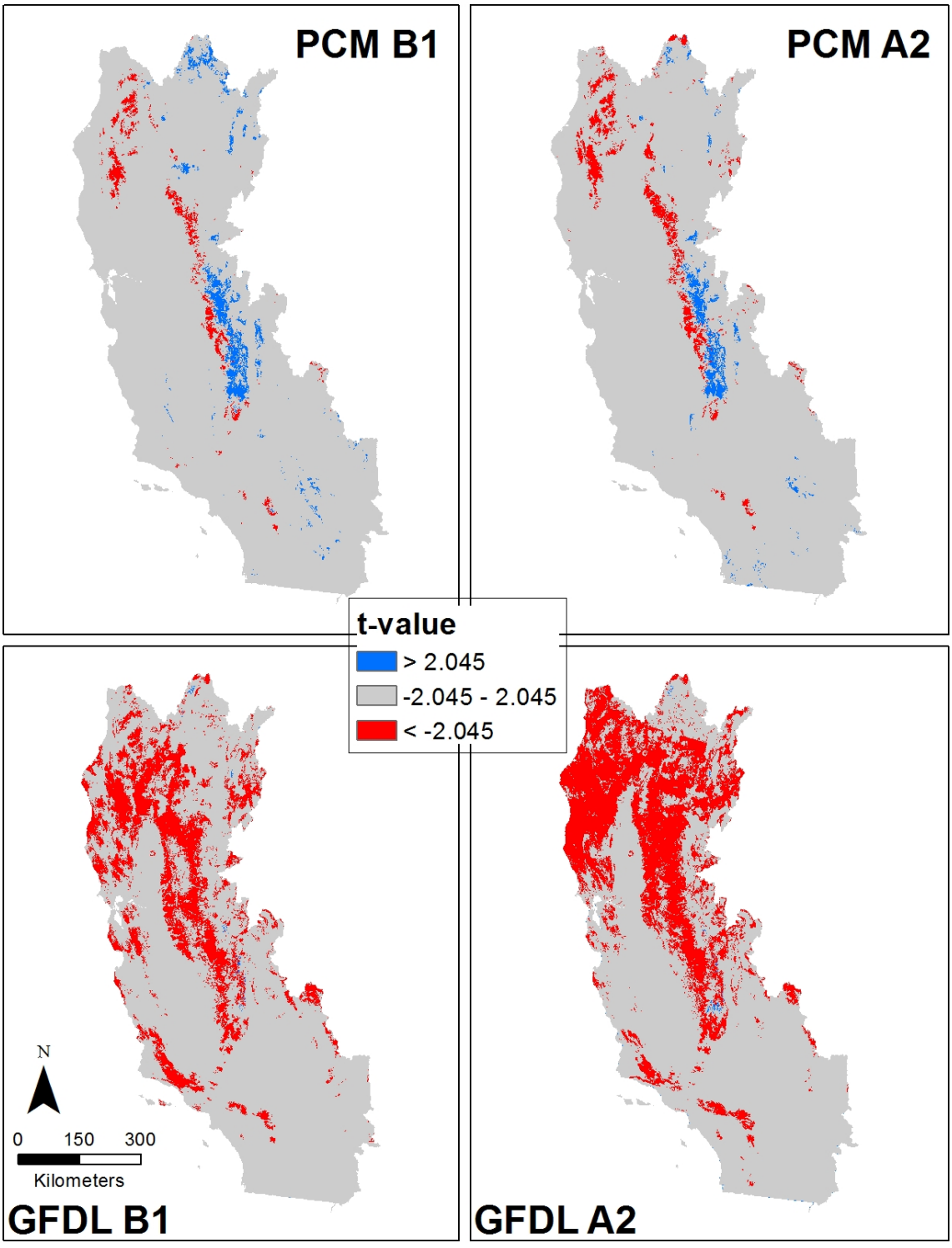

Figure 25: Statistically Significant Areas of Recharge change between Future (2071–2100) and Baseline (1971–2000), as Measured Using a T Test at α = .05 Significance Level

3.1.2.5 Climatic Water Deficit

The average climatic water deficit (CWD) for 1971–2000 ranges from 0 to 1,555 mm (Figure 9a). The northern section of the coast range, along with the Sierra Nevada, has had the lowest CWD, near or at 0, while the southern half of the central valley and the desert region in the southeast part of the state have had the highest. Changes in annual CWD between 1911–1940 and 1971–2000 were generally negative statewide (Figure 26), with slight changes in some southern California areas. The change at the HUC 12 watershed level, ranges from -151 to +115 mm, with a mean regional change of -15.9 mm. Looking at this difference relative to the standard deviation during the baseline 30 years of 1971–2000, none of the watersheds got drier by more than 1 SD, but several got wetter by more than one SD (Figure 26). Some areas of change emerge as statistically significant even though the change in at those locations is within 0.5 SD (Figure 26).

The vast majority of California is projected to have greater CWD, with all ecoregions increasing on average (Table 2), and with the GFDL projections higher than the PCM projections (Figure 27, Table 2). The highest increases are seen in the A2 scenarios along the summits and eastern sides of the Sierra Nevada. The PCM B1 scenario predicts a small decrease in CWD in small areas of the Central Valley, the northern section of the coast range, and in both the coast range and eastern part of southern California. The GFDL model does not predict any decreases in CWD. The change as measured relative to baseline standard deviations (Figure 28) shows that drying outside of 2 SD will be common in the Sierra Nevada and parts of the northern coast ranges under the A2 scenarios. These changes are also consistently statistically significant (Figure 29). It is of interest that this projection occurs for both wet and dry scenarios, which indicates the robust nature of the CWD application. This variable can be used to show that even with increased precipitation, the interaction of increases in air temperature (which have high confidence for all models) with evaporative demand and limits in soil moisture storage will result in increases in deficit across most landscapes, and drive very different growing conditions for most plants. This environmental condition, coupled with annual temperature extremes (driving growing degree days, chilling requirements, and extreme heat and cold tolerances) are likely to determine the future distribution of vegetation on our landscapes.

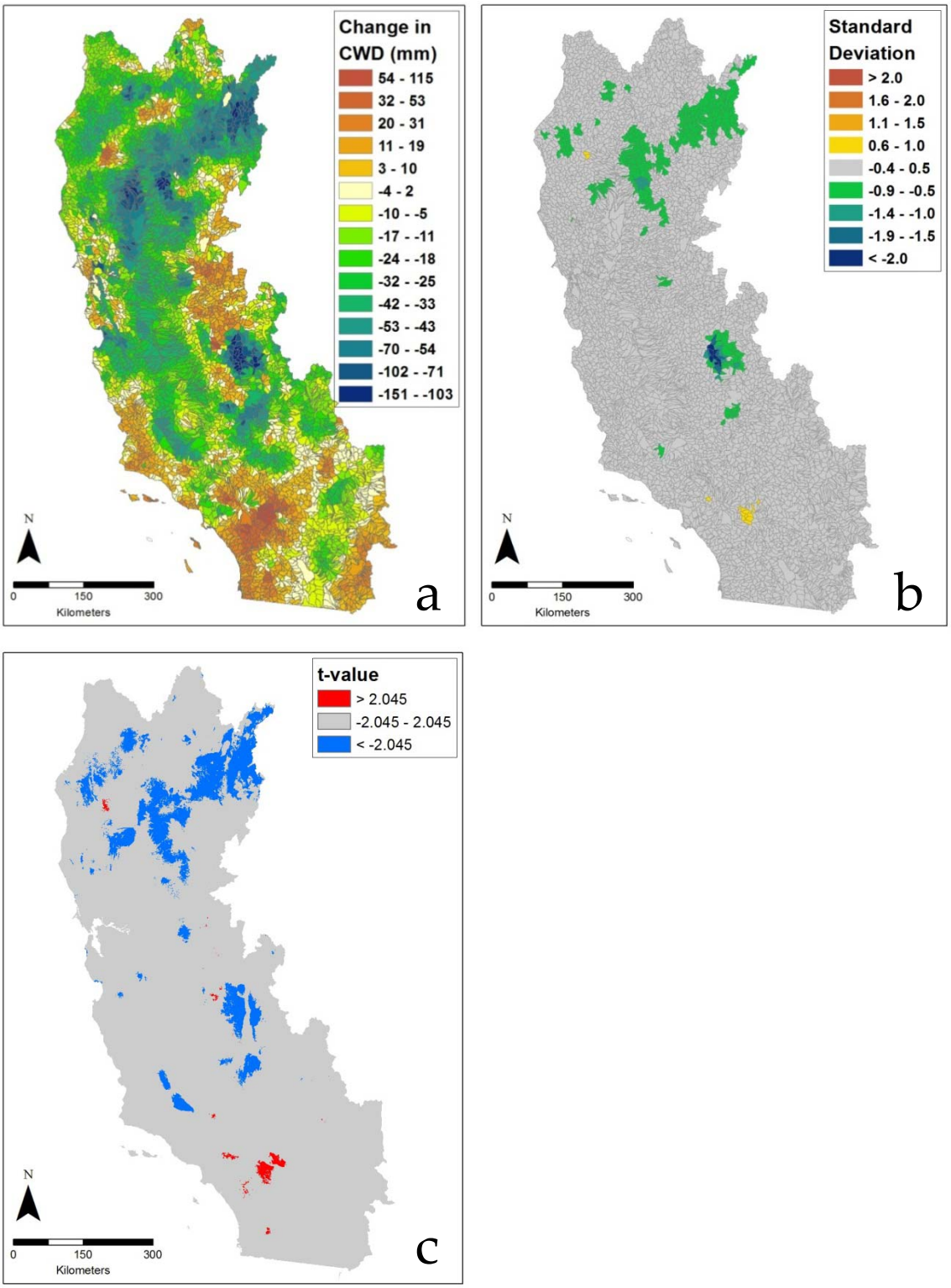

Figure 26: The Difference in Annual Climatic Water Deficit (CWD) for HUC 12 Watersheds between 1911–1940 and 1971–2000 (a), Normalized to the Standard Deviation over the 1971–2000 Period (b), and Statistically Significant Areas of Change, as Measured Using a T Test at α = .05 Significance Level (c)

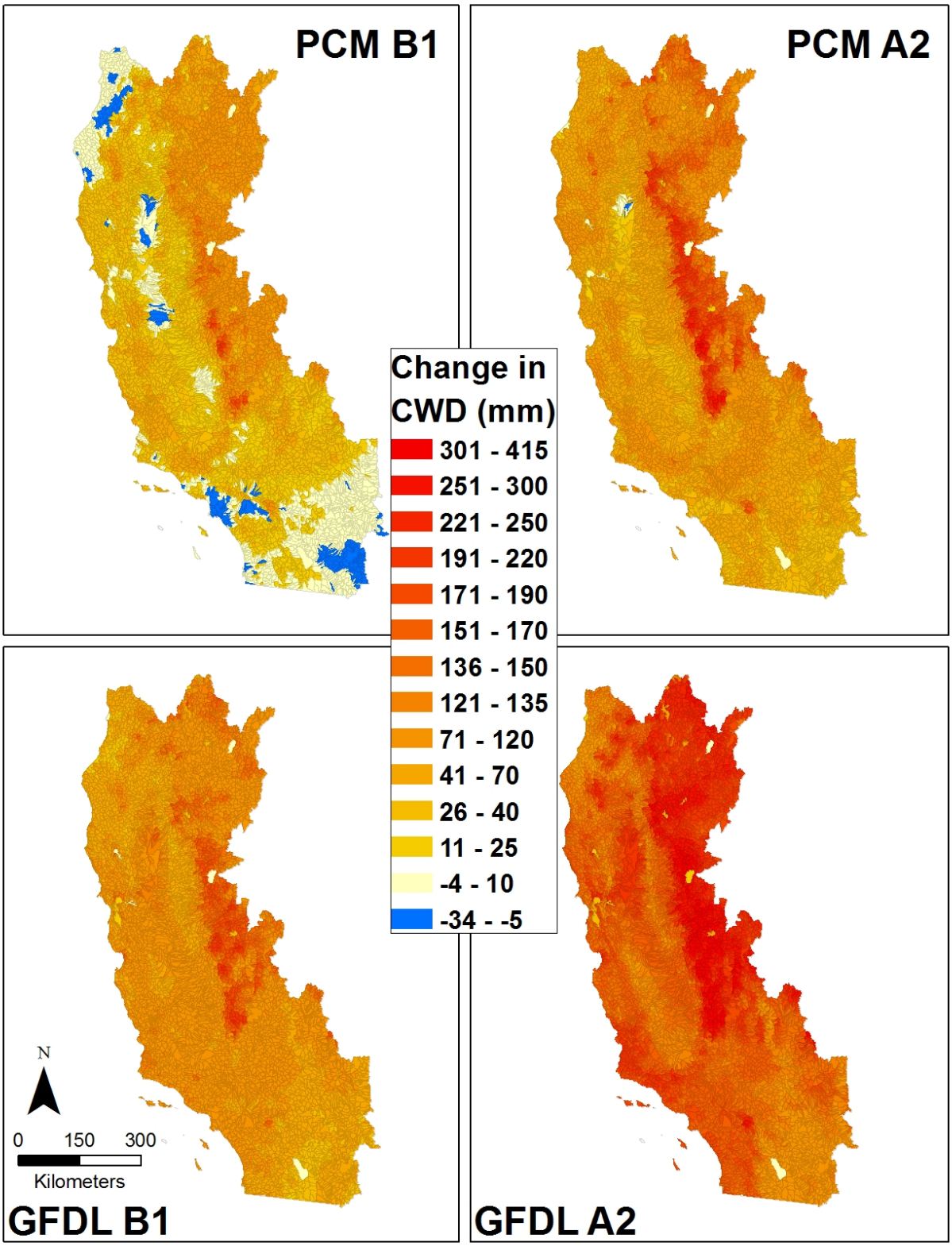

Figure 27: Difference in Climatic Water Deficit (CWD) for HUC 12 Watersheds between Future (2071–2100) and Baseline (1971–2000) for GFDL and PCM A2 and B1 Scenarios

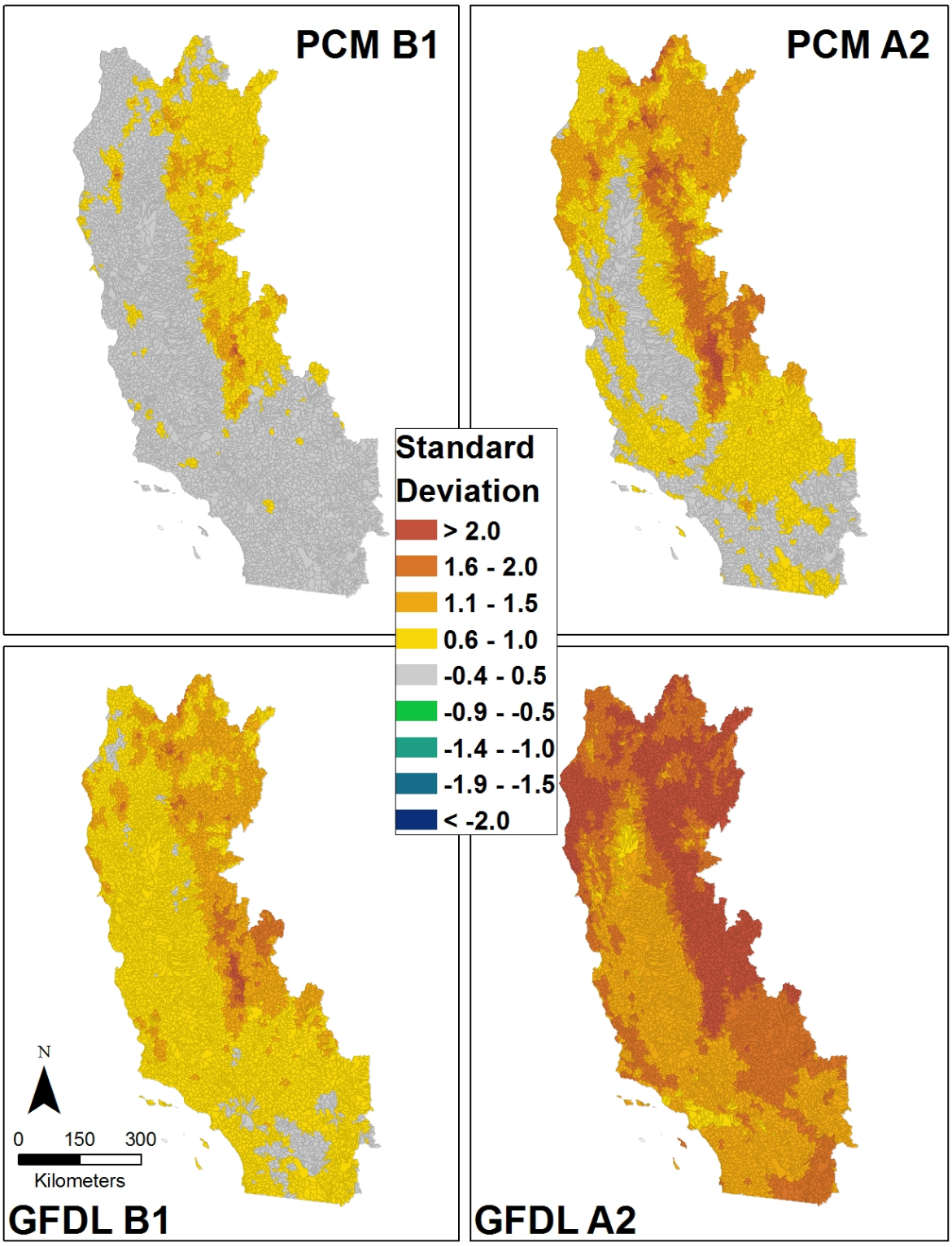

Figure 28: The Difference in Climatic Water Deficit for HUC 12 Watersheds between Future (2071–2100) and Baseline (1971–2000), Normalized to the Standard Deviation over the 1971–2000 Period for GFDL and PCM A2 and B1 Scenarios

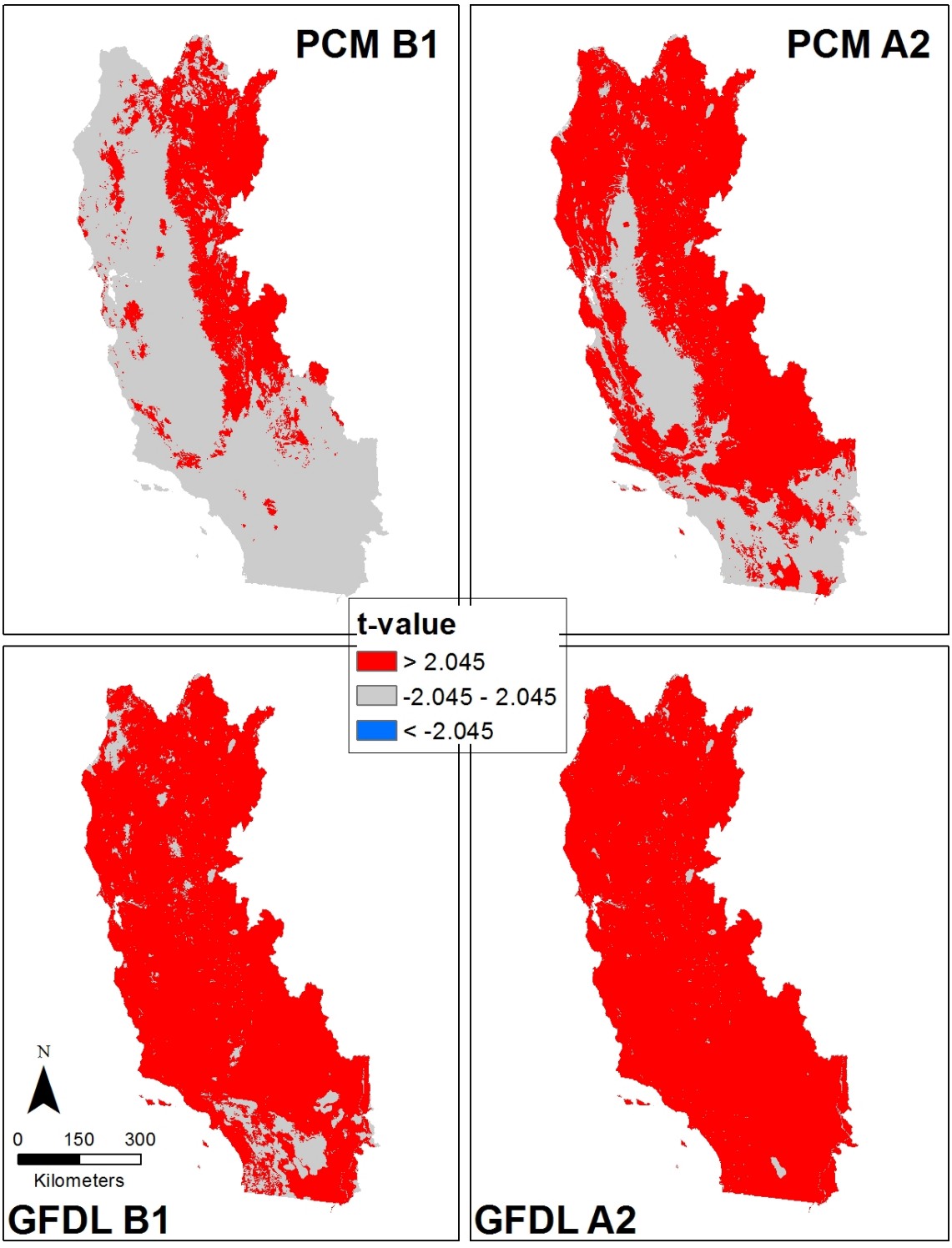

Figure 29: Statistically Significant Areas of Climatic Water Deficit change between Future (2071–2100) and Baseline (1971–2000), as Measured Using a T Test at α = .05 Significance Level

Finally, fine-scale modeling and analysis permits the influence of elevation and aspect to appear. This is shown with a comparison of the CWD for the last 30 years of the twentieth century (Figure 30, left panel) and the projected change from those baseline conditions to conditions in the last 30 years of the twenty-first century using the GFDL A2 scenario as an example (Figure 30, right panel shows the amount of change in CWD between future [2071–2100] and baseline conditions [1971–2000]). In this mountainous region straddling the lower Tulare basin and the desert of Antelope Valley, the CWD is primarily a function of elevation, with the desert floor high in deficit, and the mountain tops low in deficit. By the end of the twenty-first century, modeling shows the greatest change to be (1) in the high mountains in the west where there is diminished snowpack, and (2) on the south-facing slopes. While slope had little effect on the distribution of CWD in the baseline period, the changes indicate resilience on the north-facing slopes where lower energy loads sustain moisture and moderate temperature as the climate warms.

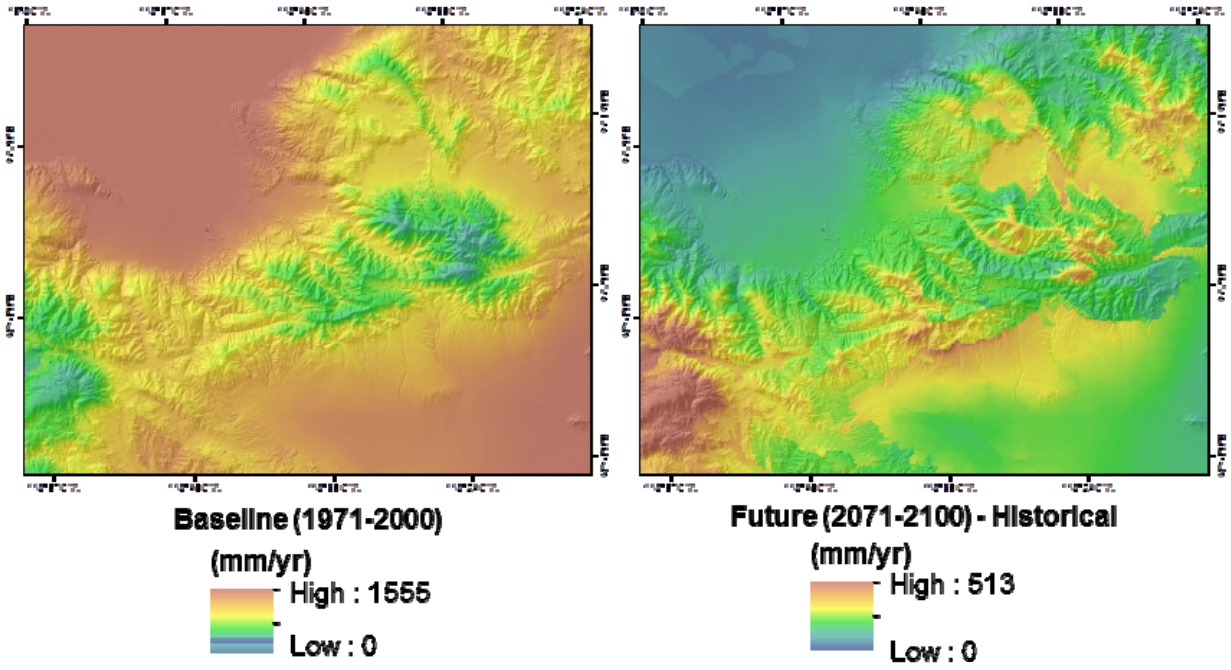

Figure 30: Current (1971–2000) Average Climatic Water Deficit, and Difference between One Scenario (GFDL A2) and Baseline

Section 4: Discussion

The dominant climatic trends that emerged from the BCM runs conducted here include increases in air temperature that drive reductions in snowpack, earlier snowmelt, and a compression of the winter season, such that runoff is increased at the expense of recharge under all precipitation scenarios. The influence of air temperature also drives the increase in climatic

water deficit regardless of precipitation changes, impacting many aspects of ecosystem health, agricultural demands, and water availability.

The projections of changes in hydrology assume no changes in land use and reflect only changes in climate. Even without changes in land use there have been large changes distributed variably across the landscape of California. Increases in precipitation during the baseline time period were recorded in all ecoregions except the deserts, but the largest changes were a result of increases in air temperature that have influenced springtime snowmelt. The extent and thickness of snowpack diminished in all but a few high-elevation locations and has large implications for the water supply of California, which relies heavily on the slow springtime snowmelt to sustain the resource through the dry summer months. These climatic changes during the baseline period affected runoff and recharge differently across the state. There were primarily increases in runoff, especially in the northern Sierra Nevada, while recharge showed variable response, with increases in most locations including where snow has diminished, and decreases on the north and south coast regions.

Climate has also driven changes during the baseline period in CWD, which proved to be most reliant on air temperature, as the modest increases in precipitation either were held in soils or became recharge or runoff early in the season, and therefore resulted in increased CWD later in the season. This is reflected throughout the state with increases in CWD, except for parts of the San Francisco North Bay, Central Coast, and North Coast regions (which experienced less of an increase in air temperature) and the northern Central Valley (where the soils are thick enough to store excess water from precipitation).

Looking across longer time periods, the results show a change in the direction of trend for a number of important hydrological variables. Historically, precipitation slightly increased, most strongly in the Sierra Nevada and northern Coast Ranges, while decreasing in the deserts. Future statewide increases in precipitation continue only under PCM B1 and reverse direction in the northern Coast Ranges and Modoc Plateau under PCM A2, while the GFDL identifies drying for nearly the entire study area under both scenarios.

Region-wide precipitation, which has trended wetter historically is the most uncertain variable in future GCM/emission projections among the scenarios investigated. The PCM models project wetter conditions (although usually not above the level of current variability) through the twenty-first century for both emissions scenarios, and the GFDL projects much drier conditions. There is model consensus on rising air temperatures. Increasing temperatures drive earlier snowmelt, and also increase the rate of PET, a hydrologically independent variable. Potential evapotranspiration predominantly showed modest increases over historic time, with a few anomalies in the high Sierra Nevada. This trend is amplified under all the future scenarios, and produces the most significant change measured in this study, with the trend ranging from 1 standard deviation of baseline PET to >2 under the GFDL A2 projections. What affects this level of increased metabolic demand will have on the many plant species in the region is undetermined, but water deficit stress well beyond the year-to-year variability currently encountered could be a way to measure where we would expect physiognomic shifts in dominant vegetation types.

Changes in runoff correspond to the uncertain direction of change in precipitation projected by the different models. Historic trends of increasing runoff are projected to increase under the wet PCM scenarios, especially in the mountainous regions, and to decrease under the dry GFDL scenarios. However, the change in runoff is mostly under 0.5 SD for both wetter and drier. The exception is in desert regions, where increases in runoff are projected to be far above current variability, but this is because there are currently very low levels of runoff, and the actual magnitude of change projected is low. It is interesting to consider that while warming is generally expected to increase spring runoff, and to make hydrological systems more "flashy" or prone to floods, the results here suggest that for many places, on a yearly basis, the total amount of future runoff is similar to current amounts. Note also that the increase in PET reduces the amount of excess water available for runoff.

Recharge, which over historic time has increased in the Sierras and northern California, while declining in the Central Valley and most of southern California, does not follow the direction of change in precipitation, due to the compression of the wet season and the dependence of recharge processes on soil moisture storage and bedrock permeability. Our projections indicate that if there is excess water afforded by increases in precipitation, it will mostly become runoff rather than recharge. Recharge is dominant during the slow snowmelt season when the soil drains slowly and provides the time for recharge. With this season becoming shorter in the future, this process becomes less significant under all scenarios.

Finally, CWD, which lessened in some areas historically, becomes much more pronounced under all future projections, with the Sierra Nevada mountains and Modoc plateau experiencing the most consistent impacts across scenarios. This trend exemplifies the increase in PET in all scenarios due to air temperature, and the limitation of the soils to hold additional water where, or if, precipitation increases. Thus, driving forces for species distributions, agricultural demands, and other processes or needs that rely on seasonal soil moisture threaten to impose much higher stress.

These results suggest that while warming continues from historic to future in a positive trend, that many of the hydrologic variables will pass through some tipping point, and that the conditions in California may become much more challenging than baseline or historic trends suggest for the future. For example, mountainous regions that have been somewhat buffered from hydrologic impacts may experience more pronounced impacts related to water shortages and CWD. Such impacts may include tree mortality due to drought, increased pathogen outbreaks, and increased fire risk—all of which may lead to significant changes in timberland species composition and structure, including outright conversion to other vegetation types. The future suitable conditions of the major agricultural regions, the Central Valley, Salinas Valley, and South Coast ranges will be highly dependent on whether the future plays out more along the PCM or the GFDL projections. Under the PCM projections, while CWD does increase in most of these areas, the increase is typically less than half a standard deviation of baseline variability. Climate water deficit increases are much greater under GFDL projections, and under these conditions farmers will likely need far more adaptive measures to address the increasing soil aridity. For natural ecosystems, the Sierra Nevada appear to be under the greatest increased stress from CWD, under all four projections, and the coastal ranges experience varying levels of

CWD increase, with PCM A2 the lowest and GFDL A2 producing similar levels of CWD as in the Sierra Nevada. These increases are likely to have both physiological impacts to plant species, and to change the background level of fire return in these ecosystems.

4.1 BCM Performance

The use of streamgage data to calibrate the BCM to accumulated upstream runoff and recharge permits an assessment of the relationship between recharge and runoff on a spatial and temporal basis. Similar types of model calibration have been performed for the solar radiation and evapotranspiration components (Flint and Flint 2007). Soil moisture and climatic water deficit could be field verified as well through spatial and temporal sampling of plant evapotranspiration rates (e.g., Ryu et al. 2008) and by measures of soil moisture (e.g., Mittelbach et al. 2011). In this study, we assembled runoff data from 138 streamgages, which permits a rough assessment of how well the BCM model performs at integrating all the hydrologic balance components.

The application of the BCM to assess unimpaired hydrologic conditions for California relies on the calibration to geology and the relative success across the state with which estimated basin discharge corresponds to measured streamflow. The application of this mechanistic model permits a look at how conditions have changed over time and provides an illustration of where in the region basins are more or less sensitive to changes in climate, where runoff or recharge processes are dominant, and where moisture stresses to the landscape are likely to be more or less profound. Generally basins with the least impairments had the best calibrations, with the exception of basins in the volcanics in the upper Klamath River basin.

Generally calibration and performance results for the BCM were satisfactory in basins throughout the state with both unimpaired and impaired (including urban and agriculture) basins providing close matches of estimated basin discharge to measured streamflow. Basins with the lowest BCM performance scores contained unaccounted-for land uses, such as agricultural or municipal diversions or return flows, or water impoundments such as reservoirs. These results provide reasonable confidence in the spatially distributed estimates of recharge, runoff, and climatic water deficit throughout the entire state, as well as for ungaged basins. However, runoff in the BCM is not routed, and basin discharge requires post-processing using measured streamflow to determine the relative contributions of recharge and runoff in a basin to gains and losses in streamflow. Once established, these components can be used to extrapolate basin discharge through time, given no changes in impairments. Uncertainties in calibration do not affect estimates of CWD, as this calculation does not rely on the bedrock permeability used to partition the excess water into recharge and runoff. Soil water conditions are a function of soil properties, available water from precipitation and evapotranspiration. Therefore, the BCM calculation of CWD, PET minus actual evapotranspiration (Stephenson 1998), reflects the uncertainties inherent in the climate data, in the soil properties from soil mapping and PET.

4.2 Model Utility and Data Limitations

The BCM is a physically based, deterministic model that provides information at a fine scale on the basis of downscaled climate input data and the most detailed maps available to represent other landscape variables used. These techniques have been tested to illustrate accuracy in representing the larger-scale climate datasets (Flint and Flint 2012). The calculation of potential evapotranspiration has been rigorously developed and calibrated to measured data throughout California (Flint and Flint 2007). Applications of the BCM to determine hydrologic response, as measured by discharge to climate, rely on maps of soil type and estimates of properties (SSURGO; NRCS, http://soils.usda.gov/survey/geography/ssurgo/) and geologic maps from which bedrock permeability is estimated. Soil properties are maintained static, but bedrock permeability is adjusted to change the ratio of recharge to runoff and improve the comparison of estimated total basin discharge to measured streamflow. If a geologic type is mapped as one type over a broad area of the state, when bedrock permeability is adjusted to improve calibration in one location, the relative proportions of recharge and runoff change correspondingly across the domain in basins with similar geologic types. Since discharge is derived from runoff and recharge, a post-processing calibration/validation may be conducted, as was the case in this study.

A useful application of the BCM beyond the estimates of spatially distributed recharge and runoff would be to estimate basin discharge at ungaged basins. To this end, there were attempts made to correlate the basin calibration parameters that were used to adjust the basin discharge to match measured streamflow in gaged basins (Appendix C) to landscape variables. The intent was to enable the extrapolation of discharge estimates to ungaged basins on the basis of mapped physical characteristics such as geology, soil properties, slope, basin area, or aridity. The concept here is that parameters that adjusted the baseflow to be high in basins with high bedrock permeability, for example, might have a correlation across multiple basins. However, none of these showed a significant relationship with model calibration parameters across all calibration and validations in California. Possible reasons for the lack of relationship include potential errors in the soils or geology maps, or in the PRISM climate data, or due to human activities that are affecting basin hydrology at the watershed scale. Since the BCM is a mechanistic model, driven by a series of physically based assumptions, we argue that the model output is of value for regional comparisons of watersheds, even in the absence of independent validation for ungaged basins. If we assume that the properties and climate are correct, the BCM hydrologic outputs are based on properties that are spatially distributed throughout the study area, and the calculations performed consistently across all basins, providing a level of confidence when using the hydrologic results for regional cross-comparisons of basins.

Some of the sources of error are well known to geographers. Soils maps are particularly prone to error, since accurate measures of soil depth are difficult to obtain, and currently unobtainable for large areas. The national State Soil Geographic (STATSGO) dataset smoothes out landscape features and generally disregards topographic controls on soil depth. County-level soils maps (SSURGO) are currently being developed for the state for application to the BCM, which will provide much better accuracy in BCM output, particularly for CWD. Improving measurements

of soil depth generally emerged as one of the most important data development agendas as a result of this study.

Human activities are extensive in California, and likely have impacts in nearly every basin. These activities that can affect the hydrologic cycle at the watershed scale include small impoundments, direct pumping from streams for urban or agricultural use, construction of impermeable surfaces, and changes to the natural land cover. These can affect variously the partitioning of input PPT to different pathways in the hydrological cycle, and also affect the actual evapotranspiration (AET) and PET calculated as part of the model. We were not able to make detailed efforts on assessing the influence of human activities on the overall model accuracy, and feel this would be a suitable agenda for future research, particularly for basins with several gages that are placed below and above areas of human disturbance.

The historical climate used for this analysis, PRISM, relies on meteorological station data, and empirical relations of numerous factors affecting the local expression of climate on the landscape, including distance from the ocean, extent of mountain ranges, and other features, to interpolate among data locations. This dataset is therefore a model, relying on data, and does not strictly honor the measured data in most locations. However, the interpolated data likely reflects better estimates of climate in locations without measurements than nearby station data at different elevations or topographic settings, and is considered a useful and competent long-term dataset.

The estimate of spatially distributed runoff does not equal basin discharge as measured at a streamgage without post-processing to determine the components of runoff and recharge that contribute to stream channel gains and losses, which must be done using some measured data for a given basin. The resultant parameters corresponding to the gains and losses generally reflect climatic conditions and geologic setting, but at the scale of hydrologic California have not been determined to a degree that allows for the direct extrapolation of basin discharge to all ungaged basins. The spatial distribution of runoff and recharge, however, provide relative differences over the region and indicate the differences in sensitivity of basins to changes in climate. The estimate of changes in soil moisture and CWD do not rely on interpretation of bedrock permeability, and uncertainties correspond more closely with those of the mapped soil properties and climate data.

Because the BCM model outputs are calculated on a grid-cell basis, results can be summarized across landscapes using summary units of any size of interest such as watersheds, ecoregions, or political boundaries. The ability to spatially project hydrological model outputs permits the cross-comparison of these landscape delineations, with mapped outputs of interest to various fields of research (e.g., Appendix F). The discharge and groundwater outputs can inform water management for storage and human consumption, and anadromous fisheries. Soil moisture and climatic water deficit are of interest for tracking suitability of rain-fed agriculture and for assessment of suitability of natural environments for component plants and animals.

The ability to calculate hydrological outputs using a transparent, mechanistic approach, and at fine spatial scales, permits a new set of predictor variables to be used in the spatial projection of

suitable plant ranges or habitats (e.g., Williams et al. 2009). This is a particularly important opportunity for ecologists and conservation biologists because species distribution models are one the primary methods of evaluating the susceptibility of species to climate change (e.g., Guisan and Thuiller 2005; Lorrie et al. 2009). One of the most important variables that BCM calculates is climatic water deficit (Stephenson 1998). Natural resource managers and field ecologists are particularly interested in this variable, as it integrates site conditions with temperature and moisture, and is therefore a factor that plants may respond to more directly than climate variables alone, particularly in regions with pronounced seasons. The strength of the BCM in portraying CWD is that different watersheds can be compared by identifying the area-weighted mean value. Therefore relative differences across hydrologic California are comparable.

Section 5: Summary and Conclusions

5.1 Development of Hydroclimatic Variables for Climate Assessments

The downscaling of historical climate data and future climate scenarios for application to the BCM to calculate hydrologic response to climate change has provided a dataset that is both rich in its regional representation of climatic and hydrologic trends, but also spatially detailed to provide fine-scale examples of local impacts of climate change on the landscape.

Landscape responses to climate change are moderated by locations with lower energy loads, such as north-facing hillslopes or coastal regions with frequent cloud cover. Soil also amplifies or moderates the hydrologic response for the landscape to climate change, depending on whether soils are thin and excess water is lost to runoff or recharge, or if they are thick and can maintain moisture longer into the season. Mountainous regions seasonally occupied by snowpack are quite sensitive to climate change, as the timing of snowmelt is enhanced by warming, thus changing the length of the wet season and extending the dry season for all regions downstream relying on snowpack for public and agricultural use.

The BCM, using the best map data available, still shows that we have not captured all the details that drive individual watershed dynamics. However, for comparative purposes across a large number of watersheds and ecoregions, the relative consistency of the model permits informative interpretations. This is, in essence, very similar to the way in which GCMs themselves run, in that they provide a platform for intercomparison of regions even while they may be more or less accurate when compared to ground-based measurements. In this regard, then, the next challenge for modelers of these physical (and biophysical) processes is to determine how to incorporate the next-finer scale of detail. Basin Characterization Model output maps indicate where on the landscape changes in the hydrologic cycle occur. If discharge or recharge boundary conditions are needed at the watershed-scale basin, then this study suggests that some local calibration is necessary. However, if the basins are purely unimpaired, then nearby or adjacent basin calibration is likely to suffice.

The consistent patterns offered by the BCM for a variety of hydroclimatic variables that relate to ecological processes to fine spatial scales make the model output of particular interest to landscape ecologists, and to those interested in modeling the biogeographic response of species and vegetation types to future changes in climate. Part of the interest derives from the fact that future moisture conditions are much more difficult to project than future temperature; a fact that emerges when comparing the outputs of future GCMs for temperature and precipitation, where there is much higher agreement between models for temperature. Having a mechanistic model that captures the dynamics of the water that is predicted permits a better estimation of hydrological conditions under varying scenarios, which in turn can provide a view to the range of potential impacts to water available for natural processes and for human uses; particularly rain-fed agriculture.

5.2 Model Refinements and Future Directions

Because of the modular nature of the Basin Characterization Model, it is possible to make two types of improvements. First, any particular module's calculations may be updated and improved. An example would be if PET values for different vegetation types could be calculated, these could be applied using an existing vegetation map to render more accuracy in the plant-driven parts of the model. Second, input data maps may be updated and improved.

Refinements are currently planned to improve the accuracy of the spatially distributed outputs, and improve confidence in estimates in ungaged basins. On the basis of a comparison the PRISM 4 km-resolution climate data used in this study, and the subsequently available PRISM 800 m-resolution climate data (Stern et al. 2011), map-based improvements for the next version of BCM projections include the incorporation of the PRISM 800 m transient climate dataset for historical BCM analyses. The 800 m transient data provides slight improvements in precipitation estimates for the state, particularly at high elevations dominated by snowpack. For future projections, a broader suite of GCM and scenarios could be developed, while awaiting the next iteration of projections from the IPCC.

To improve the snow-driven module in BCM, calibration of the snow accumulation and snowmelt calculations will be done to match measured snow-water equivalent at over 300 snow sensors and snow courses, and maps of persistent glaciers will also be included. The use of the 800 m PRISM climate data also contributes to a marked improvement in snowpack in some locations. SSURGO soils maps are far more detailed and accurate than STATSGO datasets and reflect topographic controls on soil properties. Therefore SSURGO soils maps are being developed statewide for model application. Geologic maps and local calibrations are being refined in those locations where geologic types are not well represented by the calibration basins, such as the volcanics of the Modoc Plateau and the upper Klamath River basin.

References

Alkama, R., B. Decharmen, H. Douville, and A. Ribes. 2011. "Trends in global and basin-scale runoff over the late twentieth century: Methodological issues and sources of uncertainty." *Journal of Climate* 24: 3000–3014.

Alley, W. M. 1984. "On the treatment of evapotranspiration soil moisture accounting, and aquifer recharge in monthly water balance models." *Water Resources Research* 20:1137–1149.

Anderson, E. A. 1976. *A point energy and mass balance model of a snow cover.* Technical Report NWS 19, 150 p. U.S. National Oceanographic and Atmospheric Administration (NOAA), Silver Spring, Maryland.

Bouwer, L. M., J. C. Aerts, G. M. Van de Coterlet, N. Van de Giesen, A. Gieske, and C. Mannaerts. 2004. Evaluating downscaling methods for preparing global circulation model (GCM) data for hydrological impact modeling. Climate Change in Contrasting River Basins (eds. Aerts, J. C. J. H. and P. Droogers). CAB International Publishing: London, UK, 25–47.

Breshears, D. D., O. B. Myers, C. W. Meyer, F. J. Barnes, C. B. Zou, C. D. Allen, N. G. McDowell, and W. T. Pockman. 2009. "Tree die-off in response to global change-type drought: Mortality insights from a decade of plant water potential measurements." *Frontiers in Ecology and the Environment* 7:185–189.

Bristow, K. L., and G. S. Campbell. 1985. "An equation for separating daily solar radiation into direct and diffuse components." *Agricultural and Forest Meteorology* 35: 123–131.

California Department of Water Resources. 2008. Managing an uncertain future: Climate change adaptation strategies for California's water. White paper for State of California. October.

Campbell, Gaylon. 1977. *An Introduction to Environmental Biophysics.* Springer-Verlag: New York.

Cayan, D. R., M. Tyree, M. D. Dettinger, H. Hidalgo, and T. Das. 2009. *California climate change scenarios and sea level rise estimates for the California 2008 Climate Change Scenarios Assessment.* California Energy Commission report CEC-500-2009-014-F. Available from: http://www.energy.ca.gov/2009publications/CEC-500-2009-014/CEC-500-2009-014-F.PDF.

Cayan, D. R., E. P. Mauer, M. D. Dettinger, M. Tyree, and K. Hayhoe. 2008. "Climate change scenarios for the California region." *Climactic Change* 87 (suppl 1): S21–S42. DOI: 10.1007/s10584-007-9377-6.

Chen, Z., M. L. Kavvas, L. Tan, and S-T. Soong. 2004. "Development of a regional atmospheric-hydrologic model for the study of climate change in California." *Proceedings of the American Society of Civil Engineers* 1093–1098.

Chiew, F. H. S., D. G. C. Kirono, D. M. Kent, A. J. Frost, S. P. Charles, B. Timbal, K. C. Nguyen, and G. Fu. 2010. "Comparison of runoff modeled using rainfall from different downscaling methods for historical and future climates." *Journal of Hydrology* 387:10–23.

Crimmins, S. M., S. Z. Dobrowski, J. A. Greenberg, J. T. Abatzoglou, and A. R. Mynsberge. 2011. "Changes in Climatic Water Balance Drive Downhill Shifts in Plant Species' Optimum Elevations." *Science* 331:324–327.

Daly, C., W. P. Gibson, M. Doggett, J. Smith, and G. Taylor. 2004. Up-to-date monthly climate maps for the conterminous United States. Proceedings 14th AMS Conference on Applied Climatology, 84th AMS Annual Meeting Combined Preprints, Amer. Meteorological Soc., Seattle, Washington, January 13–16, 2004, Paper P5.1, CD-ROM. http://www.prism.oregonstate.edu/pub/prism/docs/appclim04-uptodate_monthly_climate_maps-daly.pdf.

Daly, C., R. P. Neilson, and D. L. Phillips. 1994. "A statistical-topographic model for mapping climatological precipitation over mountainous terrain." *J Appl Meteor* 33:140–158.

Delworth, T. L., A. J. Broccoli, A. Rosati, R. J. Stouffer, V. Balaji, J. A. Beesley, W. F. Cooke, K. W. Dixon, J. Dunne, K. A. Dunne, J. W. Durachta, K. L. Findell, P. Ginoux, A. Gnanadesikan, C. T. Gordon, S. M. Griffies, R. Gudgel, M. J. Harrison, I. M. Held, R. S. Hemler, L. W. Horowitz, S. A. Klein, T. R. Knutson, P. K. Kushner, A. R. Langenhorst, H-C. Lee, S-J. Lin, J. Lu, S. L. Malyshev, P. C. D. Milly, V. Ramaswamy, J. Russell, M. D. Schwarzkopf, E. Shevlakova, J. J. Sirutis, M. J. Spelman, W. F. Stern, M. Winton, A. T. Wittenberg, B. Wyman, F. Zeng, and R. Zhang. 2006. "GFDL's CM2 global coupled climate models. Part I: Formulation and simulation characteristics." *Journal of Climate* 19:643–674.

Dettinger, M. D., D. R. Cayan, M. Meyer, and A. E. Jeton. 2004. "Simulated hydrologic responses to climate variations and change in the Merced, Carson, and American River basins, Sierra Nevada, California, 1900–2099." *Climatic Change* 62:283–317.

Flint, L. E. and A. L. Flint. In review. Climate Change in SF Bay Area Watersheds: Case Studies in the Russian River Valley and Santa Cruz Mountains.

Flint, A. L., L. E. Flint, and M. D. Masbruch. 2011. Input, calibration, uncertainty, and limitations of the Basin Characterization Model: Appendix 3 of Conceptual Model of the Great Basin Carbonate and Alluvial Aquifer System (eds. V. M. Heilweil, and L. E. Brooks), U.S. Geological Survey Scientific Investigations Report 2010–5193.

Flint L. E., and Flint A. L. 2012. "Downscaling future climate scenarios to fine scales for hydrologic and ecologic modeling and analysis." *Ecological Processes* 1:2.

Flint, A. L., L. E. Flint, and M. D. Masbruch. 2011. Input, calibration, uncertainty, and limitations of the Basin Characterization Model: Appendix 3 of Conceptual Model of the Great Basin Carbonate and Alluvial Aquifer System (eds. V. M. Heilweil, and L. E. Brooks), U.S. Geological Survey Scientific Investigations Report 2010–5193.

Flint, L. E., and A. L. Flint. 2007. Regional analysis of ground-water recharge. In *Ground-water recharge in the arid and semiarid southwestern United States.* Stonestrom, D. A., J. Constantz, T. P. A. Ferré, and S. A. Leake (eds). U.S. Geol Surv Prof Paper 1703: 29–59.

Flint, L. E., and A. L. Flint. 2006. Impacts of Tioga Road on groundwater flow in Tuolumne Meadows: Preliminary conceptual model and numerical analysis: Chapter 5 in Cooper, D. J., J. D. Lundquist, J. King, A. L. Flint, L. E. Flint, E. Wolf, and F. C. Lott. *Effects of the Tioga Road on hydrologic processes and Lodgepole Pine invasion into Tuolumne Meadows, Yosemite National Park.* Report prepared for Yosemite National Park. December 2006. 142 p.

Flint, A. L., L. E. Flint, J. A. Hevesi, and J. M. Blainey. 2004. Fundamental concepts of recharge in the Desert Southwest: A regional modeling perspective, in *Groundwater Recharge in a Desert Environment: The Southwestern United States,* edited by J. F. Hogan, F. M. Phillips, and B. R. Scanlon, Water Science and Applications Series, Vol. 9, American Geophysical Union, Washington, D.C., 159–184.

Flint, A. L., L. E. Flint, E. M. Kwicklis, J. T. Fabryka-Martin, and G. S. Bodvarsson. 2002. "Estimating recharge at YuccaMountain, Nevada, USA, comparison of methods." *Hydrogeology Journal* 10:180–204.

Flint, A. L., and S. W. Childs. 1987. "Calculation of solar radiation in mountainous terrain." *Journal of Agricultural Forestry Meteorology* 40:233–249.

Fowler, H. J., S. Blenkinsop, and C. Tebaldi. 2007. "Linking climate change modelling to impacts studies: Recent advances in downscaling techniques for hydrological modelling." *International Journal of Climatology* 27:1547–1578.

Franklin, J. 2010. Data for species distribution models; the environmental data. Chapter 5 in *Mapping Species Distributions: Spatial Inference and Prediction (Ecology, Biodiversity and Conservation).* Cambridge University Press: New York, 324 p.

Gee, G. W. and D. Hillel. 1988. "Groundwater recharge in arid regions: Review and critique of estimation methods." *Hydrological Processes* 2:255–266.

Girvetz E. H., C. Zganjar, G. T. Raber, E. P. Maurer, P. Kareiva, and J. J. Lawler. 2009. "Applied Climate-Change Analysis: The Climate Wizard Tool." *PLoS ONE* 4(12): e8320.doi:10.1371/journal.pone.0008320.

Guisan, A., and W. Thuiller. 2005. Predicting species distribution: Offering more than simple habitat models. *Ecology Letters* 8:993–1009.

Hannah, Lee, M. R. Shaw, Makihiko Ikegami, Patrick R Roehrdanz, Oliver Soong, and James Thorne. 2012. Consequences of Climate Change for Native Plants and Conservation. California Energy Commission. Publication number: CEC-500-2012-024.

Hay, L. E., S. L. Markstrom, and C. Ward-Garrison. 2011. "Watershed-scale response to climate change through the twenty-first century for selected basins across the United States." *Earth Interactions* 15(17): 1–37. Available online at http://EarthInteractions.org.

Heller, N. E., and E. S. Zavaleta. 2009. "Biodiversity management in the face of climate change: A review of 22 years of recommendations." *Biological Conservation* 142:14–32.

Hevesi, J. A., A. L. Flint, and L. E. Flint. 2003. *Simulation of net infiltration and potential recharge using a distributed-parameter watershed model of the Death Valley region, Nevada and California.* U.S. Geological Survey Water Resources Investigations Report 03–4090, 161 p.

Hickman, J. C. 1993. *The Jepson Manual: Higher plants of California.* University of California Press: Berkeley, California.

Hidalgo H., M. D. Dettinger, and D. R. Cayan. 2008. *Downscaling with constructed analogues-Daily precipitation and temperature fields over the United States.* California Energy Commission Report No. CEC-500-2007-123.

Hillel, D. 1980. *Fundamentals of soil physics.* Academic Press: New York.

Hopp, L. and J. J. McDonnell. 2009. "Connectivity at the hillslope scale: Identifying interactions between storm size, bedrock permeability, slope angle and soil depth." *Journal of Hydrology* 376:378–391.

Hutchinson, D. G. and R. D. Moore. 2000. "Throughflow variability on a forested hillslope underlain by compacted glacial till." *Hydrological processes* 14:1751–1766.

IPCC (Intergovernmental Panel on Climate Change). 2001. Climate change 2001, the third assessment report (AR3) of the United Nations Intergovernmental Panel on Climate Change. http://www.ipcc.ch/publications_and_data/publications_and_data_reports.htm.

IPCC. 2007. Climate Change 2007, the fourth assessment report (AR4) of the United Nations Intergovernmental Panel on Climate Change. http://www.ipcc.ch/publications_and_data/publications_and_data_reports.htm.

Iqbal, Muhammad. 1983. *An Introduction to Solar Radiation.* Academic Press: Toronto; New York.

Jackson, L., V. R. Haden, S. M. Wheeler, A. D. Hollander, J. Perlman, T. Oackso, V. K. Mehta, V. Clark, J. Williams, and A. Thrupp (University of California, Davis). 2012. Vulnerablity and Adaptation to Climate Change in California Agriculture. California Energy Commission. Publication number: CEC-500-2012-031.

Jennings, C. W. 1977. Geologic map of California: California Division of Mines and Geology Geologic Data Map Number 2, scale 1:750,000.

Jones, J. P., E. A. Sudicky, and R. G. McLaren. 2008. "Application of a fully-integrated surface-subsurface flow model at the watershed-scale: A case study." *Water Resources Research* 44: W03407, 13 pp.

Koczot, K. M., S. L. Markstrom, and L. E. Hay. 2011. "Effects of Baseline Conditions on the Simulated Hydrologic Response to Projected Climate Change." *Earth Interact* 15: 1–23.

Krawchuk, M., and M. Moritz. 2012. Fire and Climate Change in California: Changes in the Distribution and Frequency of Fire in Climates of the Future and Recent Past (1911–2099). California Energy Commission. Publication number: CEC-500-2012-026.

Lawler, J. J., and S. L. Shafer, D. White, P. Kareiva, E. P. Maurer, et al. 2009. "Projected climate-induced faunal change in the Western Hemisphere." *Ecology* 90:588–597.

Leavesley, G. H., M. D. Branson, and L. E. Hay. 1992. Using coupled atmospheric and hydrologic models to investigate the effects of climate change in mountainous regions. Managing Water Resources during Global Change, R. Herrmann, ed., 691–700.

Legates, D. R., and G. J. McCabe, Jr. 1999. "Evaluating the use of 'goodness-of-fit' measures in hydrologic and hydroclimatic model validation." *Water Resources Research* 35:233–241.

Lenihan, J. M., R. Drapek, D. Bachelet, and R. P. Neilson. 2003. "Climate change effects on vegetation distribution, carbon, and fire in California." *Ecological Applications* 13:1667–1681.

Liang, X., D. P. Lettenmaier, E. Wood, and S. J. Burges. 1994. "A Simple Hydrologically Based Model of Land Surface Water and Energy Fluxes for General Circulation Models." *Journal of Geophysical Research* 99:14415–14428.

Loarie, S. R., P. B. Duffy, H. Hamilton, G. P. Asner, C. B. Field, and D. D. Ackerly. 2009. "The velocity of climate change." *Nature* 462:1052–1055.

Lundquist, J. D., D. R. Cayan, and M. D. Dettinger. 2004. "Spring onset in the Sierra Nevada: When is snowmelt independent of elevation?" *Journal of Hydrometeorology* 5: 327–342.

Lutz, J. A., J. W. van Wagtendonk, and J. F. Franklin. 2010. "Climatic water deficit, tree species ranges, and climate change in Yosemite National Park." *Journal of Biogeography* 37:936–950.

Maurer, E. P., L. D. Brekke, and T. Pruitt. 2010. "Contrasting lumped and distributed hydrology models for estimating climate change impacts on California watersheds." *Journal of the American Water Resources Association* 46: 1024–1035. DOI: 10.1111/j.1752-1688.2010.00473.x.

Meehl, G. A., W. M. Washington, T. M. L. Wigley, J. M. Arblaster, and A. Dai. 2003. "Solar and greenhouse gas forcing and climate response in the twentieth century." *Journal of Climate* 16: 426–444.

Micheli, E., L. E. Flint, A. L. Flint, S. Weiss, and M. Kennedy. In Review. Downscaling future climate projections to the watershed scale: A North San Francisco Bay Estuary case study.

Millar, C. I., R. D. Westfall, D. L. Delany, M. J. Bokach, A. L. Flint, and L. E. Flint. *Accepted*. Forest mortality in high-elevation whitebark pine (Pinus albicaulis) forest of eastern California, USA: Influence of environmental context, bark-beetles, soil-moisture stress, and warming. *Canadian Journal of Forestry Research.*

Mittelbach, H., F. Casini, I. Lehner, A. J. Teuling, and S. I. Seneviratne. 2011. "Soil moisture monitoring for climate research: Evaluation of a low-cost sensor in the framework of the Swiss Soil Moisture Experiment (SwissSMEX) campaign." *Journal of Geophysical Research* 116: D05111, 11p. doi:10.1029/2010JD014907.

Nakic'enovic', N., J. Alcamo, G. Davis, B. de Vries, J. Fenhann, S. Gaffin, K. Gregory, A. Grubler, T. Y. Jung, and T. Kram. 2000. *Intergovernmental Panel on Climate Change Special Report on Emissions Scenarios.* Cambridge University Press: Cambridge, U.K. http://www.grida.no/publications/other/ipcc_sr/?src=/climate/ipcc/emission/index.htm .

Nalder, I. A., and R. W. Weins. 1998. "Spatial interpolation of climatic normals, test of a new method in the Canadian boreal forest." *Agricultural and Forest Meteorology* 92: 211– 225. DOI:10.1126/science.1151915.

Nash, J. E., and J. V. Sutcliffe. 1970. "River flow forecasting through conceptual models, I , A discussion of principles." *Journal of Hydrology* 10:282–290.

NRCS (Natural Resources Conservation Service). 2006. U.S. General Soil Map (STATSGO2). http://www.ftw.nrcs.usda.gov/stat_data.html, http://soils.usda.gov/survey/geography/statsgo/description.html.

Parmesan, C. 2006. "Ecological and evolutionary responses to recent climate change." *Annual Review of Ecology and Evolutionary Systematics* 37:637–669.

Pierce, D. W., T. P. Barnett, B. D. Santer, and P. J. Gleckler. 2009. "Selecting global climate models for regional climate change studies." *Proceedings of the National Academy of Sciences.* doi:10.1073/pnas.0900094106.

Priestley, C.H.B., and R.J. Taylor. 1972. On the assessment of surface heat flux and evaporation using large-scale parameters. *Monthly Weather Review* 100:81–92.

Purkey, D. R., B. Joyce, S. Vicuna, M. W. Hannemann, L. L. Dale, D. Yates, and J. A. Dracup. 2008. "Robust analysis of future climate change impacts on water for agriculture and other sectors: A case study in the Sacramento Valley." *Climactic Change* 87:S109–S122.

Ragab, R. 1996. Constraints and applicability of irrigation scheduling under limited water resources, variable rainfall and saline conditions. Food and Agricultural Organization of the United Nations (FAO) (ed.). Irrigation scheduling: From theory to Practice. Rome, Italy 149–165.

Rislsey, J., H. Moradkhani, L. Hay, and S. Markstrom. 2011. "Statistical comparisons of watershed-scale response to climate change in selected basins across the United States." *Earth Interactions* 15(14):1–26.

Ryu, Y., D. D. Baldocchi, S. Ma, and T. Hehn. 2008. "Interannual variability of evapotranspiration and energy exchange over an annual grassland in California." *Journal of Geophysical Research* 113: D09104, 16 p. doi:10.1029/2007JD009263.

Sanford W. E., L. N. Plummer, D. P. McAda, L. M. Bexfield, and S. K. Anderholm. 2001. Estimation of hydrologic parameters for the groundwater model of the Middle Rio Grande Basin using carbon-14 and water-level data. In: Cole, J. C. (ed) U.S. Geological Survey Middle Rio Grande Basin Study: Proceedings of the Fourth Annual Workshop, Albuquerque, New Mexico, 15–16 February 2000. US Geol Surv Open-File Rep 00-488, p 4–6.

Santos, M. J., C. Moritz, J. H. Thorne (UC Berkeley, UC Davis). 2012. Identifying Vulnerable Species and Adaptation Strategies in the Southern Sierra of California Using Historical Resurveys**.** California Energy Commission. Publication number: CEC-500-2012-025.

SSURGO. Soil Survey Staff, Natural Resources Conservation Service, United States Department of Agriculture. Soil Survey Geographic (SSURGO) Database for California. Available online at http://soildatamart.nrcs.usda.gov.

Stephenson, N. L. 1998. "Actual evapotranspiration and deficit: Biologically meaningful correlates of vegetation distribution across spatial scales." *Journal of Biogeography* 25:855–870.

Stern, M. A., A. L. Flint, J. A. Curtis, and L. E. Flint. 2011. Comparison of 4-km and 800-m transient PRISM climate datasets and their influence on hydrologic modeling, AGU abstracts, AGU Annual Meetings, Dec. 2011, San Francisco. *Presentation accepted.*

Stouffer, R. J., A. J. Broccoli, T. L. Delworth, K. W. Dixon, R. Gudgel, I. Held, R. Hemler, T. Knutson, H-C. Lee, M. D. Schwarzkopf, B. Soden, M. J. Spelman, M. Winton, and F. Zeng. 2006. "GFDL's CM2 global coupled climate models. Part IV: Idealized climate response." *Journal of Climate* 19:723–740.

Trnka, M., J. E. Olesen, K. C. Kersebaum, A. O. Skjelvag, J. Eitzinger, B. Seguin, P. Peltonen-Sainio, R. Rotter, A. Iglesias, S. Orlandini, M. Dubrovsky, P. Hlavinka, J. Balek, H. Eckersten, E. Cloppet, P. Calanca, A. Gobin,V. Vucetic, P. Nejedlik, S. Kumar, B. Lalic, A. Mestre, F. Rossi, J. Kozyra, V. Alexandrov, D. Semeradova, and Z. Zalud. 2012. "Agroclimatic conditions in Europe under climate change." *Global Change Biology* 17: 2298–2318.

Tromp-van Meerveld, H. J., N. E. Peters, and J. J. McDonnell. 2007. "Effect of bedrock permeability on subsurface stormflow and the water balance of a trenched hillslope at the Panola Mountain Research Watershed, Georgia, USA." *Hydrological Processes* 21: 750–769.

UNEP (United Nations Environmental Programme). 1997. *World Atlas of Desertification.* Editorial commentary by N. Middleton and D. S. G. Thomas. London: Edward Arnold.

van Mantgem, P. J., and N. L. Stephenson. 2007. "Apparent climatically induced increase of tree mortality rates in a temperate forest." *Ecology Letters* 10:909–916.

Vicuña , S., E. P. Maurer, B. Joyce, J. A. Dracup, and D. Purkey. 2007. "The Sensitivity of California Water Resources to Climate Change Scenarios." *Journal of the American Water Resources Association* 43:482–498.

Washington, W. M., J. W. Weatherly, G. A. Meehl, A. J. Semtner, T. W. Bettge, A. P. Craig, W. G. Strand, J. Arblaster, V. B. Wayland, R. James, and Y. Zhang. 2000. "Parallel climate model (PCM) control and transient simulations." *Climate Dynamics* 16: 755–774.

Williams, J. N., C. Seo, J. H. Thorne, J. N., J. K. Nelson, S. Erwin, J. M. O'Brien, and M. W. Schwartz. 2009. "Using species distribution models to predict new occurrences for rare plants." *Diversity and Distributions* 15: 565–576.

Wood, A. W., E. P. Maurer, A. Kumar, and D. P. Lettenmaier. 2002. "Long range experimental hydrologic forecasting for the eastern U.S." *J. Geophys. Res*. 107: 4429. doi:10.1029/2001JD000659.

Zar, Jerrold H., 1999. *Biostatistical Analysis - 4th Edition.* Prentice-Hall: New Jersey.

Glossary

AET	Actual Evapotranspiration
AZMET	Arizona Meteorological Network
BCM	Basin Characterization Model
CALSIM	A Water Resources Simulation Model
CIMIS	California Irrigation Management Information System
CMIP3	Coupled Model Intercomparison Project Phase 3
CWD	Climate Water Deficit
GCM	Global Climate Model
GFDL	Geophysical Fluid Dynamics Laboratory
GIDS	Gradient-Inverse-Distance-Squared
HUC	USGS hydrologic unit code
IPCC	Intergovernmental Panel on Climate Change
ISBA-TRIP	Interactions between Soil, Biosphere, and Atmosphere-Total Runoff Integrating Pathways
MODIS	Moderate Resolution Imaging Spectroradiometer
MPa	megapascals
NCAR	National Center for Atmospheric Research
NOAA	National Oceanic and Atmospheric Administration
NRCS	Natural Resources Conservation Service
NREL	National Renewable Energy Laboratory
NSS	Nash-Sutcliffe efficiency statistic
PCM	Parallel Climate Model
PET	potential evapotranspiration equations
PIER	Public Interest Energy Research
PRMS	Precipitation-Runoff Modeling System
RCH	recharge
SD	standard deviation
SSURGO	County-level soils maps
STATSGO	State Soil Geographic dataset
V&A	Vulnerability and Adaptation
UC	University of California
UNEP	United Nations Environmental Programme
UNESCO	United Nations Educational, Scientific and Cultural Organization
U.S. DOE	U.S. Department of Energy
USGS	U.S. Geological Survey
VIC	Variable Infiltration Capacity model
WCRP	World Climate Research Programme
WEAP	Water Evaluation And Planning
WEHY	Watershed Environmental Hydrology

Appendix A: Input Files and Output Files for the Basin Characterization Model

The following graphic (Figure A1) shows the needed input variables and datasets to run the different modules of the BCM.

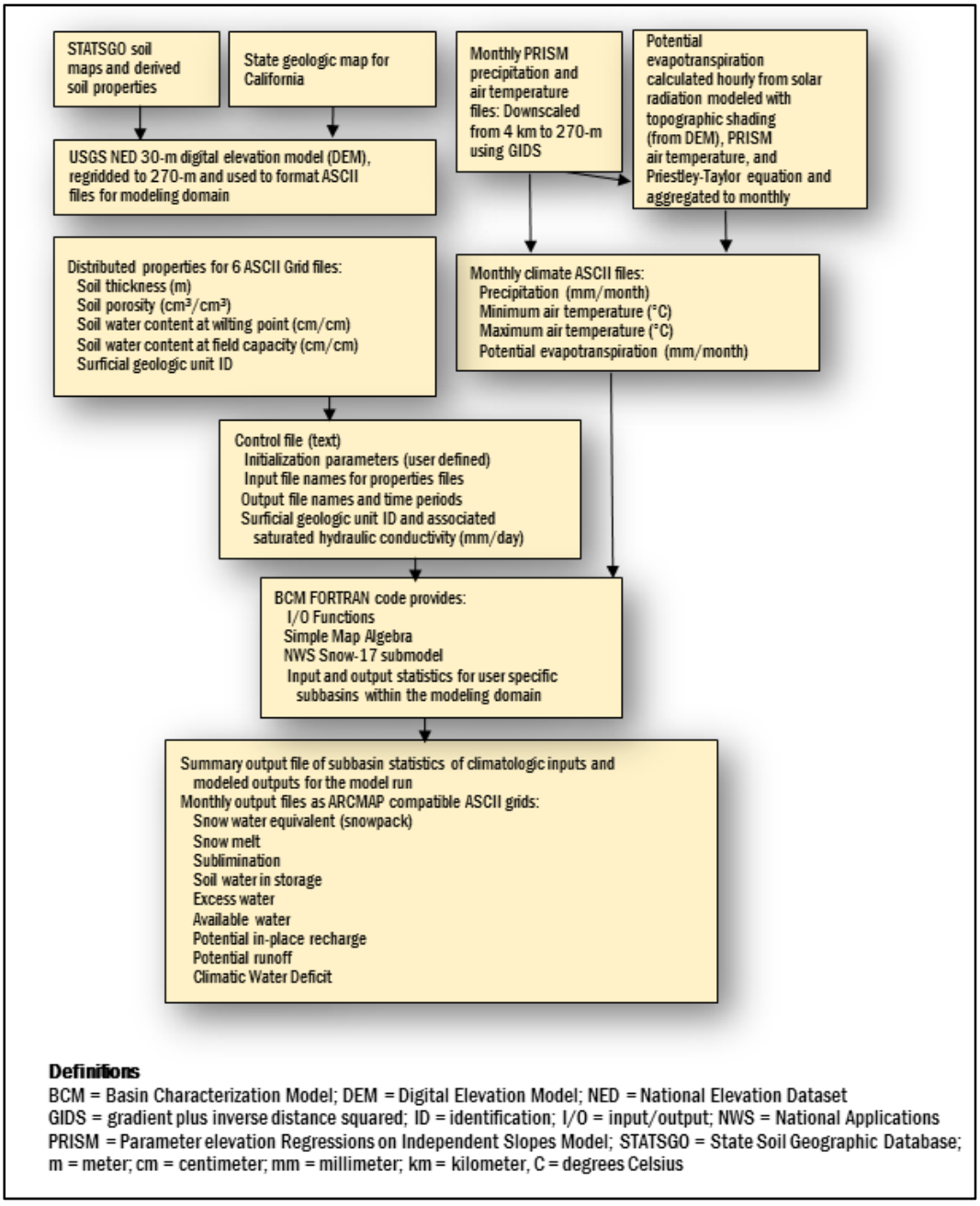

Figure A1. Flow Chart for the Basin Characterization Model Showing Needed Input Variables and Datasets

Appendix B: Description of Input and Output Variables for the Basin Characterization Model

Table B1. The input and output variables used and produced by modules of the BCM.

Variable	Code	Creation Method	Units	Equation/model	Description
Maximum air temperature	tmax	downscaled	degree C	Model input	The maximum monthly air temperature
Minimum air temperature	tmin	downscaled	degree C	Model input	The minimum monthly air temperature
Precipitation	ppt	downscaled	mm	Model input	Total monthly precipitation (rain or snow)
Potential evapotrans-piration	pet	Modeled/ pre-processed	mm	Model input	Total amount of water that can evaporate from ground surface or be transpired by plants
Snowfall	snow	BCM	mm	Precipitation if tmin below 1.5 degrees C	Amount of snow that fell
Snowpack	pck	BCM	mm	Prior month pck + snow – subl - melt	Amount of snow that accumulated per month
Sublimation	subl	BCM	mm	Calculated, applied to pck	Amount of snow lost to sublimation (snow to water vapor)
Snowmelt	melt	BCM	mm	Calculated, applied to pck	Amount of snow that melted (snow to liquid water)
Excess water	exc	BCM	mm	ppt – pet	Amount of water remaining in system, assuming potential evapotranspiration consumes maximum amount of water, for positive months only
Soil water storage	stor	BCM	mm	ppt + melt – aet – rch - run	Average amount of water stored in the soil
Actual evapotrans-piration	aet	BCM	mm	Changes in stor between field capacity and wilting point	Amount of water that evaporates and is transpired that is available in soil water storage above wilting point
Climatic water deficit	cwd	BCM	mm	pet-aet	Annual evaporative demand that exceeds available water
Runoff	run	BCM	mm	Amount of water that exceeds total stor + rejected recharge	Amount of water that becomes runoff
Recharge	rch	BCM	mm	Amount of water exceeding field capacity that enters bedrock at the rate of bedrock permeability	Amount of water that penetrates below the root zone

Appendix C: Streamgages Used for Study Basins in California for the Basin Characterization Model, Including Calibration Parameters, and Goodness-of-fit Statistics.

Table C1. This Table Lists All the Streamgages Used in the Calibration and Validation Analyses. A total of 139 gages were used, presented with their calibration parameters and goodness of fit statistics. There are 68 calibration, and 71 validation gages in the study.

							Calibration Parameters			Goodness-of-fit Statistics				
	NWIS station ID	Latitude (decimal degree)	Longitude (decimal degree)	Years of record	Jepson ecoregion	Area km2	Baseflow exponent	Runoff scaler	Recharge scaler	Mthly r2	Yrly r2	Nash-Sutcliffe Efficiency	% Urban	% Agriculture
Calibration Basins														
Aptos C A Aptos Ca	11159700	36.9763	-121.9035	14	Central Western CA	12	0.960	0.20	0.50	0.79	0.78	0.69	21.4%	0.1%
Aptos C Nr Aptos Ca	11159690	37.0016	-121.9071	14	Central Western CA	10	0.970	0.40	0.50	0.70	0.85	0.52	0.3%	0.3%
Arroyo Corte Madera D Pres A Mill Valley Ca	11460100	37.8971	-122.5372	20	Central Western CA	5	0.980	0.90	0.80	0.87	0.95	0.87	53.3%	0.0%
Arroyo Hondo Nr San Jose Ca	11173200	37.4615	-121.7705	18	Central Western CA	77	0.960	1.00	0.90	0.79	0.87	0.79	0.3%	0.0%
Arroyo Valle Bl Lang Cn Nr Livermore Ca	11176400	37.5613	-121.6849	36	Central Western CA	130	0.950	0.70	0.30	0.70	0.81	0.68	0.5%	1.0%
Bear C A Boulder C Ca	11160060	37.1277	-122.1180	15	Central Western CA	16	0.950	0.60	0.50	0.69	0.92	0.62	4.1%	0.6%
Boulder C At Boulder Creek Ca	11160070	37.1266	-122.1238	16	Central Western CA	11	0.960	0.70	0.70	0.86	0.96	0.83	12.4%	0.0%
Corralitos C A Freedom Ca	11159200	36.9394	-121.7716	43	Central Western CA	28	0.910	0.30	0.40	0.71	0.85	0.67	18.0%	26.7%
Corralitos C Nr Corralitos Ca	11159150	37.0055	-121.8091	15	Central Western CA	11	0.940	0.65	0.40	0.66	0.87	0.66	0.3%	1.5%

Coyote C Nr Gilroy Ca	11169800	37.0777	-121.4954	22	Central Western CA	109	0.970	1.00	0.30	0.69	0.82	0.68	0.2%	0.5%
Cull C Ab Cull C Res Nr Castro Valley Ca	11180960	37.7176	-122.0555	21	Central Western CA	6	0.940	0.90	0.60	0.72	0.88	0.70	2.2%	0.0%
Laguna C Nr Davenport Ca	11161590	37.0255	-122.1321	7	Central Western CA	3	0.970	0.40	0.60	0.57	0.88	0.54	8.1%	0.0%
Lagunitas C A Sp Taylor State Pk Ca	11460400	38.0268	-122.7375	17	Central Western CA	34	0.981	0.60	0.90	0.73	0.83	0.64	8.6%	0.0%
Little Pine C Nr Alamo Ca	11183700	37.8848	-121.9788	15	Central Western CA	1	0.930	0.80	0.20	0.65	0.91	0.65	1.9%	0.0%
Majors C Nr Santa Cruz Ca	11161570	36.9985	-122.1224	7	Central Western CA	4	0.960	0.40	0.70	0.75	0.88	0.75	7.3%	0.5%
Marsh C Nr Byron Ca	11337500	37.8732	-121.7282	31	Central Western CA	43	0.940	0.75	0.40	0.53	0.72	0.45	1.9%	0.5%
Novato C A Novato Ca	11459500	38.1076	-122.5811	53	Central Western CA	18	0.910	0.80	0.30	0.65	0.90	0.63	15.6%	0.1%
Pilarcitos C A Half Moon Bay Ca	11162630	37.4665	-122.4352	33	Central Western CA	27	0.950	0.60	0.60	0.73	0.81	0.67	6.2%	3.8%
Pinole C A Pinole Ca	11182100	37.9723	-122.2474	39	Central Western CA	10	0.950	0.80	0.55	0.71	0.91	0.69	3.0%	0.9%
San Antonio C Nr Petaluma Ca	11459300	38.1823	-122.6175	6	Central Western CA	29	0.930	0.80	0.50	0.89	0.96	0.89	0.5%	8.9%
San Benito R Nr Willow Creek School Ca	11156500	36.6094	-121.2040	60	Central Western CA	249	0.960	0.30	0.40	0.62	0.88	0.60	0.2%	0.2%
San Lorenzo R A Big Trees Ca	11160500	37.0443	-122.0735	63	Central Western CA	106	0.950	0.10	0.20	0.78	0.93	0.78	17.0%	0.1%
San Lorenzo R A Santa Cruz Ca	11161000	36.9907	-122.0330	20	Central Western CA	115	0.940	0.10	0.20	0.73	0.91	0.73	29.6%	0.3%
San Lorenzo R Nr Boulder C Ca	11160020	37.2066	-122.1460	24	Central Western CA	6	0.960	0.50	0.60	0.76	0.89	0.67	0.2%	0.0%
San Ramon C A San Ramon Ca	11182500	37.7729	-121.9958	47	Central Western CA	6	0.940	0.90	0.70	0.69	0.87	0.68	8.7%	0.0%
San Vicente C Nr Davenport Ca	11161800	37.0552	-122.1833	16	Central Western CA	6	0.970	0.35	0.70	0.57	0.82	0.33	8.7%	2.1%
Saratoga C A Saratoga Ca	11169500	37.2543	-122.0405	66	Central Western CA	9	0.940	0.70	0.45	0.70	0.91	0.66	9.2%	0.8%
Scott C Ab Little C Nr Davenport Ca	11161900	37.0641	-122.2305	15	Central Western CA	25	0.960	0.65	0.60	0.74	0.93	0.72	1.2%	0.1%
Soquel C A Soquel Ca	11160000	36.9913	-121.9569	49	Central Western CA	40	0.970	0.93	0.60	0.80	0.88	0.76	6.0%	3.3%
Uvas C Ab Uvas Res Nr Morgan Hill Ca	11153900	37.0927	-121.7193	21	Central Western CA	21	0.950	0.75	0.70	0.75	0.89	0.72	0.5%	0.0%

Wb Soquel C Nr Soquel Ca	11159800	37.0513	-121.9402	14	Central Western CA	12	0.960	0.50	0.70	0.85	0.89	0.81	7.0%	3.3%
Zayante C A Zayante Ca	11160300	37.0860	-122.0480	35	Central Western CA	11	0.950	0.60	0.60	0.77	0.91	0.71	4.7%	0.0%
Austin C Nr Cazadero Ca	11467200	38.5012	-123.0703	8	North Western CA	63	0.960	0.90	0.80	0.89	0.94	0.88	1.2%	0.0%
Bear C Nr Rumsey Ca	11451720	38.9448	-122.3472	25	North Western CA	100	0.950	0.80	0.40	0.85	0.91	0.85	0.2%	3.3%
Brush C A Santa Rosa CA	11466065	38.4550	-122.6800	5	North Western CA	10	0.960	1.00	1.00	0.97	0.86	0.75	43.0 %	2.4%
Dry C Nr Cloverdale Ca	11464500	38.7495	-123.0933	39	North Western CA	88	0.940	0.60	0.60	0.92	0.96	0.92	0.0%	0.0%
Dry C Nr Napa Ca	11457000	38.3562	-122.3661	16	North Western CA	17	0.940	0.90	0.60	0.74	0.93	0.74	0.1%	5.7%
Dry C Nr Yorkville Ca	11464400	38.7890	-123.1567	10	North Western CA	56	0.940	0.90	0.80	0.91	0.99	0.91	0.1%	0.7%
Ef Russian R Nr Ukiah Ca	11462000	39.1973	-123.1886	49	North Western CA	105	0.940	1.00	0.80	0.60	0.91	0.58	1.1%	9.0%
Feliz C Nr Hopland Ca	11462700	38.9720	-123.1439	8	North Western CA	31	0.960	1.00	0.80	0.88	0.98	0.83	0.0%	1.1%
Franz C Nr Kellogg Ca	11463940	38.6082	-122.6958	5	North Western CA	16	0.940	0.90	1.00	0.88	0.99	0.88	0.2%	13.3%
Maacama C Nr Kellogg Ca	11463900	38.6401	-122.7647	21	North Western CA	43	0.950	0.90	0.60	0.90	0.96	0.90	0.2%	5.9%
Mark West C NR Mirabel Heights CA	11466800	38.4940	-122.8530	5	North Western CA	251	0.920	0.20	0.70	0.84	1.00	0.85	40.4 %	25.3%
Mark West C NR Windsor CA	11465500	38.5090	-122.7700	2	North Western CA	43	0.940	0.70	0.60	0.95	1.00	0.10	6.6%	1.1%
Matanzas C A Santa Rosa CA	11466170	38.4390	-122.7020	7	North Western CA	21	0.930	0.80	0.90	0.88	0.00	0.81	23.5 %	3.3%
Milliken C Nr Napa	11458100	38.3384	-122.2705	13	North Western CA	17	0.970	1.00	0.70	0.90	0.95	0.85	10.2 %	5.6%
Napa R Nr St Helena Ca	11456000	38.4976	-122.4291	60	North Western CA	81	0.930	0.40	0.90	0.85	0.95	0.85	10.4 %	21.6%
Nf Cache C Nr Lower Lake Ca	11451500	39.0190	-122.5700	51	North Western CA	197	0.930	0.35	0.60	0.63	0.74	0.59	0.9%	0.4%
Pena C Nr Geyserville Ca	11465150	38.7004	-122.9733	12	North Western CA	22	0.930	1.00	0.90	0.87	0.97	0.86	0.0%	0.7%
Redwood C Nr Napa Ca	11458200	38.3176	-122.3452	15	North Western CA	10	0.940	0.90	0.70	0.83	0.89	0.82	1.6%	26.1%
Russian R Nr Redwood Valley Ca	11460940	39.3192	-123.2245	5	North Western CA	14	0.960	1.00	0.80	0.93	0.98	0.90	0.4%	1.2%

Russian R Nr Ukiah Ca	11461000	39.1953	-123.1961	49	North Western CA	100	0.960	0.90	0.40	0.90	0.93	0.89	4.1%	8.7%
Sonoma C A Agua Caliente Ca	11458500	38.3232	-122.4955	27	North Western CA	58	0.950	0.90	0.60	0.86	0.94	0.86	7.1%	17.3%
Warm Springs C Nr Asti Ca	11464860	38.6959	-123.0978	10	North Western CA	12	0.950	1.00	0.90	0.90	1.00	0.89	0.0%	0.0%
Big C Ab Pine Flat Res Nr Trimmer Ca	11220000	36.9163	-119.2455	20	Sierra Nevada	70	0.960	0.90	1.00	0.86	0.93	0.86	0.0%	0.0%
Big C Ab Whites Gulch Nr Groveland Ca	11284400	37.8418	-120.1859	31	Sierra Nevada	16	0.920	0.80	0.50	0.76	0.85	0.76	0.3%	0.0%
Kings R Ab Nf Nr Trimmer Ca	11213500	36.8632	-119.1252	53	Sierra Nevada	952	0.950	1.00	1.00	0.47	0.92	0.39	0.0%	0.0%
Merced R A Happy Isles Bridge Nr Yosemite Ca	11264500	37.7315	-119.5598	84	Sierra Nevada	181	0.940	1.00	0.80	0.67	0.92	0.57	0.0%	0.0%
Merced R A Pohono Bridge Nr Yosemite Ca	11266500	37.7168	-119.6673	83	Sierra Nevada	321	0.940	0.40	0.70	0.65	0.92	0.28	0.2%	0.0%
Nf Tuolumne R Nr Long Barn Ca	11284700	38.0987	-120.1007	24	Sierra Nevada	23	0.940	0.90	0.70	0.81	0.94	0.78	2.9%	0.0%
Nf Willow C Nr Sugar Pine Ca	11242400	37.3977	-119.5672	34	Sierra Nevada	17	0.960	0.70	0.70	0.57	0.78	0.41	0.0%	0.0%
Sf Kaweah R A Three Rivers Ca	11210100	36.4166	-118.9152	32	Sierra Nevada	87	0.930	0.90	0.60	0.70	0.93	0.68	0.1%	0.0%
Guejito C Nr San Pasqual	11027000	33.1159	-116.9539	35	Southwester n CA	23	0.930	0.70	0.50	0.67	0.71	0.17	0.4%	2.1%
Los Penasquitos C Bl Poway C Nr Poway Ca	11023330	32.9493	-117.0709	24	Southwester n CA	31	0.980	1.00	1.00	0.81	0.88	0.80	48.2 %	2.3%
San Diego R A Fashion Valley At San Diego Ca	11023000	32.7651	-117.1695	18	Southwester n CA	429	0.960	0.20	0.80	0.84	0.95	0.83	72.6 %	0.0%
San Diego R A Mast Rd Nr Santee Ca	11022480	32.8404	-117.0267	86	Southwester n CA	368	0.960	0.25	0.75	0.79	0.86	0.79	19.6 %	1.7%
Santa Maria C Nr Ramona Ca	11028500	33.0523	-116.9464	61	Southwester n CA	58	0.960	1.00	0.50	0.79	0.84	0.65	24.1 %	17.5%
Santa Ysabel C Nr Ramona Ca	11025500	33.1070	-116.8670	68	Southwester n CA	112	0.950	0.40	0.40	0.55	0.70	0.92	0.6%	0.8%
					mean	77	0.949	0.70	0.63	0.76	0.88	0.71	8.5%	3.4%
					unimpaired only		0.950	0.87	0.83	0.73	0.92	0.67	0%	0%

Validation basins

							Calibration Parameters			Goodness-of-fit Statistics				
	NWIS station ID	Latitude (decimal degree)	Longitude (decimal degree)	Years of record	Jepson ecoregion	Area km2	Baseflow exponent	Runoff scaler	Recharge scaler	Mthly r2	Yrly r2	Nash-Sutcliffe Efficiency	% Urban	% Agriculture
Antelope C Nr Tennant Ca	11489500	41.5464	-121.9194	27	Cascade Ranges	19	0.970	0.70	0.50	0.73	0.87	0.72	0.0%	0.0%
Cottonwood C A Hornbrook Ca	11516600	41.9181	-122.5648	7	Cascade Ranges	90	0.940	1.00	0.70	0.53	0.87	0.51	1.5%	0.6%
Deer C Bl Slate C Nr Deer Creek Meadows Ca	11382550	40.2337	-121.4661	9	Cascade Ranges	69	0.979	0.70	0.30	0.23	0.85	0.07	0.1%	0.0%
Hat C Nr Hat Creek Ca	11355500	40.6864	-121.4258	68	Cascade Ranges	162	0.981	0.20	0.30	0.31	0.31	0.31	0.0%	0.2%
Little Shasta R Nr Montague Ca	11516900	41.7528	-122.3017	21	Cascade Ranges	48	0.970	0.25	0.35	0.46	0.55	0.40	0.0%	0.0%
Pine C Nr Susanville Ca	10359300	40.6648	-120.7924	20	Cascade Ranges	226	0.940	0.35	0.20	0.22	0.72	0.55	0.0%	0.0%
Squaw C Ab Shasta Lk Ca	11365500	40.8567	-122.0878	22	Cascade Ranges	64	0.970	1.00	0.70	0.78	0.96	0.59	0.0%	0.0%
Alamo C Nr Nipomo Ca	11137400	35.0486	-120.3034	20	Central Western CA	83	0.900	0.60	0.50	0.57	0.71	0.50	0.0%	0.0%
Arroyo Seco Nr Greenfield Ca	11151870	36.2374	-121.4826	25	Central Western CA	113	0.980	1.00	1.00	0.78	0.90	0.70	0.0%	0.0%
Big Sur R Nr Big Sur Ca	11143000	36.2458	-121.7744	50	Central Western CA	47	0.983	1.00	1.00	0.68	0.90	0.63	0.1%	0.0%
Cantua C Nr Cantua Creek Ca	11253310	36.4021	-120.4345	33	Central Western CA	46	0.930	0.38	0.20	0.53	0.78	0.52	0.2%	0.0%
Estrella R Nr Estrella Ca	11148500	35.7172	-120.6412	42	Central Western CA	922	0.930	0.35	0.40	0.67	0.80	0.56	0.3%	3.1%
Pescadero C Nr Pescadero Ca	11162500	37.2607	-122.3299	49	Central Western CA	46	0.950	0.90	0.70	0.79	0.93	0.79	1.1%	0.1%
Sisquoc R Nr Sisquoc Ca	11138500	34.8397	-120.1692	57	Central Western CA	281	0.960	0.40	0.30	0.62	0.75	0.07	0.0%	0.0%
Sf Pit R Nr Likely Ca	11345500	41.2306	-120.4382	71	Modoc Plateau	247	0.978	0.60	0.40	0.59	0.67	0.55	0.0%	0.2%
Sprague River Near Beatty Oreg.	11497500	42.4470	-121.2397	38	Modoc Plateau	513	0.997	1.00	1.00	0.57	0.81	0.56	0.0%	0.0%
Sprague River Near Chiloquin Oreg.	11501000	42.5844	-121.8509	79	Modoc Plateau	1580	0.996	0.10	0.40	0.49	0.69	0.33	0.0%	0.0%

Sycan River Below Snake Creek Nr Beatty Oreg.	11499100	42.4859	-121.2800	13	Modoc Plateau	568	0.980	0.60	1.00	0.59	0.89	0.59	0.0%	0.0%
Sycan River Near Beatty Oreg.	11499000	42.5497	-121.3189	9	Modoc Plateau	540	0.987	0.85	0.80	0.58	0.74	0.50	0.0%	0.0%
Williamson River Below Sheep Creek Nr Lenz Oreg.	11491400	42.9114	-121.4778	13	Modoc Plateau	205	0.997	0.20	0.55	0.47	0.89	0.47	0.0%	0.0%
Williamson River Near Klamath Agency Oreg.	11493500	42.7400	-121.8356	44	Modoc Plateau	1290	0.960	0.00	0.45	0.01	0.53	0.34	0.0%	0.0%
Wood River At Fort Klamath Oreg.	11504000	42.6997	-121.9856	18	Modoc Plateau	90	0.995	0.00	0.58	0.00	0.00	0.50	0.0%	0.0%
Beaver C Nr Klamath R Ca	11517800	41.8942	-122.8245	5	Northwest CA	106	0.970	0.50	0.60	0.84	0.97	0.84	0.0%	0.0%
Blue C Nr Klamath Ca	11530300	41.4497	-123.8968	13	Northwest CA	120	0.970	0.70	0.80	0.89	0.96	0.88	0.0%	0.0%
Bluff C Nr Weitchpec Ca	11523050	41.2400	-123.6593	7	Northwest CA	75	0.970	1.00	1.00	0.81	0.60	0.80	0.1%	0.0%
Elk C Nr Happy Camp Ca	11522200	41.7430	-123.3568	8	Northwest CA	90	0.970	0.30	0.50	0.65	0.96	0.83	0.0%	0.0%
Grass Valley C A Fawn Lodge Nr Lewiston Ca	11525600	40.6761	-122.8317	24	Northwest CA	31	0.970	0.30	0.70	0.81	0.94	0.80	0.1%	0.0%
Hayfork C Nr Hyampom Ca	11528500	40.6258	-123.4359	21	Northwest CA	378	0.950	0.50	0.90	0.77	0.94	0.67	0.4%	0.2%
Indian C Nr Happy Camp Ca	11521500	41.8350	-123.3843	43	Northwest CA	120	0.970	0.60	0.70	0.77	0.92	0.75	0.1%	0.0%
Mattole R Nr Petrolia Ca	11469000	40.3130	-124.2848	51	Northwest CA	245	0.970	1.00	1.00	0.93	0.92	0.82	0.2%	0.2%
Mf Cottonwood C Nr Ono Ca	11374400	40.3672	-122.5742	19	Northwest CA	244	0.950	0.70	0.70	0.78	0.94	0.72	0.1%	0.0%
Napa R At Calistoga Ca	11455900	38.5770	-122.5800	8	Northwest CA	22	0.950	1.00	0.70	0.89	0.98	0.88	5.6%	22.4%
Navarro R Nr Navarro Ca	11468000	39.1720	-123.6706	49	Northwest CA	303	0.960	1.00	1.00	0.93	0.95	0.91	0.3%	1.9%
Nf Cache C A Hough Spring Nr Clearlake Oaks Ca	11451100	39.1653	-122.6211	28	Northwest CA	60	0.960	1.00	0.60	0.76	0.85	0.72	0.0%	0.0%
Nf Stony C Nr Newville Ca	11387800	39.7845	-122.4783	11	Northwest CA	63	0.910	0.80	0.70	0.78	0.92	0.78	0.1%	0.1%
Nf Trinity R A Helena Ca	11526500	40.7817	-123.1295	26	Northwest CA	151	0.970	1.00	0.80	0.70	0.88	0.63	0.0%	0.0%
Putah C Nr Guenoc Ca	11453500	38.7787	-122.5186	51	Northwest CA	113	0.960	1.00	0.90	0.89	0.89	0.87	4.5%	6.1%

Red Cap C Nr Orleans Ca	11523030	41.2400	-123.5454	7	Northwest CA	56	0.970	0.70	0.50	0.65	0.86	0.40	0.0%	0.0%
Redwood C A Orick Ca	11482500	41.2991	-124.0524	48	Northwest CA	277	0.970	1.00	0.75	0.70	0.89	0.46	0.1%	0.0%
Salmon R A Somes Bar Ca	11522500	41.3775	-123.4787	76	Northwest CA	751	0.950	0.30	0.80	0.70	0.89	0.67	0.0%	0.0%
Scott R Nr Fort Jones Ca	11519500	41.6405	-123.0162	58	Northwest CA	653	0.970	0.70	0.80	0.71	0.96	0.69	0.4%	8.0%
Scotts C Nr Lakeport Ca	11449100	39.0953	-122.9628	20	Northwest CA	55	0.940	1.00	0.90	0.81	0.96	0.80	0.4%	5.7%
Sf Gualala R Nr Annapolis Ca	11467500	38.7048	-123.4242	25	Northwest CA	161	0.960	1.00	0.70	0.93	0.91	0.93	0.2%	0.5%
Sf Salmon R Nr Forks Of Salmon Ca	11522300	41.2219	-123.2523	8	Northwest CA	252	0.960	0.80	0.70	0.81	0.99	0.79	0.0%	0.0%
Sf Trinity R A Forest Glen Ca	11528100	40.3747	-123.3287	6	Northwest CA	208	0.950	0.80	0.70	0.57	0.90	0.38	0.0%	0.0%
Trinity R Ab Coffee C Nr Trinity Ctr Ca	11523200	41.1111	-122.7067	42	Northwest CA	149	0.970	0.90	1.00	0.29	0.91	0.14	0.2%	0.0%
Weaver C Nr Douglas City Ca	11525800	40.6706	-122.9439	11	Northwest CA	48	0.950	0.80	0.70	0.70	0.84	0.68	3.0%	0.0%
Willow C Nr Willow C Ca	11529800	40.9469	-123.6621	15	Northwest CA	41	0.967	1.00	0.80	0.71	0.81	0.62	0.0%	0.0%
Bell C Nr Pinecrest Ca	11283200	38.1626	-119.9443	16	Sierra Nevada	9	0.950	1.00	1.00	0.76	0.97	0.64	0.0%	0.0%
Clark Fork Stanislaus R Nr Dardanelle Ca	11292500	38.3637	-119.8723	44	Sierra Nevada	68	0.970	0.80	0.70	0.61	0.95	0.59	0.0%	0.0%
Esperanza C Nr Mokelumne Hill Ca	11307000	38.3165	-120.5965	9	Sierra Nevada	17	0.950	1.00	0.80	0.90	0.98	0.89	0.1%	0.0%
Golden Trout C Nr Cartago Ca	11185300	36.3718	-118.2899	12	Sierra Nevada	24	0.980	0.40	0.75	0.55	0.90	0.54	0.0%	0.0%
Maxwell C A Coulterville Ca	11269300	37.7160	-120.1909	20	Sierra Nevada	17	0.940	0.50	0.50	0.77	0.93	0.76	0.0%	0.0%
Miami C Nr Oakhurst Ca	11257100	37.3935	-119.6553	20	Sierra Nevada	11	0.960	0.40	0.80	0.63	0.88	0.63	0.0%	0.0%
Nf Of Mf American R Nr Foresthill Ca	11433260	39.0240	-120.7196	20	Sierra Nevada	89	0.960	1.00	0.80	0.73	0.96	0.70	0.0%	0.0%
Oak C Nr Mojave Ca	10264600	35.0499	-118.3588	29	Sierra Nevada	16	0.940	0.30	0.10	0.26	0.61	0.12	0.0%	0.0%
San Joaquin R A Miller Crossing Ca	11226500	37.5104	-119.1983	47	Sierra Nevada	249	0.970	0.00	0.90	0.70	0.89	0.62	0.0%	0.0%

Wf Chowchilla R Nr Mariposa Ca	11258900	37.4204	-119.8756	23	Sierra Nevada	34	0.950	0.60	0.70	0.80	0.94	0.78	1.0%	0.0%
Combined flow Falls C nr White Water + Div Ca	10257501	33.8690	-116.6720	15	Southwestern CA	4	0.970	0.30	0.50	0.62	0.75	0.60	0.0%	0.0%
Cuyama R Nr Ventucopa Ca	11136500	34.6889	-119.3588	14	Southwestern CA	90	0.955	0.10	0.10	0.58	0.87	0.43	0.1%	0.7%
Jamul C Nr Jamul Ca	11014000	32.6376	-116.8850	53	Southwestern CA	70	0.990	0.50	0.55	0.53	0.42	0.44	4.0%	7.0%
Little Rock C Nr Little Rock Ca	10264000	34.4630	-118.0196	48	Southwestern CA	49	0.950	0.50	0.40	0.63	0.88	0.63	0.4%	0.0%
Malibu C At Crater Camp Nr Calabasas Ca	11105500	34.0778	-118.7027	49	Southwestern CA	105	0.950	0.40	0.80	0.70	0.82	0.62	26.9 %	1.1%
Pine C Nr Palmdale Ca	10264530	34.6025	-118.2485	6	Southwestern CA	2	0.930	0.15	0.10	0.72	0.85	0.65	0.5%	8.1%
Reyes C Nr Ventucopa Ca	11136480	34.6941	-119.3191	6	Southwestern CA	5	0.940	0.70	1.00	0.63	0.74	0.53	0.0%	0.0%
San Gorgonio R A Banning Ca	10256300	33.9311	-116.8287	1	Southwestern CA	44	0.950	0.20	0.60	0.99	0.00	0.99	0.9%	0.6%
Snow C And Div Combined Ca	10256501	33.8706	-116.6820	46	Southwestern CA	11	0.970	0.70	0.50	0.79	0.91	0.73	0.1%	0.0%
Sweetwater R Nr Descanso Ca.+ Div Ca	11015001	32.8348	-116.6239	21	Southwestern CA	45	0.910	0.20	0.50	0.49	0.83	0.26	3.3%	0.8%
Temecula C Nr Aguanga Ca	11042400	33.4592	-116.9245	42	Southwestern CA	131	0.970	0.15	0.20	0.75	0.74	0.74	1.8%	2.8%
Wagon Rd C Nr Stauffer Ca	11136400	34.7089	-119.2088	6	Southwestern CA	18	0.920	0.30	0.30	0.83	0.86	0.82	0.0%	0.0%
					mean	188	0.960	0.61	0.64	0.66	0.82	0.61	0.8%	1.0%
					unimpaired only		0.964	0.57	0.64	0.61	0.81	0.58	0%	0%

Appendix D: Available Datasets for the 14 Climate and Hydrologic Variables

After running the BCM, water year summaries, and linear regression models, we were able to create five sets of data (historic, and two GCMs with two emission scenarios). These five sets are summarized in the six columns of Table D1 below. It is important to note the file sizes at the bottom of the table are for only one of the five scenarios we processed.

Table D1. Mapped Datasets Produced for this Study, Their Formats and Storage Sizes

		Monthly		30-yr Water Year Summary		30-yr Monthly Summary	
		ASCII	GRID	ASCII	GRID	ASCII	GRID
Maximum Temperature	tmax	yes	no	yes	yes	yes	yes
Minimum Temperature	tmin	yes	no	yes	yes	yes	yes
Precipitation	ppt	yes	no	yes	yes	yes	yes
Potential Evapotranspiration	pet	yes	no	yes	yes	yes	yes
Runoff	run	yes	no	yes	yes	yes	yes
Recharge	rch	yes	no	yes	yes	yes	yes
Climatic Water Deficit	cwd	yes	no	yes	yes	yes	yes
Actual Evapotranspiration	aet	yes	no	yes	yes	yes	yes
Sublimation	subl	yes	no	yes	yes	yes	yes
Soil Water Storage	stor	yes	no	yes	yes	yes	yes
Snowfall	snow	yes	no	yes	yes	yes	yes
Snowpack	pck	yes	no	yes	yes	yes	yes
Snowmelt	melt	yes	no	yes	yes	yes	yes
Excess Water	exc	yes	no	yes	yes	yes	yes
Approx. size (all variables, 1 scenario, uncompressed)		2.3TB		47GB	16GB	525GB	200GB
Approx. size (all variables, 1 scenario, compressed)				3.17GB	2.85GB	19.8GB	18.1GB

These data were intended to be available for any members of the PIER V&A study who wanted to use them. The advantage in using them is that results are cross-comparable with other studies that also use them. To get a copy of the data, please contact Jim Thorne or Ryan Boynton at the University of California, Davis.

Some additional processing was conducted for a few groups, such as 10-year summaries for the historic data rather than 30-year summaries, and extracting the data by watersheds used in individual studies.

Appendix E: Summary of Climate Conditions through Time Using the 5128 HUC 12 Watersheds as Units of Analysis

Table E1. This table summaries the variables within each of the 5128 watersheds in California, and produces mean, standard deviation, minimum, and maximum values for the whole region from this compilation.

		min	max	mean	std
Precipitation	**Historic (1911-1940)**	41.9	3202.7	545.4	467.2
	Historic (1941-1970)	47.3	3525.2	607.5	542.0
	Current (1971-2000)	63.5	3548.5	625.8	535.0
	PCM B1 (2070-2099)	89.4	3742.4	691.7	567.4
	PCM A2 (2070-2099)	81.1	3511.9	662.4	535.4
	GFDL B1 (2070-2099)	60.4	3291.7	551.2	469.4
	GFDL A2 (2070-2099)	54.1	3146.7	513.0	444.2
Potential Evapotranspiration	**Historic (1911-1940)**	856.8	1601.2	1229.8	187.4
	Historic (1941-1970)	835.3	1581.1	1223.6	187.9
	Current (1971-2000)	837.2	1620.5	1240.0	192.1
	PCM B1 (2070-2099)	900.3	1672.5	1291.0	193.0
	PCM A2 (2070-2099)	924.3	1698.9	1317.0	193.4
	GFDL B1 (2070-2099)	904.7	1680.4	1298.8	192.9
	GFDL A2 (2070-2099)	939.3	1728.4	1343.9	194.7
Runoff	**Historic (1911-1940)**	0.0	2243.2	113.1	200.1
	Historic (1941-1970)	0.0	2547.6	138.3	248.5
	Current (1971-2000)	0.0	2559.3	149.0	251.5
	PCM B1 (2070-2099)	0.0	2711.1	181.6	285.3
	PCM A2 (2070-2099)	0.0	2512.0	166.2	263.3
	GFDL B1 (2070-2099)	0.0	2312.5	110.8	206.2
	GFDL A2 (2070-2099)	0.0	2213.9	107.1	197.2
Recharge	**Historic (1911-1940)**	0.0	1198.3	115.7	195.8
	Historic (1941-1970)	0.0	1313.8	134.7	227.6
	Current (1971-2000)	0.0	1295.1	131.9	215.5
	PCM B1 (2070-2099)	0.0	1270.3	131.5	206.4
	PCM A2 (2070-2099)	0.0	1190.0	127.0	199.9
	GFDL B1 (2070-2099)	0.0	1177.8	103.8	180.4
	GFDL A2 (2070-2099)	0.0	1105.9	95.9	164.7
Climatic Water Deficit	**Historic (1911-1940)**	16.8	1509.2	850.0	360.2
	Historic (1941-1970)	12.4	1506.9	832.7	370.4
	Current (1971-2000)	5.8	1513.2	834.1	366.4
	PCM B1 (2070-2099)	17.2	1532.9	874.5	349.6
	PCM A2 (2070-2099)	18.3	1579.2	916.9	342.1
	GFDL B1 (2070-2099)	18.0	1577.2	924.1	353.0
	GFDL A2 (2070-2099)	20.0	1635.2	1008.1	340.5

Appendix F: Identify Vulnerable Species and Adaptation Strategies in the Southern Sierra of California Using Historical Resurveys

The majority of this deliverable is submitted as a separate paper with Drs. Maria Santos and Craig Moritz as lead authors (Santos et al. 2012). However, one of the vegetation outputs sought for this effort, as well as for the statewide assessment, was the development of the MC1 dynamic vegetation model outputs using the 270 m grids produced in this study. The following paragraphs describe the baseline state of development of that model. Note that while the MC1 outputs have been delayed, the research using California Wildlife Habitat Relationship (WHR) landcover types through historic conditions has been advanced using an occupancy modeling approach which has led to an almost completed manuscript described in the Santos paper (Santos et al. 2012). Additionally, research on developing a method to predict TDew Mean, a measure of the monthly average dew point temperature and a requirement for MC1 to run, raises in its own right interesting questions for a climate research program.

The most problematic issue for the running of the new MC1 is the accurate development of future climate grids representing dew point. Relative humidity, or dew point, is an important component of MC1, and potentially for vegetation models generally. Therefore, we decided that this was a worthwhile area to study.

In previous runs of the MC1 model for California, the dew point was assumed to equal the minimum monthly temperature (Tmin). In a sensitivity analysis of the utility of Tmin to portray TDew Mean, we found that while this metric works for about three-quarters of the continental United States, it does not work for the southwest (Figure F1); moreover, in California it is inaccurate over about three-quarters of the state for at least four to six months out of the year (Figure F2). We worked with Dr. Alan Flint on a number of ways to address this issue, and tried four separate approaches to developing accurate projections of the TDew Mean for future climates. These have all involved using the TDew Mean values provided in the baseline PRISM historical data to develop some type of correlation between climate variables that would permit future projections.

First, we looked at Tmin = TDew Mean. This is what has been used in previous versions of the MC1 run for California. As mentioned above, this approach produced very low R^2 values for Southern California, the Sierra, and the Central Valley.

Second, we looked at the relationship between PET and Tmin, with the hypothesis that a high potential evapotranspiration might help improve our correlations. However this similarly had unsatisfactory results.

Third, we compared precipitation with Tmin, but that also did not produce suitable results.

Finally, we calculated relative humidity (Campbell 1977; Iqbal 1983) for each month using TDew Mean and Tmin from the 800 m historical PRISM data. This permitted calculation of TDew Mean using the new, modified Campbell equations (Bristow and Campbell 1985). This

approach permitted us to compare TDew Mean as we calculated, compared to PRISM values. For the great majority of California, this returned monthly values within 6°C (42.8°F) from the PRISM values (mostly from 0°C–4°C, or 36°F–39.2°F). We decided to use this approach to prepare future projections of TDew Mean for use in the MC1 model. This approach requires the assumption that the spatial patterns of relative humidity will remain constant into the future, i.e., that it will be much lower in the desert southwest and higher in the Pacific Northwest. We finished preparing these monthly values for use in the MC1 model and sent the data to the lab at Oregon State University where MC 1 is produced. The model baseline is being spun up. Results will be forwarded when these are made available.

Figure F1: Monthly Correlation of TDew Mean with Tmin for January, Showing that Tmin is a Decent Predictor of Dewpoint for the Wetter Parts of the U.S., but That This Relationship Does Not Hold for the Arid Southwest

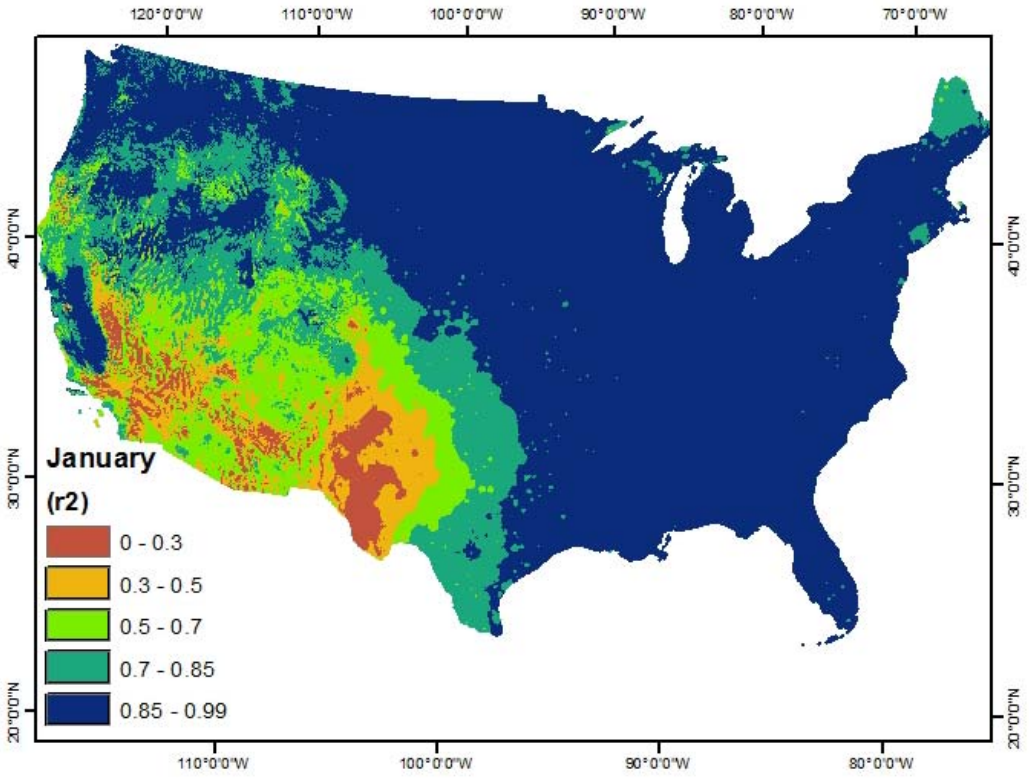

Figure F2: Monthly Correlation of Tmin to PRISM TDew Mean, Showing That Minimum Temperature Correlates Poorly with Dew Point for Large Portions of California, in the Month of April